K I N E T I C S O F P H A S E S E P A R A T I O N

I N B I N A R Y P O L Y M E R ~~M I X T U R E S~~ BLENDS.

by

Robert G. Hill

A Thesis Submitted for the Degree of Doctor of Philosophy of the University of London

Department of Chemical Engineering and Chemical Technology
Imperial College of Science and Technology
London S.W.7.

JUNE 1985

A B S T R A C T

This thesis describes the design and construction of a Small Angle Light Scattering Instrument and its subsequent use along with small angle neutron and X-ray scattering to study spinodal decomposition in polymer mixtures. Three mixtures were studied: Oligomer mixtures of Polystyrene with Polybutadiene and high molecular weight mixtures of Solution Chlorinated Polyethylene with Poly(methyl methacrylate) and with Ethylene vinyl acetate Copolymer.

The data is analysed using the spinodal decomposition theory of Cahn and Hilliard. This theory satisfactorily predicts the observed exponential growth of the wavevector maximum during the early stages- but fails to predict the wavevector cut-off, or the wavevector dependence of the growth rate. The Cahn-Hilliard theory fails to account for the non exponential growth of the wavevector maximum and its movement to smaller wavevectors during the late stages. The results are compared with predictions made for Polymers by de Gennes, Pincus, Binder and van Aartsen. None of these theories satisfactorily predict the initial scale of phase separation in all three systems. The Poly(methylmethacrylate)/Solution Chlorinated Polyethylene system phase separates on a scale much smaller than has previously been observed in polymer mixtures. The initial correlation length being comparable to the radius of gyration of the polymer coils in agreement with the theories of de Gennes, Pincus and Binder that take into account the entangled nature of polymers.

A C K N O W L E D G E M E N T S

I would especially like to thank the following:

Dr. P. Tomlins for help with the SAXS studies on the PMMA/SCPE mixtures and for bringing to my attention the PS/PB system.

Dr. A. Maconnachie for carrying out gel permeation chromotography.

Dr. R. Ghosh for his helpful advice and particularly for setting up the real time SANS experiments.

Dr. A. Wright for his help with D11 and his constructive comments.

Dr. C. Nave for his assistance with SAXS at Daresbury
Unilever Colworth House for use of their Kratky camera.

Malcolm Dix for designing and help with the building of the interface for the Small Angle Light Scattering Instrument.

Ian Drummond for his support with the elemental analysis of the Solution Chlorinated Polyethylenes.

Drs. H. Snyder (Dupont), T. Russel (IBM), D. Walsh, S. Rostami, Professor Koningsveld (DSM) and Monica Olivera (Cavendish Laboratory) for useful discussions and copies of papers prior to publication.

Joyce Burberry for completing the typing.

Finally, I would like to thank my supervisor, Dr. J.S. Higgins, for her support and encouragement during this work.

C O N T E N T S

Page No.

Abstract

Acknowledgements

Contents

CHAPTER 1

INTRODUCTION 1

CHAPTER 2

THERMODYNAMICS

Phase Stability 3

Thermodynamics of Polymer Miscibility 4

Thermodynamics of Practical Systems 6

CHAPTER 3

POLYMER MOTION 8

CHAPTER 4

THEORIES OF PHASE SEPARATION

Introduction 13

Early Stage Theories 17

Late Stage Theories 26

Modifications for Polymers 27

CHAPTER 5

SMALL ANGLE SCATTERING

Introduction 33

Theory 34

Scattering from a System Undergoing Spinodal Decomposition 38

Page No.

Scattering from a System Undergoing Nucleation and Growth 41

General Considerations 45

CHAPTER 6

PREVIOUS EXPERIMENTAL STUDIES OF SPINODAL DECOMPOSITION

Introduction 53

Alloys 55

Glasses 58

Liquids 59

Polymer/Solvents 61

Oligomers 62

Polymers 65

CHAPTER 7

MATERIALS

Choice of Systems 73

Thermodynamics of Systems Studied 75

Material Preparation and Characterisation 78

Sample Coding 84

Blend Preparation 84

CHAPTER 8

DESIGN OF SMALL ANGLE LIGHT SCATTERING INSTRUMENT

Introduction 88

Design Requirements 88

Description Instrument 91

Characteristics 96

Page No.

CHAPTER 9

TECHNIQUES

Determination of Phase Boundaries 98

Transmission Electron Microscopy 100

Light Microscopy 101

Dynamic Mechanical Analysis 101

Small Angle Light Scattering 102

Small Angle Neutron Scattering 104

Small Angle X-ray Scattering 108

CHAPTER 10

RESULTS AND DISCUSSION

Polystyrene/Polybutadiene Oligomers 114

Ethylene-vinyl-acetate/Solution Chlorinated Polyethylene 123

Poly(methylmethacrylate)/Solution Chlorinated Polyethylene 136

CHAPTER 11

DISCUSSION 155

References 163

Tables 174

Figures 218

CHAPTER 1

INTRODUCTION

During the last ten years there has been considerable interest in polymer-polymer miscibility with the emphasis on establishing phase diagrams and explaining them in terms of thermodynamic theories,[1,2,3]. In contrast there have been very few studies of the demixing process and its dynamics.

The study of the kinetics of phase separation processes in polymer mixtures is of interest for four reasons.

Firstly, studying the kinetics of a process often leads to a more complete understanding of the thermodynamics.

Secondly, very little is known about the validity of the current theories of polymer motion in the melt state and few measurements of polymer diffusion coefficient exist. Kinetic studies of phase separation of polymers may test some of these theories.

Thirdly, polymer mixtures are good model systems in which to study fundamental phase separation processes, for example, spinodal decomposition. Because of their long entangled nature polymer

molecules, have low diffusion coefficients compared with small molecules. Furthermore unlike glasses and metals they phase separate on a comparitively large scale, this results in the phase separation process proceeding slowly, enabling the kinetics of the process to be studied in detail.

The mean field approximation on which spinodal decomposition theory is based has been shown recently to be more valid for polymers than for small molecule systems.

Finally much greater control can be exercised with phase separation experiments on polymers than on any other system. For example, phase boundaries can be readily manipulated to a given temperature, crystallinity can be eliminated by random copolymerisation and the mobility of the component polymers can be varied by altering their molecular weight.

Fourthly, the study of the kinetics of phase separation in polymer blends may well enable new polymer materials to be made by stopping the phase separation process at different times in order to give a known microstructure. Such materials may have useful mechanical properties, or be useful as potential membranes.

CHAPTER 2

THERMODYNAMICS

A precursor to the study of the dynamics of phase separation in polymer mixtures is a knowledge of their thermodynamics. A brief discussion of the important aspects will follow :

PHASE STABILITY

The free energy of mixing two species is given by :

$$\Delta Gm = \Delta Hm - T\Delta Sm$$

Where :

ΔHm is the enthalpy of mixing

ΔSm is the entropy of mixing

A plot of the free energy of mixing as a function of composition is shown in Fig.1, temperature and pressure being constant. If ΔGm is a convex function over the entire composition range then one single homogenous phase will exist. Alternatively, if ΔGm is convex only over a portion of the composition range, then regions of stability and

metastability will exist. These regions give rise to different mechanisms of phase separation which will be discussed fully in Chapter 4.

THERMODYNAMICS OF POLYMER MISCIBILITY

In general most low molecular weight mixtures have favourable free energies of mixing and are, therefore, miscible, whilst high molecular weight polymers have unfavourable free energies of mixing and are immiscible. In small molecule mixtures the entropy term dominates, whereas with polymers the entropy of mixing is almost negligible because the polymer back-bone restricts the number of positions available to the monomer units. This is illustrated schematically in Fig.2. Obviously, as the chain length increases the number of possible arrangements decreases and the entropy of mixing diminishes. This concept is expressed mathematically in the Flory-Huggins Lattice model,[5,6]

$$\frac{\Delta G}{kT} = \underbrace{\frac{\phi}{N_A}\ln\phi + \frac{1-\phi}{N_B}\ln(1-\phi)}_{\text{Combinatorial Entropy Term}} + \chi\phi(1-\phi)$$

Where :

k is the Boltzman constant

T is the temperature (K)

N_A is the degree of polymerisation of polymer A

N_B is the degree of polymerisation of polymer B

ϕ is the volume fraction of component A

χ is the Flory-Huggins interaction parameter

The combinatorial entropy component is the entropy that arises from the number of possible ways of arranging the two polymers on the lattice. This model also includes a χ term to allow for any slight changes in enthalpy caused by interactions between the two components.

The Flory-Huggins lattice model predicts an upper critical solution temperature phase diagram, for high molecular weight polymer mixtures, but in reality they have lower critical solution temperature behaviour (LCST)

Later Flory and others [7,8, 9] proposed an equation of state theory to take into account expansion and pressure coefficents as well as trying to predict LCST behaviour. It has been used [10,11] in modelling polymer-polymer phase boundaries. The equation of state theory

includes the combinatorial entropy terms, an interaction term χ_{12} and an empirical parameter Q_{12}. This latter term represents an additional contribution from a non combinatorial entropy of mixing. In many cases it is included in the definition of X_{12} which then becomes :

$$\bar{X}_{12} = X_{12} - T\tilde{v}\, Q_{12}$$

Where :

T is the temperature in K

$\tilde{v}$ reduced volume of the mixture

rather than being expressed as a separate term.

THERMODYNAMICS OF PRACTICAL SYSTEMS

Miscibility of polymer mixtures occurs in three situations.

1. Polymers of very low molecular weight which no longer have a negligible entropy of mixing.

2. Polymers which are chemically almost identical having a very small unfavourable heat of mixing.

3. Polymers which show specific interactions between the component monomers resulting in favourable heats of mixing.

Polymers that fall into category 1 are generally of no commercial interest, however, they are very useful model systems for academic studies of the thermodynamics of miscibility and dynamics of phase separation.

Examples of category 2 are not very common. Examples include; chlorinated polyethylene with poly(vinyl-chloride)[12] and possibly deuterated polymers with the equivalent hydrogenous polymer.

Category 3 is by far the most common and the most commercially important group. Such systems often exhibit partial miscibility and have lower critical solution temperature phase behaviour [13], [14].

CHAPTER 3

POLYMER MOTION

A knowledge of the physics of polymer motion particularly translational diffusion is necessary to understand phase separation in polymer blends.

At temperatures below the glass transition, Tg of a polymer there will be no translational motion, however, it must be remembered that because of the viscoelastic nature of polymers the glass transition measurement will be frequency dependent.[15]

Studies on polymer diffusion, are hampered because translational diffusion coefficients are extremely low. Few measurements have been made, particularly for high molecular weights. Polymer diffusion has been recently reviewed by Tirrel.[16]

Recent studies have almost exclusively been concerned with de Gennes theory of reptation [17], [18], based on the tube model of Edwards. [19] This model envisages a polymer chain trapped in a tube of entanglements formed by other polymer chains (Fig.3). Only chains above a given molecular weight will form entanglements, this value

is termed the entanglement molecular weight (Ne). Values for Ne are determined experimentally from viscoelastic studies as a function of molecular weight.

The entanglements are assumed to be immobile during the time it takes for the polymer chain to extricate itself by Brownian motion from the tube.

The reptation model predicts that the self diffusion coefficient (D) will be dependent on the degree of polymerisation (N) and the frictional mobility within the tube (μ). The translational diffusion coefficient D is predicted to scale as :

$$D \propto N^{-2}$$

Early work by Klein[20,21,22] and by Leger et al[23] using different techniques were in very good agreement with the above scaling law. Klein[24] also demonstrated that the matrix molecular weight had no influence on the measured diffusion coefficient of a labelled chain. However, both the techniques utilized by Klein and Leger et al were not suitable for studying very high molecular weight chains. However, the reptation model fails to explain viscoelastic data on polymers, in particular it predicts an exponent of 3.0 for the viscosity dependence on the degree of polymerisation (N), whilst an

exponent of 3.4 is always found in practice.[25]

The model also fails to explain the N^{-2} behaviour rather than the N^{-1} behaviour expected on a Rouse model[26] for polymer diffusion below the entanglement molecular weight.[27,28] This casts doubts on the strict validity of the reptation model. More recently Smith et al[29] using fluorescence redistribution after pattern photobleaching (FRAPP) demonstrated that for high molecular weight labelled chains the diffusion coefficient obtained was dependent on matrix molecular weight in contradiction to the reptation theory. Klein[30] has recently investigated the diffusion of branched star molecules for which de Gennes[31] predicts a much slower diffusion coefficient and also found deviation from the reptation theory. He suggests that for very high molecular weights or star molecules where reptation is slow tube renewal effects become important, i.e., the tube is no longer fixed during the time the polymer chain is contained within the tube.

Studies using the Neutron Spin Echo technique on Poly(methylsiloxane) melts by Richter et[32]al. demonstrate only Rouse type motion for chains above the entanglement molecular weight. They suggest that the reptation model is only valid for the self diffusion case.

However, an unpublished study by Higgins and Roots[33] using the same technique, but with polytetrahydrofuran demonstrates the presence of two modes of relaxation for molecular weights above Ne, whilst only the faster mode is observable for molecular weights below Ne. The shorter relaxation time corresponds to local Rouse type motion, whilst the longer relaxation time is believed to correspond to reptation. Their data suggests that the time scale observed by Richter et al was too short to observe reptation and, therefore, only the Rouse type motion was observed.

Studies looking at the relaxation of orientated melts nearly always gives rise to Rouse behaviour rather than reptation. For example, Boué et al[34] found the relaxation of polymer melts after step deformation to be accurately modelled by Rouse behaviour even for molecular weights in excess of entanglement values.

Recently it has been shown that the diffusion of polycaprolactam (PCL) into poly(vinylchloride) (PVC) went as N^{-1} and not the N^{2} behaviour expected[35]. de Gennes[36] has explained this in term of being the result of an N^{-2} diffusion coefficient and a thermodynamic driving force favouring mixing which is proportional to the number of monomers in the chain (N). In the case of PCL/PVC blends there is a large negative enthalpy of mixing arising from a specific interaction

between the component monomers. Though the explanation of de Gennes for the N^{-1} diffusion coefficient behaviour seems very plausible, the data could also be explained by Rouse type behaviour occuring. At present, it is not clear how polymers will diffuse during phase separation, however, diffusion in polymer blends is unlikely to be modelled exactly by a reptation model, even when one of the polymers can be effectively assumed to be immobile with respect to the other. It is clear though that the average chain length will have a pronounced effect on diffusion. Thus polymers with a high frictional tube coefficient (due to bulky side groups), high degrees of polymerisation or are branched are likely to phase separate slowly.

It might be expected that in a polymer mixture the shorter chains will diffuse faster than the longer chains and thus a range of diffusion coefficient exist. Alternatively, there may be a lot of co-operativity between chains and only one diffusion coefficient may thus exist for a given blend composition.

Because of our limited knowledge of polymer diffusion, the best approach will be to utilize as near monodisperse molecular weight distributions as practically possible to avoid any potential complications.

CHAPTER 4

THEORIES OF PHASE SEPARATION

I N T R O D U C T I O N

There are many theories of phase separation, no one theory satisfactorily predicts the phase separation process. Most theories are applicable only for a short time scale for one or two systems. Some general features of phase separation will be discussed before any detailed theory.

Consider a phase diagram with a miscibility gap as shown in Fig.4a. If a polymer mixture with a composition Xo is quenched from a high temperature T_1 to a lower temperature T_2, then the composition will initially be the same throughout the mixture and its free energy will be Go on the free energy curve in Fig.4b. However, the polymer mixture will be immediately unstable because small fluctuations in composition that produce A rich and B rich regions will cause the total free energy to decrease. Therefore, "uphill" diffusion takes place until the equilibrium concentrations X_1 and X_2 are reached. This is shown schematically in Fig. 5 a. The above process can occur for any polymer mixture composition where the free energy curve has a negative curvature i.e.,

$$\frac{\delta^2 G}{\delta \phi^2} < 0$$

Thus the polymer mixture must lie between the points of inflection on the free energy curve. The locus of the points where $\delta^2 G/\delta\phi^2 = 0$ is termed the spinodal.

If the polymer mixture lies outside the spinodal, but within the binodal (defined by the points of common tangent) small fluctuations from the mean concentration lead to an increase in the free energy and the fluctuations decay. Large fluctuations can, however, result in a decrease in the free energy. Such a fluctuation is termed a nucleus and can arise by a thermal,or density fluctuation giving rise to homogenous nucleation; alternatively a nucleus can be formed by a foreign particle or surface enriched layer in which case heterogenous nucleation occurs. The nucleus has an excess surface energy compared with its surroundings and is strongly held together with the result that molecules flow in by conventional down hill diffusion. Unlike the totally unstable phase separation process nucleation and growth requires an activation energy and the system is, therefore, metastable between the binodal and spinodal. This process is shown schematically in Fig. 5 b.

Not all theories recognise the spinodal as the limit of metastability. Binder[37] claims that the spinodal is "unphysical" since the barrier to

phase separation never quite goes to zero only becoming less than $k_B T$. He proposes a cluster model that can account for decomposition in both the metastable, and the unstable region of the phase diagram.

Studies of the nucleation stage of nucleation and growth are difficult due to the necessity of eliminating foreign particles from the system.

This thesis is mostly concerned with the phase separation mechanism of spinodal decomposition that occurs within the spinodal.

The characteristic features of this process are :-

1. It is an unstable process requiring no activation energy and is, therefore, very rapid.

2. An order parameter that describes the system obeys a local conservation law thus the decomposition is limited by diffusion like processes. The diffusion is uphill and, therefore, the diffusion coefficient has a negative sign.

3. Temperature fluctuations play no part.

4. The process occurs coherently; the composition of the phases changes continuously. For isotropic materials the waves have random orientations and phase angles, so the spinodal structure is random and interconnected.

All the theories of phase separation avoid describing the molecular details of the system and instead concentrate on describing phase separation using macroscopic variables. In practice phase separation kinetics have often been described in terms of power law expressions. For example, the time dependence of the maximum scattered intensity may be given by :

$$Im \propto t^{\gamma}$$

Similiarly the time dependence of the average correlation length may be given by :

$$Dm \propto t^{\circ}$$

An alternative method of analysing phase separation data is that used by Goldburg[38] who recognised that the behaviour of a system phase separating was very dependent on the time scale over which the phase separation was observed. He therefore interpreted his data in terms of a reduced unit approach where :

$$\tilde{Q}m = QmDm \quad (t = o)$$

$$\tau = t\bar{D} \quad (t = o) \; / \; (Dm)^2 \quad (t = o)$$

where both $\tilde{Q}m$ and τ are dimensionless quantities completely determined by experiment.

This approach has recently been used by Snyder.[39]

Early Stage Theories

The Cahn-Hilliard Theory

Cahn and Hilliard[40-43] described the free energy G of an inhomogenous binary mixture composed of small molecules (e.g., A and B) in an incompressible system as :

1. $$G = \int dv \left(G(\phi) + K\phi^2 + \ldots\right)$$

Where K is the gradient energy coefficient

where G (ϕ) is the free energy density of the system having composition ϕ of one component (e.g., A) which is uniform everywhere in space and the second term is the excess free energy arising from the concentration gradient. By taking the variational derivative of equation 1 the chemical potential difference ($\mu A - \mu B$) is obtained. The flux of each component JA or JB is then obtained from M ($\mu A - \mu B$). An application of the continuity equation dc/dt = div JA to JA results in :

2. $$\frac{d\phi}{dt} = M \frac{\partial^2 G}{\partial \phi^2} \nabla^2 \phi - 2MK\nabla^4\phi + \text{non linear terms}$$

where M is the interdiffusion coefficient which is approximately constant, having a slight concentration dependence. For most practical purposes it can be regarded as being equivalent to a diffusion coefficient. It is useful to compare equation 2 with a conventional diffusion equation expression.

3. $$\partial\phi/\partial t = D\nabla^2\phi$$

This gives rise to the concept of the Cahn-Hilliard diffusion coefficient ($\tilde{D}$) being.

4. $$\tilde{D} = M(\partial^2 G/\partial\phi^2)$$

Neglecting non-linear terms the solution to equation 2 is obtained by :

5. $$\phi(r) - \phi(o) = \sum_{Q} \exp\left(R(Q)t\right)\left[A_{(Q)}\cos\left(Q.r\right) + B\left(Q\right)\sin\left(Q.r\right)\right]$$

where the growth rate R(Q) is given by.

6. $$R(Q) = -MQ^2 \left[\left(\frac{\partial^2 G}{\partial \phi^2} \right) - 2KQ^2 \right]$$

Because K is always positive $\delta^2 G/\delta\phi^2$ governs the sign of the growth rate. Positive values of $\delta^2 G/\delta\phi^2$ yield negative values of R(Q) and all instabilities decay. As $\delta^2 G/\delta\phi^2$ becomes zero long wavelengths will grow and as it becomes negative shorter wavelengths become capable of growing. The linear theory of Cahn-Hilliard can be used to predict the wavevector, Qm of the spatial composition fluctuations that grow most rapidly and the critical wave ector (Qc) below which fluctuations decay in the spinodal region. From equation 6 it follows that :

7. $$Qm^2 = \left(\frac{Qc}{\sqrt{2}}\right)^2 = - \frac{\partial^2 G}{\partial \phi^2}/4K$$

and, therefore

8. $$R(Qm) = M \left[\left(\frac{\partial^2 G}{\partial \phi^2} \right)/8K \right]$$

The conclusion to be drawn from these two equations is that Qm

is controlled only by thermodynamics while R(Qm) is controlled also by the interdiffusion coefficient.

At the spinodal point :

9. $$\frac{(\delta^2 G)}{(\delta\phi^2)} = 0 \quad T = T_S = 0$$

and as a result

$$Qm^2 = R(Qm) = 0$$

At $Q \ll Qm$, R(Q) is dominantly controlled by diffusion, the contribution of which is such that the larger Q the larger R(Q). If, however, $Qc > Q \gg Q_m$ R(Q) is now dominantly controlled by thermodynamic properties.

Thus where R(Q) is controlled by diffusion

$$R(\text{diffusion})\ (Q) \simeq Q^2 D$$

and where R(Q) is controlled by thermodynamics

$$\Omega(\text{thermodynamics})\ (Q) \simeq \left[-\left(\frac{\partial^2 G}{\partial \phi^2}\right) - 2KQ^2\right]$$

It is, therefore, apparent that the dynamics in the linear spinodal regime are determined by the terms M, $(\delta^2 G/\delta\phi^2)$ and K.
From C/H theory the scattering wavevector maximum can be shown to be given by :

10. $$Qm^2 \propto \frac{\partial^2 G}{\partial \phi^2}$$

Assuming regular solution theory and a temperature independent value for K Cahn[44] demonstrated that :

11. $$\frac{\partial^2 G}{\partial \phi^2} \propto \left(\frac{Ts-T}{Ts}\right)$$

Thus a plot of Qm^2 against temperature should be linear and extrapolate to zero. Assuming M to be temperature independent it also follows that the Cahn-Hilliard diffusion coefficient is given by :

$$\bar{D} \alpha \left(\frac{Ts-T}{Ts}\right)$$

The slope of $\bar{D}$ against temperature should be linear and extrapolate to zero at the spinodal.

The linearized C/H theory predicts an exponential growth in scattered intensity with time, a negative diffusion coefficient and phase interconnectivity, all of which occur at early times during the phase separation process.

However, the C/H theory also predicts a sharp transition in behaviour at the spinodal, a constant Qm at a given temperature and a continuous exponential growth of scattered intensity all of which are not found.[45],[46]. In practice Qm gets progressively smaller, there is no sharp boundary between nucleation and growth and spinodal decomposition and the exponential growth only occurs for the first few percent of the phase separation process.

Even during the initial stages of the phase separation C/H theory cannot quantitatively predict the rate of phase separation.

All these faults are due to assumptions made in deriving the C/H theory. Various workers have modified the C/H theory and others have started afresh with completely new theories.

The problems with the C/H approach are[47] :-

1. It is difficult to interpret the parameter $G(\phi)$.

2. The coarse graining is assumed to be done on a scale much larger than molecular distances but not larger than the correlation length of concentration fluctuations. A result of this is that G can be defined in a meaningful way for :

   (UCST) $0.95 < T/Ts < 1.0$

   but not for deeper quenches. In polymer blends the phase sizes are likely to be much larger than the molecular distances compared with metallic alloys, ceramics, or glasses and this might extend the temperature range.

3. Near the spinodal the thermodynamic driving force for phase separation will be small and as a result the rate will be slow and nucleation processes will contribute significantly to the phase separation process.

4. The theory totally neglects the non-linear terms which become more important as the phase separation proceeds.

5. The theory neglects hydrodynamic terms, viscous flow and changes in volume.

6. The theory assumes the thermodynamics of the phase separating system are modelled by regular solution theory, thus the phase separation is brought about by the reduction in the favourable $T\Delta S$ term as the temperature is lowered. The theory will still be valid for polymer systems having UCST phase behaviour where the phase separation is brought about by the reduction in the combinatorial entropy term as the temperature is lowered. However, most partially miscible polymer mixtures have LCST phase behaviour and their thermodynamics are dominated by favourable enthalpies of mixing.

In these cases the temperature dependance of Qm and $\bar{D}$ will not be as predicted by Cahn, but both parameters will obviously go to zero at the spinodal, assuming no nucleation and growth taking place.

Experimentally there is often not a sharp spinodal boundary. Cook[48] has explained this phenomena in terms of the C/H theory failing to incorporate thermal fluctuations. Park et al[49] have pointed out that:

13. $Qc/Qm = \sqrt{2}$

is only valid when thermal fluctuations are included in the C/H theory at $T = 0^0K$.

The expression with thermal fluctuations included becomes :-

14. $$\frac{Qm}{Qc} = \left[\frac{Ts-T}{2Ts}\right]^{\frac{1}{2}} \quad (\text{UCST case})$$

Binder[47] has criticised this approach of incorporating thermal fluctuations for systems with short range interactions. He does not believe thermal fluctuations to be large enough or localized enough to round off the spinodal.

Langer and coworkers[50,51] have modified the C/H theory to take into account the neglected non-linear terms as well as thermal fluctuations, which has resulted in the Langer, Bar-on and Miller theory[52] (LBM theory). This theory predicts:

$$Dm \propto t^{0.212}$$

$$Im \propto t^{0.81}$$

Where Im is the intensity at Qm.

This theory fits the limited early time data for the spinodal decomposition of solids such as metallic alloys, but not the spinodal decomposition of fluids, such as lutidine/water mixtures. This led Kawasaki and Ohta[53] to suggest that long range hydrodynamic forces are important during the early stages of spinodal decomposition. They incorporated hydrodynamic terms into the LBM Theory to correct for the

hydrodynamic interactions. This has become known as the K/O theory and fits the data for lutidine/water fairly well. However, hydrodynamic effects are most important during the later stages of phase separation for which the K/O theory does apply since it is based on LBM theory and thus C/H theory which assumes only a small amount of phase separation takes place.

Late Stage Theories

The late stage starts when there is no more increase in the phase concentrations and the phases adjust their sizes by a variety of mechanisms to minimise their surface energy.

The first process considered is that of Ostwald ripening also known as the constant volume evaporation model[54]. Ostwald ripening can follow nucleation and growth or spinodal decomposition mechanisms. Ostwald ripening is the dissolution of small droplets to further the growth of large droplets. Lifshitz and Slyozov[55] have put forward a theory predicting the time dependance of the average droplet size as

$$Dm \propto t^{0.33}$$

In spinodally decomposed samples with the classical interconnected morphology there is an alternative mechanism proposed by McMaster[56] of interfacial tension driven viscous flow. He has interpreted this

mechanism in terms of Tomotika's[57] analysis of the break-up of one thread of viscous Newtonian Liquid in another Newtonian liquid. This analysis gives rise to an exponential growth in the phase size and McMaster found such an effect.

Siggia[58] extended the K/O theory to late times. He suggests that the mechanism of constant volume evaporation for the late stages when the drops are much larger than the initial correlation length is not so important for liquids. He argues that the volume fraction of precipitate actually produced in most phase separation experiments probably favours direct coalescence. When the minority phase is continuous as in a quench at the critical concentration, surface tension effects cause a crossover from $Dm \propto t^0$ to $Dm \propto t$.

Modifications for Polymers.

Polymer blends are viscous fluids in the melt state when they phase separate, thus hydrodynamic effects during the early stages are likely to be more important than in metallic alloys, but not as important as in liquids. Coherency assumed in the C/H theory is likely to be a more valid assumption for polymers than for metals. The C/H theory assumes an homogenous state prior to phase separation and for many polymer blends with crystalline regions present this will be an invalid assumption.

Theoretical studies by Binder[59] and de Gennes[60,61] demonstrated that the mean field approximation, on which the theory of Cahn-Hilliard is based is more valid for polymers than for small molecule systems. The mean field approximation is more valid when assumed over a distance scale larger than molecular forces operate, but shorter than the wavelength of the decomposing fluctuations. Polymers decompose on a much longer wavelength than do alloys and glasses. This will extend the temperature range over which the mean field approximation is valid.

Binder[59] also recognises in contrast to his view for small molecule mixtures that the spinodal has a physical significance in polymer-polymer mixtures. Binder also demonstrates that homogenous nucleation and growth will be so slow as to be insignificant in high molecular weight entangled polymer mixtures.

Modification of theories of phase separation may or may not be necessary for polymer mixtures. It is important to consider what features distinguish polymers from other materials. These include, their long entangled nature, presence of long range interactions and their reduced entropy due to the polymer backbone restricting the number of positions in space open to the monomer units.

Binder[59] de Gennes[62] and Pincus[63] have discussed what modification these factors will have on the theory of spinodal decomposition, their theories will be discussed later.

Others[39] have stressed the similiarities between the polymer phase separation and that of glasses, alloys and liquid mixtures.

van Aartsen[64] utilized Flory-Huggins theory and C/H theory to derive the following expression for the size scale of phase separation in polymer solvent mixtures.

$$15. \quad Dm = 2\pi\ell\left[3\left(1-\frac{T}{T_s}\right)\right]^{-\frac{1}{2}}$$

where ℓ is the range of molecular interaction, Ts and T are the temperature of the spinodal and sample respectively.

An almost identical expression can be derived using Debye's theory of non-homogenous solutions and C/H theory. The van Aartsen expression has been simply modified for polymer mixtures having LCST behaviour by replacing the term (1-T/Ts) by (T/Ts-1). For polymer/polymer mixtures it can be shown that:

$$16. \quad \ell = Rg/\sqrt{3}$$

where Rg is the radius of gyration. It is normally assumed that both component polymers have identical radii of gyration. For a high molecular weight polymer mixture Rg is typically about 200Å and Dm will, therefore, be approximately 5000Å a few degrees inside the

spinodal.

Binder[59] de Gennes[62] and Pincus[63] have attempted to modify the C/H theory for the effects of entanglements and reptation. They assume the free energy of the blend is described by the Flory-Huggins Lattice model, has a positive χ favouring segregation and the degree of polymerisation (N) is very large. Their theories give rise to a second view that believes spinodal decomposition will start on a scale the order of the radius of gyration of the polymer molecules or less.

As yet no studies have been carried out to look for this small scale phase separation. The techniques of SANS and SAXS that could be used are not widely available. de Gennes first considered theoretical aspects of phase separation of polymer blends. He obtained

17. $$\tau q^{-1} = q^2 M(q)\left[\frac{1}{N\phi(1-\phi)} - \frac{2\chi+(aq)^2}{36\phi(1-\phi)}\right]$$

where τq^{-1} is the relaxation spectrum for a single relaxation.

In the intermediate wavevector regime $Ne^{-1} > q > Rg^{-1}$ a scaling argument was used giving:

$$M(q) \sim q^2$$

This was based on a single relaxation time for a mode of wavevector

q of a non-interacting chain in a melt.

Later de Gennes[65] modified his theory to take into account two modes of relaxation, this theory was subsequently reconsidered and corrected by Pincus who showed:[63]

$$M(q) \propto q^{-2}$$

and found that the most unstable mode immediately after quenching is molecular weight dependent. Pincus predicts the initial unstable mode q to be given by:

18. $$q^{-1} \cong \frac{Rg}{6} \sqrt{3} \left(\left(\frac{\chi}{\chi_s} - 1 \right) \right)^{-\frac{1}{2}}$$

for $(\chi/\chi s - 1) << 1$ near the spinodal and:

19. $$q^{-1} = Rg/6 \left(\text{In } 6\chi/\chi s \right)^{-1}$$

for a deep quench $\chi >> \chi s$. The corresponding expressions for the growth rate are:

20. $$R \cong \text{Trep}^{-1} \left(\frac{\chi}{\chi s} - 1 \right)^2 \left(\frac{\chi}{\chi_s} - 1 << 1 \right)$$

$$R \propto \tau_{rep}^{-1}\left(\frac{\chi}{\chi_s}\right) \qquad (\chi \gg \chi_s)$$

Close to the spinodal the growth rate, R undergoes a critical slowing down and the spinodal decomposition may be masked by nucleation processes.

The essential predictions made by Pincus are; 1. The unstable mode has a wavelength comparable to the ideal chain radius and therefore, should vary as N with only a weak concentration dependence providing the final temperature is not too close to the spinodal. 2. The corresponding growth rate is proportional to the reptation diffusion coefficient of the melt, this is also predicted by Binder.
3. Finally for very deep quenches a transient microphase separation may occur on a scale $Ne^{\frac{1}{2}}$ (the distance between entanglements) as discussed by de Gennes for crosslinked blends. This requires $\chi/\chi s \gg$ N/Ne which Pincus considers will be unlikely to be achieved.

C H A P T E R 5

Small Angle Scattering

I N T R O D U C T I O N

Small angle scattering is probably the best technique for studying phase separation, since it enables both the concentration gradient and the size scale of phase separation to be measured. However, there are considerable difficulties in the interpretation of small angle scattering data. Many other techniques notably various types of microscopy are often very useful in conjunction with small angle scattering techniques.

Microscopy though not ideally suited to quantitative studies, permits the direct observation of the morphology of the blend and more importantly the nature of the interface between phases.

Spectroscopic techniques that can determine the environment of the polymers in the one and two phase regions are also useful in conjunction with scattering techniques.

No extensive review of small angle scattering theory will be undertaken, numerous excellent reviews of small angle light[66-69], neutron[70, 71] and X-ray scattering[72, 73] have been published. Nearly all the experimental and theoretical studies published deal with scattering from dilute suspensions of isolated particles of fixed volume and concentration. The interpretation of scattering from a phase separating system is not a trivial matter. Only the general features of small angle diffraction will be covered and a comparison of the three techniques used, followed by a review of the scattering behaviour expected from systems undergoing a nucleation mechanism and a spinodal decomposition mechanism.

Theory

Consider the situation shown in Figure 7. If radiation is scattered from two points in a medium a distance D apart then the path difference between the two scattered rays is:

$$2P \sin \theta/_2$$

where $P = D \sin (\phi - \theta/_2)$ is the projection of D onto the plane bisecting the incident and scattered rays and θ is the scattering angle.

If there are two phases present and their scattering properties are different then an interference pattern will be formed. Not only can there be interference of scattered waves from the same particle as illustrated in the figure, but also interference of scattered waves from two or more particles. The condition for interference to occur is that the path length $2P \sin \theta/_2$ must correspond to approximately the diameter of the particles or the interparticle spacing and should be approximately the magnitude of the wavelength of the incoming radiation.

One of the major differences between the three scattering techniques is their wavelength. Thus the source of radiation determines the scale of phase separation observed. The range accessable to the three small angle techniques is illustrated schematically in Figure 8.

In a scattering experiment it is usual to describe events in terms of the wavevector of the radiation. The wavevector of the incident beam $\underline{ki}$ is related to that of the scattered beam $\underline{ks}$ via $\underline{K} = \underline{ks} - \underline{ki}$. For neutrons the wavevector is simply called the Q vector, for photons the K vector and for Xrays the H vector. All wavevectors will be called Q for convenience in this thesis.

If there is no energy lost or gained during the scattering event i.e., the collision is totally elastic then:

22. $$Q = |Q| = \frac{4\pi}{\lambda} \sin(\theta/2)$$

In the light scattering case the refractive index n of the scattering medium compared to vacuum must be taken into account. The refractive index governs the velocity of light and thus the wavelength in the medium. The new wavelength is given by

23. $$\lambda' = \lambda/n$$

Thus Q is given by

24. $$Q = \frac{4\pi n}{\lambda} \sin(\theta/2)$$

The wavelength of neutrons and X-rays is almost unaltered by the nature of the scattering medium.

All sorts of systems will give a scattering pattern including an extremely ordered array of atoms in a crystal in which case the

experiment becomes the Bragg diffraction case, the projection P becomes the distance between planes and a series of peaks are observed in the scattering pattern. The case for constructive interference will then exist.

$$2d \sin \theta/_2 = n\lambda$$

$$d = 2n \Pi/Q$$

However even a random arrangement of molecules in a gas with an average spacing will cause at least one scattering peak.

The second requirement for scattering to occur is that the scattering property must be different for the two phases. This scattering property known as contrast is the second major difference between the three techniques. With light it is polarizabilities or refractive index, for Xrays the electron density and for neutrons the neutron crosssection. The refractive index and electron density difference can be readily estimated for a material, the neutron crosssection is a complex term and can not be readily predicted.

Scattering from a System Undergoing Spinodal Decomposition

The amplification factor in the C/H theory has a sharp maximum at:

25. $$\beta m = \frac{\beta c}{\sqrt{2}} = \tfrac{1}{2}\left[-\left(\frac{\partial^2 G}{\partial \phi^2}\right)/K\right]^{\frac{1}{2}}$$

thus one particular wavelength becomes dominant, the system can be approximated to a sinusoidal concentration of this wavelength. It can be assumed for a given system that the concentration is proportional to the scattering property. The Fourier transform of a sinusoidal fluctuation gives rise to a scattering pattern with a single well defined peak at wavevector Qm where:

26. $$Qm = \frac{4\Pi}{\lambda} \sin\left(\theta/_2\right)$$

Thus it can be seen that there is an equivalence between β and Q. Rundman and Hilliard were the first to carry out small angle scattering on a spinodally decomposing system and pointed out that it was not necessary to transform the scattering pattern into real space. It was also demonstrated that for a system undergoing spinodal decomposition:

27. $I(Qm) \propto \exp 2R(Qm)t$

Thus at early times, where the non linear terms are unimportant spinodal decomposition is characterised by the exponential growth of a single scattering maximum at a fixed wavelength. Because a spinodally decomposing system is highly periodic and dominated by the most rapidly growing wavevector a Bragg type expression can be used to determine the correlation length from the position of the scattering maximum.

28. $$Dm = \frac{\lambda}{2 \sin(\phi/_2)}$$

The Bragg type expression is only strictly valid for a purely sinusoidal wavelength fluctuation random in space and is not valid for any other wave type that may be formed during the late stages, such as a square wave.

In practice most spinodally decomposing systems are not dominated completely by the most rapidly growing wavevector. There exists a range of wavevectors greater than Qm up to a wavevector Qc, the critical wavevector given by:

$$Qm = \sqrt{2}.Qc$$

above which fluctuations decay. The C/H theory predicts both Qc and Qm to be time invariant, however the implicit assumption that the $\delta^2G/\delta\phi^2$ term remains constant in the C/H theory as phase separation proceeds is incorrect. This assumption breaks down sooner for wavevectors close to Qc, since the polymer molecules do not have to diffuse so far; resulting in the intensity (I) not growing exponentially for so long and the scattering pattern becoming sharper on the high Q side. Conversely wavevectors at very low Q grow exponentially for the longest times.

In many studies of spinodal decomposition the Bragg type analysis is used and scattering maxima are attributed to sinusoidal fluctuations often without any evidence. This approach implicitly assumes a spinodal decomposition mechanism before any data is even analysed. Many of the features of spinodal decomposition could arise by a nucleation and growth mechanism.

Scattering from a System Undergoing Nucleation and Growth

There has been some debate as to whether a scattering maximum can be formed by a nucleation and growth mechanism and whether a scattering maximum provides evidence of spinodal decomposition. Therefore it is useful to consider how scattering maxima are formed.

In a small angle scattering experiment a distinct scattering maximum can arise in three ways.

1. The formation of a dominant spacing such as between polymer rich phases.

2. The formation of monodisperse particle arranged randomly.

3. A combination of both 1 and 2.

Homogenous nucleation and growth would not be expected to give rise to monodisperse particles and the occurence of a predominant spacing would not be expected on a random nucleation model. However, a diffuse maxima can arise because there is a restriction

below which nucleated particles can not be formed termed the critical radius. The maximum arises in this case from both the interference from particles and between particles. This type of scattering maximum is clearly distinguishable from a maximum formed by spinodal decomposition, because as more and more particles nucleate the particle interference term becomes smaller and the maximum moves to higher Q vectors.

Heterogenous nucleation arising from a large number of identical nuclei will give a distinct scattering maximum based on the formation of a diffusion depletion zone mechanism originally proposed by Walker and Guinier[75]. This model assumes each particle consists of a spherical nucleus of radius R_1 surrounded by a shell of radius R_2 (measured from the centre of the particle). The model could equally well describe a system of closely packed particles where each pair of particles is separated by a well defined distance which introduces a short range order to the system, without any large range order. Walker and Guinier showed that their model leads to a scattering maximum and that the scattered intensity is zero at $Q = 0$. It was also demonstrated that if R_2 is greater than about $2R_1$ then the intensity distribution on the high Q side of the maximum can be accurately modelled by the Guinier equation[76] (19) where $R \equiv R_1$ since the

$$(2.9) \quad I(Q) \propto QR^6 \exp(-R^2Q^2/5)$$

depletion zone effects the scattering behaviour predominantly on the high Q side of the maximum.

Both types of nucleated maximum will be modelled by the Guinier equation, however a maximum formed by a spinodal decomposition mechanism would not generally be modelled by the Guinier equation, since equation 6 predicts a different Q dependence of the intensity on the high Q side of the scattering maximum and only in very exceptional circumstances would the data fit a Guinier plot.

Both types of nucleation formed maxima are heavily dependent on the volume of the precipitating phase in contrast to spinodal decomposition.

Nucleation mechanisms are likely to give rise to much larger correlation lengths than spinodal decomposition since the unfavourable surface energies associated with the sharp interface formed during nucleation and growth will promote the formation of larger particles since a large particle has a smaller surface to volume ratio.

Later, during the growth stage of nucleation and growth the particles will coarsen, obviously as the nuclei do not all develop at the same time, both nucleation and growth will be occuring at the same time. The driving force for the growth stage is the unfavourable surface energy. Small particles will therefore disappear at the expense of larger particles either by an Ostwald ripening or a coalescence mechanism and the scattering peak will move to lower Q in a similar fashion to that expected from a spinodal decomposition mechanism.

It can be useful to deconvolute the scattering pattern into its two components the interparticle structure factor S(Q) and the particle form factor P(Q) especially if the full I(Q) scattering pattern with good statistics is available. This approach is useful since it can give much more accurate data on the particle size and gives valuable information on the distribution and arrangement of the phases. Wright et al[77],[78] have utilized this approach in the study of nucleation and growth of ceramics and glasses, deconvoluting I(Q) plots taken at different times during the separation process.

Other features of spinodal decomposition besides the scattering maximum could also arise by a nucleation and growth mechanism, including the wavevector maximum growing exponentially whilst at a

fixed Q. If there were appropriate changes in P(Q) and S(Q) I(Qm) could remain fixed. During the nucleation stage of nucleation and growth the scattered intensity would be expected to go as R^6 where R is the particle radius. This process could easily be falsely interpreted as exponential growth from a spinodally decomposing system.

General considerations

Although small angle scattering by light, X-rays and neutrons involves the same basic principles, the nature of the radiation has a very marked influence on the design of the experiment and on the data analysis.

Ideally the radiation source should be intense enough to permit real time experiments as this results in the minimisation of errors and is a highly efficient way of using high flux neutron and Xray sources.

Most sources have a distribution of wavelengths and therefore some form of monochromator must be used. In practice this may be carried out by Bragg reflection or velocity selection. The chosen method of monochromating the beam will always be a compromise

between obtaining the desired flux and getting the required wavelength resolution. The scattered radiation affects the detection system used, however area detectors are preferred particularly for SANS and SAXS where the flux is low and the statistics can be improved dramatically by counting over 2Π and subsequently radially averaging the data. Ideally the main beam and transmitted beam fluxes should be monitored continuously to enable the data to be properly scaled and transmission corrections made if necessary.

A dedicated computer is the final component of a small angle scattering experiment and is particularly important for real time experiments. It is used to control the experiment and ideally should display the collected data continuously so that the progress of the experiment can be followed.

Small Angle Light Scattering

Unlike neutron and X-ray sources light sources are relatively inexpensive and widely available. Lasers are readily available and offer a convenient method of obtaining an intense monochromatic beam. Light sources have very high fluxes compared with neutron and Xray sources.

Detection of the scattered light can be by use of photographic film, photomultplier tubes, or photodiodes. The choice of detection system depends on the intensity of the scattered light, however more recently small angle scattering instruments have tended to utilise photodiodes, since these can be bought commercially as linear and area arrays along with optical multichannel analysers. Most materials have considerably different refractive indices so contrast between phases is normally good unlike neutron scattering and X-ray scattering. However the large difference in refractive index between materials also means that wavelengths and angles have to be corrected for refraction effects. This can complicate the data analysis considerably and also limit the d-spacing or Q range that can be studied since at large angles a total internal reflection condition can be set up. Refraction effects also occur from surface defects causing spurious scattering. The major experimental difficulty is however that extraneous foreign particles also have a good refractive index difference, often greater than the difference between the two phases being studied resulting in additional scattering. Great care therefore has to be taken to remove foreign particles.

Small angle Neutron Scattering

Neutron small angle scattering facilities are not widely available.Time for SANS studies is therefore limited. The wavelength of the neutron determines the Q range that can be studied. One of the major advantages of SANS is that with cold neutron sources a Q range overlapping with SALS at low Q and SAXS at high Q can be studied.

The contrast in a SANS experiment is determined by the difference in the neutron scattering lengths. There is not a systematic variation of scattering lengths with atomic number, as for example with Xrays and because the neutron scatters off the nucleus each isotope has a different scattering length. Most organic molecules have very similar total coherent scattering lengths, so attention has to be paid to obtaining sufficient contrast. The isotope deuterium fortunately has a markedly different scattering length from hydrogen enabling the possbility of labelling one component.

The coherent intensity in a neutron experiment is described by the crosssection $d\Sigma/d\Lambda$, which is the probability that a neutron will be scattered into a solid angle Λ for a unit volume of the sample. The crosssection is effectively an expresson for the scattering power of the sample and is analagous to the Rayleigh ratio used

in light scattering. For the case of a polymer mixture

$$30. \quad \frac{d\Sigma}{d\Omega} = \left[\left(b_A - b_B \right) \frac{V_A}{V_B} \right]^{S(Q)}$$

where b_A and b_B are the total coherent neutron scattering lengths for the monomers of polymer A and polymer B. V_A and V_B are the volumes occupied by polymers A and B. S(Q) is the structure factor for the system.

In a phase separation experiment the terms b_A and b_B will not correspond to the actual monomer cross-sections, but to an average monomer cross-section for a concentration of monomers somewhere between that of the initial composition and the composition defined by the co-existence curve. Thus it is almost impossible to calculate absolute cross-sections, however it is possible to readily calculate relative scattering cross-sections.

Coherent scattering lengths for carbon, hydrogen, deuterium, oxygen and chlorine are given in Table 1. V_A/V_B will be approximatly unity. Table 2 shows the relative cross-sections for a variety of poly(methylmethacrylates) with solution chlorinated polyethylenes of differing degrees of chlorination. It can be seen that the

scattering cross-section is larger for high degrees of chlorination of the SCPE with hydrogerous PMMA, than it is with low degrees of chlorination. Using deuterated PMMA improves the scattering cross-section dramatically. The final column of the table compares the relative times to obtain an I(Q) scattering pattern with suffcient statistics, based on some experimental data obtained from a hydrogerous PMMA/SCPE blend quenched during the early stages of spinodal decomposition. It is clear that without using deuterated PMMA it is impractical to study PMMA/SCPE blends with degrees of chlorination much less than 70 weight per cent. Replacing the hydrogenous PMMA by fully deuterated PMMA enables the possibility of performing real time kinetic experiments.

Many other systems can be studied by deuterium labelling one of the components, including polystyrene/polybutadiene oligomer mixtures.

Small angle X-ray Scattering

X-rays have a much shorter wavelength than neutrons derived from a cold source, however X-ray detectors have a spatial resolution an order of magnitude better than neutron detectors. In theory then it should be possible to study an identical Q range to that of SANS. In practice it is difficult to overcome the problem of

parasitic scattering close to the main beam. Although this parastic scattering can be removed in the data treatment there is always some uncertainty about scattering data taken at such low Q vectors.

In small angle X-ray scattering the contrast arises from the electron density, the number of electrons in a given volume. Each electron has a scattering length of 0.95×10^{-12} cm so the electron density (ρ) can be calculated using the following expression:

$$\rho = \frac{\Sigma b_i}{V}$$

where bi is the scattering length and V the volume. The contrast is then given by :

$$\bar{\rho} = \bar{\rho}_A - \bar{\rho}_B$$

where ρ_A and ρ_B are the electron density of components A and B respectively.

Most organic molecules have a very similar electron density unless they have an electron dense atom present, such as sulphur,

chlorine or bromine. Such atoms are frequently used in SAXS experiments however unlike deuterium labelling in SANS experiments these atoms have an appreciable absorption. Assuming the Lambert Beer law applies the scattered intensity would be proportional to the thickness of the sample, however absorption by the sample increases exponentially with sample thickness.
Therefore to get optimum results it is important to use a suitable sample thickness.

The linear absorption coefficient μ is given by

$$\mu = \left[\sum_{n=1}^{i} \left(\frac{\mu}{\rho} P_i \right) \right] \bar{\rho}$$

where μ/P is the mass absorption coefficient of the ith element

$\bar{\rho}$ is the mean density of the entire sample

ρi is the mass fraction of the ith element

The optimum sample thickness is then calculated by

$$Topt = 1/\mu.$$

CHAPTER 6

Previous Experimental Studies of Spinodal Decomposition

INTRODUCTION

Spinodal decomposition has been studied in a wide range of materials, including; alloys,[71,79,80] glasses,[81-83] gels,[84] mixtures of oligomers,[85,86] small molecules,[91-93] polymers with solvent,[87] and polymers.[88-96]

Despite these extensive studies the spinodal decomposition mechanism of Cahn has never been conclusively demonstrated. Experiments on phase separation are fraught with experimental difficulties, some of these are discussed below, because they dictate the type of experiment carried out and limit our understanding of the processes involved.

The spinodal decomposition theory assumes an homogenous state prior to phase separation, that is difficult to obtain experimentally, particularly for glasses, ceramics, alloys and to a lesser extent polymer mixtures.

In nearly all phase separating systems and particularly small molecules the mobility of the components is so high that the phase separation process occurs very rapidily. In nearly all cases only the late stages can be observed. To overcome this problem two types of experiments

have been performed.

The first type has involved looking at very shallow quenches into the spinodal in order to minimise the $\delta^2G/\delta\phi^2$ term driving the phase separation. Typically ΔT is the order of 10mK. This approach has been most widely used with mixtures of small molecules. Experimentally shallow quenches result in a poor contrast difference between the two phases, because the final concentrations defined by the coexistence curve are very close. The data analysis is complicated by Debye [94] critical scattering that occurs close to the spinodal. The second approach has been used mostly with metallic alloys and glasses and involves performing deep quenches into the two phase region. This method relies on a marked reduction of the mobility of the components with temperature. Attempts have often been made to utilise experimental systems where the phase boundary lies close to some restriction in the mobility e.g., a glass transition or melting point in order to ensure a low mobility for a deep quench. The major disadvantage of such an approach is the mean field approximation on which the spinodal decomposition theory is based will be even less valid. Secondly it becomes difficult to establish phase boundaries accurately near to a restriction in the mobility of the mixture.

The study of solid systems such as metals, glasses and ceramics are complicated by the lack of coherency and strain effects.

Many systems are crystalline initially invalidating the homogeneity criterion or crystallise as the phase separation proceeds complicating the data analysis.

Most metallic alloys, glasses and ceramics have phase boundaries at elevated temperatures making real time experiments difficult, if not impossible. Nearly all studies on such systems have been carried out using quenched samples and it is never certain that no additional separation occurs during the quench. Metallic alloys, and glasses and ceramics require very thin samples for SAXS studies that are difficult to prepare.

Most systems apart from polymer and oligomer mixtures have initial correlation lengths (a few degrees away from the spinodal) that are only accesable by SANS or SAXS and these techniques are not widely available.

Alloys

The spinodal decomposition theory was originally developed for metallic alloys, despite this comparatively few detailed studies have been undertaken. There has been a tendency to ascribe all periodic interconnected structures to spinodal decomposition even though such a morphology can arise by a nucleation and growth mechanism. Spinodal decomposition has been reviewed in alloys recently.[95, 96] Only kinetic studies will be considered here.

Aluminium Zinc Alloy

The first study was carried out with an aluminium/zinc alloy by Rundman and Hilliard[74,79] and this system has been extensively studied. Rundman and Hilliard utilized SAXS to study the phase separation. They noted that it was unnecessary to transform the SAXS pattern into real space. Samples were quenched from 400^{0}C in the solid state to 65^{0}C. They found an initial decrease in the scattered intensity at high Q values, but later LnI(Q) against time plots were linear and Qm remained fixed during this time period.

Gerold and Merz,[97] however, claimed that the reduction in scattered intensity initially was due to partial phase separation occuring at 400^{0}C prior to Rundman and Hilliards experiments at 65^{0}C and that the C/H theory was, therefore, not valid. They suggested that the increase in scattered intensity was due to domain growth.

Agarwal and Herman[80] repeated Rundman and Hilliards experiments, but quenched from the melt state to avoid creating structure in the samples prior to annealing at 65^{0}C. They again used SAXS and their data confirms Rundman and Hilliards conclusions. They additionally show the cut-off wavevector Qc to be fixed and no crossover to occur at all. The time invariant Qc result agrees with the C/H prediction. They

plot R(Q) against Q^2 and show marked curvature as opposed to the linearity predicted from C/H theory. Agarwal and Herman studied the morphology of the spinodally decomposed alloy using transmission electron microscopy and demonstrated an interconnected diffuse edged structure.

Junqua et al [98] claimed that a scattering maximum found in studies of spinodal decomposition in the Al/Zn alloy could be taken as evidence of a change in mechanism from nucleation and growth to spinodal decomposition. However, a more vigorous analysis of this system by Laslaz et al [99] using SANS with its lower Q range has demonstrated that a scattering maximum at low Q can occur by a nucleation and growth mechanism. This study has shown that only where a scattering maximum is present at the earliest stages of phase separation can it be claimed as evidence of spinodal decomposition. They demonstrate that there is no sudden change in mechanism at the spinodal and that the spinodal decomposition theory does not apply for shallow quenches. In a later study using transmission electron microscopy Laslaz et al[100] observe an interconnected diffuse edged morphology for deep quenches typical of spinodal decomposition. Because they find an ill defined spinodal they favour the cluster theory approach of Binder.

Cartraud et al[101] have studied deep quenches and demonstrated the

Cahn-Hilliard theory to be valid for very early times using SAXS and mechanical hardening measurements.

Glasses

Many workers claim evidence of spinodal decomposition in glasses from the observation of an interconnected morphology. Only two kinetic studies of the spinodal decomposition process have been undertaken in glasses. The first in Soda-Silica glasses and the second in Lead-borate glasses.

Soda-Silica Glasses

Nielsen[91] looked at spinodal decomposition in two compositions of soda-silica glass close to the critical composition. This SAXS study is complicated by the fact that the glasses are quenched to room temperature from the melt state (before thermal ageing in the spinodal) and undergo considerable partial phase separation. Nielsen estimates that the one composition is 35% phase separated and the other 60% phase separated. For this reason the application of C/H theory to the analysis of the data is suspect.

Nucleation and growth is initially observed to occur. The SAXS data

initially fits a Guinier plot and discrete dispersed particles are observed in the transmission electron microscope. Later the scattered intensity grows exponentially and an interconnected morphology is observed. For the more phase separated composition a plot of Qc^2 against temperature is linear and extrapolates to the spinodal. The 35% phase separated sample undergoes more nucleation and growth and the data does not fit C/H theory so well as the 60% phase separated sample.

Lead Borate Glasses

Srinivisan et al[92] investigated spinodal decomposition using SAXS in the B_2O_3-PbO-Al_2O_3 system. They demonstrate theoretically that the theories of Cahn and Cook do not lead to the occurence of a crossover point in SAXS curves during the early stages of the decomposition in a conventional down quenching experiment. The occurence of observed crossovers during the eary stages in up quench experiments is taken to indicate phase separation prior to the spinodal ageing treatment.

Liquid-Liquid Systems

Two small molecule liquid systems have been studied. These are

Isobutynic acid/water and Lutidine/Water. Most studies have been restricted to critical mixtures using very shallow quenches ($\Delta T \simeq 10mK$) and following the resultant phase separation by SALS. Data analysis is complicated by Debye critical scattering.[94] Because of the high mobilty of these mixtures it is impossible to follow the early stages and C/H theory does not apply. This has stimulated the development of completely new theories.

In general power law expressions have been used to describe the results, for example

$$Im \propto t^{\theta}$$

$$Qm \propto t^{\phi}$$

where Im is the maximum in the scattered intensity and Qm is the wavevector maximum. θ and ϕ are exponents having a range of values.

Wong and Knobler [92] have made extensive studies on isobutynic acid/water mixtures. They found the θ and ϕ exponents to be dependent on the quench depth for critical mixtures, but the exponents were independent of quench depth for off critical mixtures.

Goldburg et al [91], [93] have carried out studies on the Lutidine/water system

and demonstrated that Im and Qm for different ΔT. plotted against a scaled separation time τ yielded a single composite curve that was in qualitative agreement with the LBM theory and the cluster theory of Binder. The rate of increase in Im and the decrease in Qm were, however, more rapid than both theories predict. Goldburg et al suggest that long range hydrodynamic interactions as proposed by Kawasaki and Ohta[53] were also important.

Polymer Solvents

Smolders and van Aartsen[97] looked at phase separation in poly(phenylene oxide)/caprolactam mixtures. They showed the early stages to be described by C/H theory since the scattered intensity grew exponentially. However, they calculate Qc from the scattering maximum (assuming $Qm = \sqrt{2}\ Qc$) and then plot Qc^2 against temperature. The error in the determination of Qc is large, but the plot extrapolates back to 180^0C whilst it is known that the spinodal is at 130^0C clearly in disagreement with the theory. They claim this arises from a temperature dependence of the range of molecular forces (1) and do not consider the alternative expplanations; that the thermodynamics of this system are not modelled by Flory Huggins theory or that K in equation 6 is dependent on the temperature.

Oligomers

The dynamics of phase separation have only been studued in two oligomer mixtures: polystyrene/poly(methylphenylsiloxane) (PS/PMPS) and poly(styrene)/polybutadiene. (PS/PB).

Polystyrene/Poly(methylphenylsiloxane)

A series of papers have been published on this system.[85,102,103] The polystyrene component has an $\bar{M}w$ of 9000 and $\bar{M}w/\bar{M}n$ of 1.09. It is therefore not strictly speaking an ologomer. The PMPS has an $\bar{M}w$ of 2,800 and $\bar{M}w/\bar{M}n$ of 1,57. As this system exhibits an upper critical solution temperature (UCST) phase behaviour typical of oligomers, it will be considered as an oligomer mixture.

Most UCST systems are extremely sensitive to molecular weight so the polydispersity of the PMPS may well result in the system not having a sharp spinodal locus. Since there is no data on the molecular weight dependance of the phase boundary this effect can not be assessed.

Experiments were performed by temperature jumping into the spinodal. Typical jumps took approximately one minute and were up to 10^0C. The scattered light from the sample was followed as a function of time

using a scanning diode that took approximately two minutes to scan the resulting scattering pattern. The poor temperature jumps and the slow detection system effectively means that the early stages of the phase separation are lost, though this important point is not appreciated by the authors. The correlation length is never time invariant or even approximately so and the intensity grows non exponentially. Power law expressions are used to describe the growth of the intensity (I) and Qm in an identical fashion to Goldburg,[38] where the exponents Θ and ϕ for Qm and I have a range of values. Like small molecule liquid mixtures the exponents are approximately 3x larger for the critical mixture. Because at no stage does Qm remain fixed or I(Q) grow exponentially the authors favour the theories of Binder and Langer. They scale their data in an identical fashion to Goldburg and show that the rescaled data superimposes with that for small molecule liquids. They conclude that phase separation in polymers is essentially identical to small molecule mixtures, despite the fact that the distinctive features of polymers, namely the long entangled nature is not present in their samples. Furthermore, the modified theories of spinodal decomposition proposed by the theoreticians are based on an entangled-reptation model, for polymer translational diffusion.

Polystyrene/Polybutadiene

Russel et al[86] investigated phase separation in PS/PB oligomers. Unlike the previous authors they performed sharp temperature jumps and had a fast detection system. On theoretical grounds it would be expected that PS/PB oligomers of the molecular weight used in this study would phase separate in the SAXS Q range, so these authors used SAXS. Unfortunately, Qm was too small to follow by SAXS and the analysis was limited to the high Q end of the scattering pattern, corresponding to very short wavelengths. They show an exponential growth in I(Q) and calculate the Cahn-Hilliard diffusion coefficient to be 10^{-13} cm^2s^{-1}. This value is much lower than the diffusion coefficients for polystyrene published recently[34] indicating that early stages of spinodal decomposition are not being followed as claimed by these authors.

They also note an increase in Qc with increasing quench depth into the spinodal. By plotting Qc^2 against temperature and extrapolating Qc^2 to zero they obtain the spinodal temperature. This analysis is incorrect if thermal fluctuations are included, Park et al have shown that it is Qm that changes with temperature whilst Qc remains fixed when the phase separation is driven by the effect of temperature on the entropy.

Polymer-Polymer Mixtures

An extensive study of the dynamics of the demixing process in polystyrene/poly(vinylmethylether) (PS/PVME) blends has been undertaken by a number of workers. Only two other polymer blends have been studied; these are polystyrene/poly(o-chlorostyrene) and poly(methylmethacrylate)/Styrene acrylonitrile copolymer.

Polystyrene/Poly(vinylmethylether)

Nishii et al[99] carried out the first study of the dynamics of phase separation in PS/PVME blends. They used a combination of techniques including, optical microscopy, turbidity measurements and nuclear magnetic resonance spectroscopy. They used turbidity measurements to determine the phase diagram. Microscopy was used to determine the crude position of the spinodal, observation of an interconnected morphology providing evidence of being within the spinodal and a dispersed phase structure as being within the meta-stable region. Unlike most studies of spinodal decomposition Nishii et al utilized the following difference between spinodal decomposition and nucleation and growth. During spinodal decomposition the concentration of the two polymers will change continuously from the original concentration to the concentrations defined by the coexistence curve, whilst during

nucleation and growth only compositions corresponding to that at the coexistence curve and that of the original mixture will exist. Using nuclear magnetic resonance T_1 spin relaxation measurements Nishi et al demonstrated that the environment of the two polymers changes continuously within the spinodal thus providing evidence for spinodal decomposition.

Gelles and Curtis[104] have similarily monitored the concentrations of the two polymers during phase separation using an excimer fluorescence technique. They show that the concentration difference between the two phases changes rapidly during short times and changes more slowly over longer times. They approximate the plot of the short time data to a straight line and assume Dm to be about lum in order to obtain a rough estimate of the Cahn-Hilliard diffusion coefficient.

Gelles and Curtis[105] have also investigated the effect of molecular weight of the PS component on the rate of phase separation. This paper is full of assumptions concerning the data analysis including an assumption that they are following spinodal decomposition. They estimate R(Qm) for two PS/PVME blends containing two monodisperse polystyrenes of $\bar{M}w$ = 100,000 and $\bar{M}w$ = 1,800,000. Both the polystyrene molecular weights are above the entanglement value. The molecular weight of the PVME component remains unchanged, is very polydisperse

and a proportion of it will be below the entanglement value. The cloudpoint curve for both systems is determined visually at a 5^0C min^{-1} heating rate and they assume this corresponds to the binodal. This is unlikely at such fast heating rates particularly for the high molecular weight polystyrene blend. A scaling analysis based on a reptation concept derived by Pincus to predict the Cahn-Hilliard growth rate is used to compare their data on the two different molecular weights. The growth rate dependence on molecular weight is much less than predicted by Pincus at approximately identical quench depths and temperature and they suggest this is due to the low molecular weight unentangled component in the polydisperse PVME strongly affecting the kinetics of the early stages. Because of the very many questionable assumptions in this paper little information of any significance is obtained.

Hashimoto et al[106] have studied phase separation in PS/PVME blends by SALS using a He/Ne laser light source. A high molecular weight monodisperse PS and a polydisperse PVME were used. Experiments were carried out at room temperature after annealing samples inside the spinodal for a given time.

No scattering maximum is observed during the time period that the scattered intensity grows exponentially i contradiction to C/H theory. It is claimed this is a result of the low diffusion coefficient of this system. Snyder[107] however believes that the absence of a scattering maximum results, from total internal reflection of the scattered light from the sample washing out the maximum. He claims to avoid this problem by utilizing a shorter wavelength He/Cd laser light source.

A close examination of Hashimoto et al's data shows them to be utilizing very shallow quenches and for their data to show intense scattering at small angles. This suggests that significant nucleation and growth is occuring and possibly dominating the phase separation process initially. It is likely that all three reasons contribute towards the non observation of a scattering maximum during the early stages. Because they do not observe a maximum in the early stages, it can not be demonstrated that Qm is time invariant. Indeed when a scattering maximum does appear in their data it is at very large Q suggesting the further possiblity that a scattering maximum was not observed because it was at too a high a Q. It seems very likely that Hashimoto et al fortuitously obtained apparent exponential growth. They go on to calculate Cahn-Hilliard diffusion coefficients, $\bar{D}$ using a fixed Q_m at three temperatures

close to the spinodal and linearly extrapolate the plot of $\bar{D}$ to the spinodal temperature claiming that Qm will not vary close to the spinodal clearly according to equation 10 Qm should go rapidly to zero at the spinodal.

Snyder et al [8,9,10,103] have published a series of papers on phase separation in PS/PVME. A polydisperse PS was used ($Mw = 6.0 \times 10^4$ $Mn = 1.5 \times 10^4$) some of which will be below the entanglement molecular weight (Ne) and a PVME $\bar{M}w = 4.6 \times 10^4$ $\bar{M}n = 2.1 \times 10^4$

The first paper[103] of the series measures the total integrated scattered intensity for three compositions over a 20^0C range as a function of time. It is demonstrated that initially the total integrated intensity grows exponentially. The wave vector maximum is measured during the early stages and using this value they calculate the Cahn-Hilliard diffusion coefficient ($\bar{D}$). These values plotted against temperature linearly extrapolate to the spinodal. However, their data is inconsistent with the C/H/Flory-Huggins model when examined closely, since to be completely consistent Qm^2 should also extrapolate to zero linearly as a function of temperature and it clearly does not. The plot of $\bar{D}$ against temperature must therefore be apparently linear because the absence of an increase in Qm is compensated for by an increase in the diffusional

mobility as the temperature is raised.

In a second[98] and third paper[90] Snyder et al investigate the critical composition at fixed temperature (150^{0}C) looking at the full angular scattering pattern as a function of time. They show the scattered intensity at the wave vector maximum to grow exponentially, whilst its position remains approximately time invariant. At later times the scattering peak becomes sharper and the maximum moves to lower Q vectors. During no time period does the maximum obey a power law expression consistent with Ostwald ripening or coalescence mechanisms.

A plot of the $R(Q)/Q^2$ against Q^2 is not linear as predicted by C/H theory but exhibits significant curvature. They conclude that phase separation of PS/PVME blends is broadly in agreement with C/H theory.

In a final paper Snyder et al[39] compare their data with data on glasses and alloys as well as small molecules using Goldburgs reduced unit scaling approach. They conclude that phase separation in polymers is very similar to these systems.

Polystyrene Poly(-o-Chlorostyrene)

Stein et al[109] studied this blend by SALS. Samples were prepared by coprecipitation and pressing. Both component polymers had molecular weights greater than the entanglement value (Ne). At no stage was the correlation length time independent.

Observation of the total integrated scattered intensity was used to demonstrate whether new phases were being created. Initially, the total integrated intensity increased slightly demonstrating the creation of new phase, however Ln(I) against time plots were non linear. Over most of the experimental time period the integrated intensity remained constant indicating that the late stages of domain growth were being observed. It is suggested that the domain growth occurs according to McMasters viscous flow model and that minimal break-up of the interconnected spinodal structure occurs. Recently, SANS studies have demonstrated this system to be inhomogenous prior to phase separation.[110]

Poly(methyl-methacrylate) Styrene-acrylonitrile Copolymer

McMaster[69] studied phase separation in this polymer mixture using transmision electron microscopy. There is no natural contrast

between the component polymers, however, McMaster observes the development of phase structure with time in the electron beam. He suggests that this is due to reaction of the styrene-acrylonitrile phase with vacuum oil in the microscope. This is almost certainly not the case and instead it is the etching away of the poly(methylmethacrylate) component by the electron beam that gives the contrast. McMaster cites the observation of an interconnected morphology as evidence of spinodal decomposition. He observes the coarsening of the interconnected structure and claims it only breaks down to a dispersed phase structure when the wavelength is approximately the thickness of the specimen. He proposes a novel viscous flow mechanism of coarsening to explain his observed results.

C H A P T E R 7

MATERIALS

Choice of Systems for Study

An ideal blend system for studying the kinetics of phase separation does not exist. Such an ideal mixture of polymers would possess the following properties.

(1) The thermodynamics of its miscibility would be well characterised.

(2) It would form completely homogeneous mixtures, by at least one, and preferably two, methods of preparation.

(3) The phase boundary should be at an easily accessible temperature.

(4) Both component polymers should be available in a range of monodisperse molecular weights.

(5) The phase separation process would be suitable for following by small angle light scattering, small angle neutron scattering and small angle X-ray scattering; therefore there would have to be suitable differences in the refractive index, neutron scattering cross-section and electron density of the two polymers.

The first system chosen was an oligomer system of polybutadiene and polystyrene having an upper critical solution temperature. This system's thermodynamics of miscibility have been studied and mixtures are miscible primarily due to the large combinatorial entropy associated

with the oligomers. The spinodal can be measured directly by pulse-induced critical scattering, and an attempt is presently being made to measure the thermodynamic interaction parameter as a function of temperature.

The second system chosen for study was ethylene-vinyl-acetate copolymer with chlorinated polyethylene. The thermodynamics of this system have been studied in detail at Imperial College.[114] This mixture is particularly suited for study by small angle scattering techniques because the chlorine present provides a large refractive index, neutron scattering cross-sections and electron density difference. It is also closely related to poly(vinylchloride)/ethylene-vinyl-acetate blends used commercially. The major disadvantage is that both the chlorinated polyethylene and the ethylene-vinyl-acetate copolymer have a broad molecular weight distribution.

The third system to be studied was poly(methyl-methacrylate) with chlorinated polyethylene. This blend was studied because a preliminary investigation showed that the phase separation occurred on a much smaller scale than that normally found. A second reason for studying this blend is that the thermodynamic interaction parameter is presently being studied[115] as a function of temperature.

Thermodynamics of Miscibility of the Systems Studied

Thermodynamics of polymer miscibility has already been briefly reviewed in Chapter 2. The section below gives detailed information on the thermodynamics of the polymer mixtures studied.

Polystyrene (PS)/Polybutadiene (PB) Oligomers

This system is an example of category 1. The entropy of mixing is comparitively large; as a result, phase boundaries are upper critical solution temperature and highly dependent on the molecular weight of the two components[116]. The heat of mixing of these oligomers has been measured and is unfavourable for mixing[117]. Deuterating either component shifts the phase boundary upwards to high temperatures, broadens the spinodal curve around the critical point and reduces the metastable gap[118]. It is surprising that deuteration should affect such phase boundaries, deuterium being indistinguishable chemically from hydrogen. Deuteration is known to shift the crystallisation temperature of poly(ethylene)[119] and the phase boundary of poly(styrene) in cyclohexane[120]. Recently Stein et al.[121] have demonstrated the LCST of high molecular weight mixtures of polystyrene/poly(vinylmethylether) to move up to 40°C upwards, on deuterating the polystyrene component. These effects exist where there is a delicate balance in the free energy. They are attributable to the changed vibrational amplitude and specific volume caused by deuteration[122].

Poly(methylmethacrylate) (PMMA) and Ethylene-Vinyl-Acetate Copolymer (EVA) with Solution Chlorinated Poly(ethylene) (SCPE)

These two blends are examples of category 3 and have a strong specific interaction. Both blends have a negative enthalpy of mixing[123,124] which is believed to result from a weak hydrogen bond (Fig. 9) between the hydrogen adjacent to the Cl in the SCPE and the oxygen of the carbonyl group in either the PMMA or the EVA. The phase boundaries of both systems have been modelled using the Flory equation of state approach[125,126] and it has been shown that a negative non-combinatorial entropy (Q_{12}) unfavourable for mixing is required in order to get phase separation in these blends. However, this analysis assumes that heat of mixing data is independent of temperature and that the enthalpy of mixing obtained experimentally for oligomers is directly transferable to high polymers.

It has been shown that the PMMA/SCPE phase boundary is only dependent on the molecular weight below $\overline{M}_w \simeq 5 \times 10^4$ [125] and that the phase boundary is not very sensitive to deuterating the PMMA component[127]. Neutron scattering studies have demonstrated the radius of gyration of the PMMA to be consistent with a single coil[128], providing strong evidence that this blend is a homogeneous mixture on a molecular level. The phase boundary moves to high temperatures as the percentage chlorination of the SCPE is increased, until at 62% the system is completely miscible[129], no phase boundary being detected below the thermal decomposition temperature of the SCPE.

Heats of mixing studies using oligomeric PMMA with chlorinated octadecane show a more favourable enthalpy of mixing as the degree of chlorination of the octadecane is increased[130]. The enthalpy of mixing is only negative for degrees of chlorination greater than 45 ± 4% and PMMA is only miscible with SCPE with degrees of chlorination greater than 48 ± 4%. The heat of mixing of the analogues does not exhibit any appreciable temperature dependence up to 90°C. These results strongly support the view proposed by Chai et al.[131] that the miscibility of PMMA/SCPE blends is determined primarily by the specific interaction present.

The heat of mixing of sec-octyl acetate and chlorinated paraffins, analogues of EVA and SCPE, are negative and again become more negative as the degree of chlorination is increased[132]. Unlike the PMMA/chlorinated octadecane system, the heat of mixing is markedly temperature dependent[133], becoming less negative with increasing temperature (Fig. 10). Phase boundaries of EVA/SCPE blends have been shown to be dependent on the vinyl-acetate content of the EVA and on the degree of chlorination of the SCPE[134]. The lower critical solution temperature rises as the concentration of the interacting groups is increased. Direct evidence of the specific interaction has been obtained from Fourier-Transform infra-red studies[135]. The carbonyl-stretching vibration of the EVA in the presence of the SCPE at room temperature is shifted several wavenumbers and broadened.

On raising the temperature to 130°C well into the two-phase region, the carbonyl peak shifts back to that corresponding to the pure EVA copolymer (Fig. 11).

Material Preparation and Characterisation

Commercial Chlorinated Polyethylenes

Chlorinated polyethylene, code number H48 was obtained from Dupont. Before use it was dissolved in tetrahydrofuran to give a 5% solution, then centrifuged to remove talc added by the manufacturer, reprecipitated in water, and finally vacuum-dried. The molecular weight distribution is given in Table 3 along with its elemental analysis.

Polyethylene is chlorinated commercially using a suspension technique[136]. As a result, the product is not evenly chlorinated. Polymer molecules at the centre of the suspended particle are not chlorinated at all, whilst polymer molecules at the surface are heavily chlorinated. The unchlorinated polyethylene retains its crystallinity and spherulites were observed between cross polars in light microscopy.

The presence of such large potential nuclei and the variation of the chlorination level were disadvantages of this material. Preliminary experiments indicated that these spherulites were initiating

nucleation and growth during spinodal decomposition. To eliminate the complexity of dealing with two potential phase separation mechanisms, solution chlorinated polyethylenes were prepared.

Solution Chlorinated Polyethylene (SCPE)

Solution chlorinated polyethylene is an analogue of the commercially important polymer poly(vinylchloride) (PVC). Unlike PVC the chlorine atoms are randomly distributed along the polymer backbone and this eliminates any crystallinity.

The method used for the preparation of solution chlorinated polyethylene has been previously described by Chai et al.[137]. High density straight chain polyethylene (20 g) is dissolved in chlorobenzene at 130°C to give a 20% by weight solution. Dried chlorine gas is bubbled through the solution at 35 ml min^{-1} to give the required degree of chlorination.

The reaction is a free radical chlorination and the mechanism is probably:

$$Cl_2 \xrightarrow[H_v]{\text{Heat}} 2Cl^{\cdot}$$

$$Cl^{\cdot} + RH \rightarrow RCl + H^{\cdot}$$

$$H^{\cdot} + Cl^{\cdot} \rightarrow HCl$$

The required chlorination time was calculated assuming a 50% reaction efficiency. The chlorination was then stopped and the SCPE precipitated in a ten times excess of ice-cold methanol. The precipitated SCPE was allowed to stand in methanol overnight and then vacuum-dried.

The level of chlorination could be estimated approximately by the weight increase of the reaction flask and its contents prior to precipitation of the SCPE. An accurate measurement of the degree of chlorination was obtained by elemental analysis for hydrogen and carbon and assuming the balance to be chlorine.

The chlorination has been shown by Chai et al.[138] to be random along the polymer backbone, providing the amount of chlorine present is above 50% by weight. Below this level of chlorination, segments of unchlorinated CH_2 groups exist.

The percentage chlorination has a marked effect on the glass transition temperature of the SCPE, particularly at high percentages. Glass transitions (T_gs) are associated with the segmental motion of the polymer backbone; increasing the chlorine content will have little effect at low degrees of chlorination where the chance of a chlorine on two adjacent carbon atoms is small. However, at high degrees of chlorination this possibility will exist and adjacent

chlorines will severely restrict the rotation of the polymer backbone. A plot of T_g against weight percent chlorine content is shown in Fig. 12.

The original polyethylene is very polydisperse so the SCPE made from it is also polydisperse. A number of SCPEs were fractionated to eliminate the potential complication of having a wide range of diffusion coefficients present. The theory of polymer fractionation has been reviewed by Koningsveldt[139]. A combination of adding non-solvent to a dilute solution of the polymer and cooling were used. The SCPE was dissolved in benzene to form a 2% solution by weight. Isopropanol was then added until the solution became turbid. The flask was then warmed to 40°C to redissolve the precipitate formed and then cooled slowly back to room temperature. The precipitate was allowed to settle, then the benzene and isopropanol decanted off. The precipitate was redissolved in chlorobenzene and reprecipitated in methanol. The process was repeated to give successive fractions. Later fractions were cooled to 4°C to help reduce the amount of non-solvent required and to speed up the settling of the precipitate.

The molecular weight details of the polydisperse unfractionated and fractionated SCPEs are listed in Table 3.

Ethylene Vinylacetate Copolymer

Two samples were obtained from ICI called Evatone 40 and Evatone 45, with specified vinylacetate contents of 40% and 45% by weight respectively. This was confirmed by elemental analysis. Fractionation was carried out with the Evatone 45 in an identical manner to that for SCPE.

It was suspected that the EVAs might contain some block copolymer and therefore possess crystalline polyethylene phases. Such crystalline regions could have a pronounced effect on the phase separation mechanism acting, for example, as nucleating particles. Polyethylene crystals would be more dense than the surrounding polymer and therefore have a different refractive index and electron density. Both pure materials gave no significant scattering by SAXS or SALS and therefore can be regarded as totally amorphous materials. They are probably genuine random copolymers containing no block copolymer.

Polyvinylacetate[140] is known to be highly branched. It is therefore very likely that the ethylene vinylacetate copolymer is branched to some extent.

Poly(methylmethacrylate)s (PMMA)

Hydrogenous and deuterated poly(methylmethacrylate)s were used. All were prepared by free radical polymerisations and thus the poly-(methylmethacrylates) will all have essentially atactic stereo-chemistry. PMMA was bought from Polysciences and is a suspension polymerised material.

PMMA (D) was a laboratory synthesised material prepared from fully deuterated methylmethacrylate monomer and subsequently molecular weight fractionated using acetone/methanol mixtures. The sample used was the fourth fraction.

Polystyrene Oligomers

These samples were obtained from Polymer Laboratories and were made by an anionic polymerisation.

Polybutadiene Oligomers

Samples of polybutadiene oligomers PB 960 and PB 2660 were purchased from Goodyear Chemical Company. PB (D) was a fully deuterated material specially prepared by L. Fetters[141]. The microstructure of the samples as given by the manufacturers are listed in Table 7a, and their molecular weight details in Table 7b.

The molecular weight details and glass transition temperatures can be found in Tables 3 - 7 for all the polymers studied.

Sample Coding

Solution chlorinated polyethylenes are coded according to the degree of chlorination, the first two digits defining the degree of chlorination and the next digit the fraction number. For example, $SCPE^{50/5}$ would be the 5th molecular weight fraction of solution chlorinated polyethylene with 50 weight percent chlorine.

An identical procedure is used for coding EVA samples except now the first two digits define the vinylacetate content.

A 'D' in brackets after the sample indicates the sample is a fully deuterated material.

Blend Preparation

There are four potential methods of preparing polymer blends:

(1) Mechanical mixing in the melt.

(2) Coprecipitation from a common solvent followed by hot pressing.

(3) In-situ polymerisation of one polymer in the presence of another.

(4) Solvent casting from a common solvent.

Mechanical mixing was not considered a practical proposition for preparing blends for phase separation studies of high polymers,

because the very low diffusion coefficients of polymers would lead to very long times being required to ensure a homogeneous blend. The high shear mixers that are conventionally used to overcome the problem of low diffusion coefficients are not suitable for small sample volumes. Mechanical mixing, however, was used for preparing oligomers of polystyrene and polybutadiene.

Coprecipitation followed by hot pressing was found not to be a satisfactory method for preparing homogeneous blends as phase separation occurred during the coprecipitation step.

In-situ polymerisation was not investigated, though it does offer a potentially very easy way of forming homogeneous blends. The second polymerisation frequently results in the formation of block/graft copolymer and it is not very easy to control the molecular weight of the second polymer.

Solvent casting from a common solvent was widely used, though frequently partial phase separation occurred during the casting technique. This technique of making blends is often highly dependent on the choice of solvent. Care has to be taken to ensure that all of the solvent is removed and this restricts the thickness of polymer film that can be satisfactorily cast. However, this is not a problem for preparing blends for small angle scattering techniques, since thin films are required to ensure no multiple scattering occurs.

Preparation of Samples

Polystyrene/polybutadiene oligomer mixtures were prepared for SALS just prior to use by mixing preweighed amounts of PS and PB in stoppered tubes containing a magnetic stirrer at 120°C. This process took about 3 minutes to achieve a homogeneous mixture. Crude sample cells were formed by taking a drop of the homogeneous mixture and sandwiching it between two coverslips to give an even film 20-50 μm thick containing no air bubbles.

SANS samples were prepared by mixing the oligomers under vacuum in quartz cells to remove trapped air bubbles at 120°C. They were then vacuum-sealed.

Blends of SCPE with EVA and SCPE with PMMA were prepared by solvent casting. Dried Analar methylethylketone and Analar chlorobenzene were used as the common solvents for EVA/SCPE and PMMA/SCPE respectively. A 5% solution of the two polymers (in the desired proportions) in the appropriate solvent was made. This solution was then spun using MSE (25) centrifuge at 10,000 rpm to remove any foreign particles and dust. Samples for use with the Turbidimeter and for SANS and SAXS studies were prepared by pouring enough of the centrifuged polymer blend solution into a petridish to give a final film thickness of 0.2 mm after evaporation of the solvent. Petridishes excluded dust and gave a slow rate of evaporation of the

solvent. Samples for SALS studies were prepared by placing several drops of polymer blend solution onto clean 19 mm diameter coverslips contained in a petridish. The drops were dispersed over the surface of the coverslip to give an even film thickness. Typical final film thicknesses were 10 - 50 μm.

CHAPTER 8

DESIGN OF A SMALL ANGLE LIGHT SCATTERING INSTRUMENT

Introduction

Preliminary studies were carried out to define the requirements of a small angle light scattering instrument for carrying out phase separation experiments on polymer blends. A decision was taken to do real time experiments, because this enables rapid data acquisition with the minimisation of errors due to variation in thickness between samples and quenching. Real time experiments also enable more results to be obtained from a limited amount of material; this is an important consideration when molecular weight fractionation has been carried out.

Design Requirements

The temperature jump

It is important to be able to jump from the one-phase region of the phase diagram into the two-phase region as rapidly as possible. The simplest way this can be achieved is by means of a temperature jump. A survey of the literature and some preliminary experiments found that the majority of phase boundaries for partially compatible blends were between room temperature and 200^{o}C. Studies using a simple experimental apparatus consisting of a heated block, a helium/cadmium laser, a photomultiplier tube and a chart recorder, were

carried out on poly(ethylene oxide)/poly(ethersulphone) (PEO/PES) and ethylene vinylacetate copolymer/solution chlorinated poly(ethylene) blends (EVA/SCPE). A significant increase in the scattered intensity was found to occur in about 300 s for the EVA/SCPE blend and in less than 1 s for a PEO/PES blend only $1^{o}C$ inside the phase boundary. Plots of ln I against time had significantly different slopes at two temperatures only $3^{o}C$ apart with the EVA/SCPE blend. On these preliminary results the following requirements were decided upon.

(1) A temperature range from room temperature to $250^{o}C$.

(2) A temperature jump time of less than 5 s.

(3) The ability to maintain a preset temperature to within $0.5^{o}C$ over several hours.

(4) The temperature should be automatically monitored.

(5) The apparatus should be suitable for doing temperature scans to enable phase boundaries to be determined.

The Detection System

Preliminary experiments were carried out using strips of photographic film and a camera shutter to provide estimates of the angular range and resolution required of the detection system. Scattering maxima were found initially at about 30^{o} for an EVA/SCPE blend

and the maxima moved to small angles over several hours until at about 3^{o} it became impossible to resolve from the laser beam. The light intensity of the angular maximum was measured early on during the phase separation and found to be 6 μW cm^{-2} 30 cm from the sample.

The specification below was agreed upon on the basis of these studies and the previous studies.

(1) Angular resolution about 2^{o}.

(2) Angular range 50^{o}.

(3) Sensitivity at least 6 μW cm^{-2} at 420 nm.

(4) A response time for measuring the intensity over the angular range of less than 0.25 s.

(5) The detection system should preferably enable scattering patterns to be viewed visually during an experiment.

Light source

The light source should ideally be monochromatic, collimated and preferably of variable wavelength. Its output should be constant over the longest experimental time, i.e. at least 8 hours.

Description of the Instrument

The instrument designed around these specific requirements is illustrated schematically in Fig. 13. The apparatus consists of a horizontally-mounted, 5 mW vertically-polarised laser. Two choices of laser are available, a He/Ne Aerotech model 1105P (λ = 633 nm) or a He/Cd Liconix model 4110 (λ = 420 nm). This enables the wavelength of the light source to be varied, enabling a useful check on the validity of scattering patterns. Both lasers have advantages and disadvantages. The He/Ne laser has the advantage of shifting scattering maximum to larger angles; this is particularly useful for large correlation lengths that become difficult to resolve from the laser beam. The He/Cd laser is useful for short correlation lengths where the angle of scattering with the He/Ne laser becomes so large that a total internal reflection condition can be set up.

For convenience of loading samples into the apparatus, the optical axis is vertical. This is achieved by a 1" prism mounted on a sprung adjustable base that bends the laser beam through a right angle. Three screws passing through the prism base allow the prism to be tilted a few degrees in two directions, enabling the easy alignment of the laser beam with the collimating holes and sample holder (see Fig. 14). For convenience, for safety and to try and

avoid spurious scattering from dust particles, the apparatus is enclosed in a light-proof box. The laser beam passes up through the collimating holes, and enters the sample block via a 5 mm diameter hole on its underside. The sample block is illustrated in Fig. 15. The laser beam passes through the sample holder which consists of a thin brass plate with a 19.5 mm diameter, 0.5 mm deep indentation on the upper surface and a 3 mm diameter hole at the centre of the indentation that allows the laser beam through. The samples are solution cast onto 19 mm coverslips that fit into the indentation in the sample holder. The sample holder slides in and out of the brass sample block facilitating the loading and unloading of samples. A large hole is cut in the upper surface of the block to enable light scattered at large angles to escape. Both exit and entry holes for the laser beam are glazed to maintain a uniform temperature inside the block. The surface of most of the brass sample block is covered by an insulating jacket to minimise heat losses. Two thermocouples pass through the insulating jacket and into the block. One senses the temperature for display and the other is connected to a temperature control unit. Four 18 W soldering iron heaters within the brass block can heat the block to 200°C. They are connected to the temperature control unit and can maintain a predetermined temperature to within ±0.5°C over 8 hours, or alternatively be used to raise the temperature of the block at a set rate.

The detection system consists of a laboratory-built diode array. The diodes used were obtained from Radio Spares, Part Number 308-067. They were chosen because they had a good sensitivity even to blue light, low noise, a linear response, a very short rise and fall time, as well as built-in amplifiers. Their properties are listed in Table 8. The array consists of a curved aluminium plate, 5 mm x 10 mm x 90 mm with a radius of 16 cm into which are mounted 16 diodes. Each diode is approximately 8.5 mm in diameter. They are arranged in two rows with a half stagger (Fig. 16). The array is mounted on a holder that slides in a groove, such that the diodes are set on a fixed radius 16 cm from the sample. This arrangement locates the diodes at 2^{o} intervals. The 16 diodes therefore span an arc of 32^{o}. The holder and groove are calibrated, so the diode array can be moved readily to alter the Q range of the instrument.

Two additional diodes are used. One is mounted directly behind the prism and measures the intensity of the laser beam prior to passing through the sample. A second diode measures the intensity at 0^{o} and is used to check that only a small percentage of the beam is being scattered by the sample. This ensures that multiple scattering events are not occurring. The diodes are connected to a multiplexer and a 12-bit A/D convertor that forms an interface with a BBC model B microcomputer. The connection of the interface to the computer is via the 1 MHz bus line.

The linearity of the response of the diodes was checked using a fixed light source. The voltage output of each diode was measured as a function of distance from the light source. The potential V was proportional to $1/(\text{distance})^2$ confirming that the output voltages of the diodes are proportional to the light intensity. The linearity of the A/D conversion was checked by inputting known voltages using a mV calibrator in place of the output from the diodes and checking the response via the microcomputer.

The intensity/voltage response of the diodes, although linear, were all slightly different, presumably due to slight variations in the gain of amplifier component. The intensity of light scattered from a drop of milk is constant over the angular range from 0 to 20^{o}. This fact was used to measure the relative responses of the diodes, the data then being used to normalise the output from the diodes automatically, using the microcomputer.

This operation was performed by first measuring the dark signal from each diode then with the diode array set at 0^{o} and a drop of milk in the laser beam, the output of each diode was measured. The dark response was subtracted from the milk response to give a set of normalisation values. The dark response and the normalisation values are stored on floppy disk for subsequent automatic normalisation of the collected data by the computer.

Computer Programmes

Three programmes were written, two for carrying out kinetic experiments and one for carrying out phase boundary determinations.

All three programmes ask for the experimental details; date, sample, composition, laser type, time interval between readings and the file name for storage on floppy disk. All the programmes automatically normalise the intensity of the diodes.

"Polymer" is a programme for carrying out kinetic experiments. It is written entirely in BBC Basic and it carries out the normalisation procedure, reads each diode in the array once between time intervals, displaying the data collected continuously and storing it on floppy disk for subsequent data analysis.

A second programme "Kmean" is identical to "Polymer" but contains a subroutine written in machine code for speed of operation that samples the diode array ten times and takes a mean for each time reading. This programme was written specifically for use with the He/Cd laser that has a high frequency noise.

The final programme "Cloud" was written for measuring phase boundaries. It is similar to "Polymer", but also displays the temperature, the time, and monitors the intensity of the incoming laser beam, and corrects the data from the diodes for any change that might occur.

Characteristics of the SALS Instrument

The stability of the output of both lasers, the helium/cadmium and the helium/neon, was measured by monitoring the response of the diodes with a drop of milk in the laser beam. The intensity in arbitrary units and the standard deviation of the mean over ten readings at 5 s intervals and ten readings at 100 s intervals are shown in Table 9. Typically the coefficient of variation is less than 1% for the helium/neon, and less than 6% for the helium/cadmium. These errors are for a fairly strongly scattering system and experimental errors, particularly during the early stages of phase separation where the scattering is weak and speckling is occuring, will be greater than this.

The diode normalisation procedure was carried out ten times and the mean and standard deviation are listed in Table 10 for both lasers.

The major errors associated with the instrument are not systematic errors, and therefore cannot be quantified readily. These errors were scattering from dust particles contaminating the film, parasitic scattering from the optics and scattering from surface irregularities.

The Q range of the instrument is dependent on the laser wavelength and the refractive index of the polymer mixture studied, but using

both lasers a Q range from approximately 8×10^{-5} A^{-1} to 2×10^{-3} A^{-1} can be studied. The Q resolution of the instrument varies considerably with the scattering angle deteriorating rapidly at small angles.

CHAPTER 9

EXPERIMENTAL TECHNIQUES

Determination of Phase Boundaries

In general it is satisfactory to determine a crude phase boundary and most studies are not concerned about whether the boundary concerned corresponds to a binodal or spinodal.

There are essentially two common ways of determining phase boundaries in polymer mixtures. The first method involves determining the presence or absence of two glass transitions, such techniques include differential scanning calorinetry, dielectric relaxation and dynamic mechanical relaxation. These methods are not very sensitive even when there is a large difference in the glass transition temperatures of the two polymers. The second method involves scattering from the two phases present by light, Xrays or neutrons. Of these small angle light scattering or turbidity measurements are the most readily available. Most polymers have a large difference in their refractive indices making this method very sensitive. Phase boundaries determined by this method are termed cloud point curves, since the samples become visually cloudy.

Most phase boundaries in this thesis were determined using a small

angle light scattering instrument called a "Turbidimeter". The instrument was built by Chong and is fully described is his Phd thesis.[117] Briefly it consists of a heated sample block capable of holding four sample holders. These consist of a split brass rod in which is placed a thin film of the polymer blend sandwiched between two pieces of glass. A projector lamp is focussed onto the blend and light scattered at 45^0 is focussed onto a photodiode. The block temperature is controlled by a temperature ramp enabling it to be heated or cooled at rates from 0.1 to 1.0 $^0C\ min^{-1}$. The temperature for each sample is monitored by a thermocouple. The diode and thermocouple in each channel are interfaced to a data logger so the intensity and temperature changes can be followed automatically. A typical plot of intensity against temperature is shown in Figure. 17. The sudden change in the intensity corresponds to the cloudpoint. The cloudpoint can be improved upon by monitoring the scattered intensity as a function of time at fixed temperatures above and below the suspected phase boundary.

This instrument suffers from two disadvantages. A comparitively large amount of sample is required and it gives no indication whether the cloudpoint curve obtained corresponds to the binodal or spinodal.

Cloudpoints were also determined using the small angle light scattering instrument described in Chapter 8. This instrument utilizes a much smaller amount of sample and because it has a

multiangle detector, the presence or absence of a scattering maximum can be determined, a scattering maximum providing some evidence for the spinodal being determined. The instrument was used in two modes carrying out heating or cooling runs at 1^0C min^{-1} or isothermal experiments over eight hours.

Small angle Xray scattering was used to obtain the phase boundary in PMMA/SCPE blends that did not give sharp cloudpoint transitions in the Turbidimeter. Because of a poor refractive index difference between the PMMA and SCPE and an initial phase size too small to be observed by light scattering. Sample films ($1cm^2$x 0.2mm) were heated for one minute at 10^0C intervals from 90^0C to 180^0C for each composition. Each film was then placed in a Kratky camera[142] and run for 100s to determine the scattering pattern. If there was a significant increase in scattered intensity compared with the control blend the sample was judged to have been in the two phase region of the phase diagram. In this way a crude phase diagram could be constructed that was refined by repeating the procedure above and below the suspected phase boundary using a longer heat treatment time of five minutes.

Transmission Electron Microscopy

Samples for transmission electron microscopy were thin films

approximately 0.2mm thick. To obtain a sufficient rigidity during sectioning they were embedded in cold curing epoxy resin. Only PMMA/SCPE[67] blends were studied and because this system has a glass transition above room temperature the sectioning was comparitively straightforward. Thin sections 1000-2000 Å were cut using standard procedures and collected on 400 mesh copper grids. These were then examined using a Jeol 100KV Tem scan electron microscope. No staining procedure was necessary due to the electron dense chlorine present.

Light Microsopy

Samples for light microscopy were thin films solution cast onto 19mm diameter coverslips to give a final film thickness of 5-10 μm. These samples were heated for known times using the heating block of the light scattering instrument and then examined immediately using differential interference contrast light microscopy.[143]

Dynamic Mechanical Analysis

Dynamic Mechanical Analysis has been reviewed by Billmeyer[144]. Measurements were carried out using a Rheovibron model DDV-2(Tokyo Measuring Instrument Company Limited). A strip

of film 20 x 5 x 0.2mm was mounted in the jaws of the instrument. An oscillatory frequency of 11 Hz was used for all the measurements. The temperature was scanned from 0^0C to 200^0C at a $1^0C\ min^{-1}$ heating rate and a plot of tan δ against temperature obtained. The maximum in tan δ was taken as the glass transition temperature.

Small Angle Light Scattering

Kinetic experiments were performed using the purpose built SALS instrument. The sample block and holder are preheated to the desired temperature, the sample holder withdrawn and the coverslip supporting the polymer film loaded into the holder which is then slid back into the block. With practice this operation can be performed in about 3s. The thermal heat capacity of the block and sample holder is much greater than that of the coverslip ensuring the sharp temperature jump of the polymer film.

The scattered intensity from the polymer blend is monitored as a function of time and displayed on the visual display unit enabling the progress of the experiment to be followed.

Data Analysis

The optics of the SALS instrument could be aligned so well that no corrections for parasitic scattering were necessary. The D spacing for each angle was calculated using the following expression:

$$Dm = \frac{\lambda}{2n \sin \theta/2}$$

Refractive indices for polymers can not be measured easily. For most common polymers measurenents have been made on their oligomers. D spacings and Q vectors are not extremely sensitive to the refractive index so estimates of the refractive index were made by simply meaning the refractive index of the component polymers. The values for refractive index were taken from the Polymer Handbook[145]

The main problems with the instrument were the low resolution at low Q and the complication of total internal reflection occuring at large scattering angles. This latter complication was overcome by neglecting measurements were the scattering maxima was at angle greater than 50^0 and taking measuremnts with both the He/Ne and the He/Cd lasers.

The He/Cd laser was the preferred choice for short correlation lengths, since the shorter wavelength will result in the scattering maximum being at a smaller angle than if the He/Ne laser had been used. In this way the problem of total internal reflection was minimised.

SMALL ANGLE NEUTRON SCATTERING

Description of the Instrument

The small angle neutron scattering experiments were carried out at the Institute Laue-Langevin, Grenoble, on the small angle camera D11. This instrument has been described in detail by Ibel,[145] but a brief description of the principle features will be given here. The neutron source for this instrument is a high flux nuclear reactor. The neutrons are moderated first using liquid D_2O, then using liquid deuterium. A guide tube leaves the second moderator chamber, the first few metres of which are curved to eliminate gamma radiation and high energy neutrons, the low energy long wavelength neutrons are totally internally reflected along the evacuated guide. The white beam is monochromated using a helical velocity selector which has a wavelength resolution. $(\Delta\lambda/\lambda)$ of 0.1. The beam is collimated after velocity selection by means of altering the internal diameter of the neutron wave guides and by means of diaphrams. The apparent source can be set at distances from 2-40m from the sample. The beam passes through a uranium fission counter, so the flux can be measured continuously, this type of counter has a low cross-section so most of the beam is transmitted and it also has a high counting efficiency. The collimated beam typically has a diameter of about 10mm. The neutron beam passes through the sample and some of the neutrons are scattered into the detector. This consists of an array of 64 X 64

1 cm^2 cells formed by vertical and horizontal electrodes in a plate like glass vessel filled with BF_3. The address of a neutron striking the detector is determined by observing the coincidence of pulses at the horizontal and vertical electrodes. Because the unit cell of the detector is comparitively large, resolution at small angles is achieved by moving the detector back away from the sample. The detector can be positioned at 5 points from 2-40m from the sample. This is not ideal, because the scattered intensity falls as $1/(\text{distance})^2$. Thus the choice of sample-detector distances and the wavelength to give the desired Q range is determined as a compromise between the loss of flux by using long wavelengths and the reduction in the number of counts at the detector. To prevent the main beam saturating the detector a beam stop is placed in front of the detector.

The operation of the instrument and the analysis of data are described in two reports of the Institute Laue Langevin [147], [148]. Two types of SANS experiments were carried out: quenched sample experiments using the PMMA/SCPE[72] system and real time experiments using PS with deuterated PB and deuterated PMMA with SCPE[67]

Quenched Sample Experiments

Quenches were carried out using the heated sample block of the small angle light scattering instrument. The sample block and holder were preheated to the required temperature, then the holder withdrawn and the polymer film, 12mm X 12mm sandwiched between two

coverslips dropped into the sample holder and it slid back into the block. After the required time the sample was removed from the block. The SCPE and the PMMA both have glass transition temperatures much higher than room temperature ensuring that the structure of the blend will remain "frozen in" indefinitely. The quenched samples were taped over an 8.5mm diameter hole in a cadmium sample holder. Then run on D11 using a sample to detector distance of 10.6m and a wavelength of 5Å or 10Å as appropriate for 12 minutes each.

Real Time Experiments
On Poly(methylmethacrylate) Solution Chlorinated Polyethylene Mixtures

Using fully deuterated poly(methylmethacrylate) it is possible to carry out real time kinetics of phase separation experiments on poly(methylmethacrylate)/SCPE blends. It is not possible to measure the transmission of the neutron beam during real time experiments. To ensure that transmission corrections would not be necessary and to facilitate sharp temperature jumps polymer blend films 0.2mm thick were used. This thickness is much thinner thanoptimum (about 1mm), the disadvantage of using such thin films is that the statistics will be poorer.

A specially designed sample jig (Fig.18) was built for real time SANS experiments. Its design is similar to that for the purpose

built SALS apparatus. Briefly it consists of a brass block mounted on two pillars. The block contains two 12mm diameter quartz windows to allow the passage of the neutron beam. The sample film is placed between two pieces of aluminium foil and secured firmly in the sample holder, which consists of a brass plate 2mm thick containing a 12mm diameter hole. The sample holder is mounted on an arm which is located on the shaft of a solenoid. In the sample "out" position the sample holder makes contact with the block and heats up, because the sample is thin it maintains reasonable thermal equilibrium with room temperature. On activating the solenoid the sample holder slides into the block performing a rapid temperature jump and locating the sample in the neutron beam. The parts of the brass block exposed to the neutron beam are covered by cadmium foil. The block is covered on the incoming beam side by a sheet of cadmium containing a 9.5mm diameter hole centred on the 12mm diameter windows. This defines the final beam at the sample and prevents scattering occuring from within the block. Scattering patterns were measured continuously using a 10s time slice. Thirty two spectra could be obtained continuously before the available storage space of the Camac was filled.

<u>On Polystyrene/Polybutadiene Oligomers Mixtures</u>

Real time experiments were performed using the PS1460/PB.2660 system on the 80/20 composition containing a small proportion of

deuterated PB. Quenches were carried out by taking the quartz sided neutron cells from an oven at 120^0C and plunging them into an ice/water mixture at 0^0C. They were held at this temperature for three minutes then placed in the neutron beam at room temperature. Because of the large mass of the sample and the poor thermal conductivity of the quartz a slow temperature quench will occur. An identical quenching cycle was performed using an identical cell but replacing the PS/PB mixture by silicone oil containing a thermocouple. The response of the thermo couple is shown in Fig. 19.

Data Treatment

Corrections were made for the response of the area detector using the incoherent scattering from water. The data was isotropic and the data was therefore radially summated. Pairs of consecutive scattering patterns were summed to improve the statistics of some runs. No corrections for parasitic scattering or sample background scattering were necessary.

SMALL ANGLE X-RAY SCATTERING

Description of the Instrument

Small angle Xray scattering was carried out at the Daresbury SRS using the small angle camera on port 7. The synchroton radiation

source was required in order to carry out real time experiments.

A detailed descripton of the SAXS facility has been reported previously in a series of papers describing the optics,[149] detectors[150,151] and applications of the instrument.[152] Small angle X-ray scattering has found less widespread use in material science and polymer science compared with SANS and for this reason the small angle scattering instrument at Daresbury shares many of its features with the protein crystallography camera.

Briefly the beam from the synchrotron storage ring is focused by a platinum coated mirror from the storage ring and then monochromated by a cut germanium (III) crystal, the beam is focused to a point in front of the detector. This arrangement gives a wavelength of 1.608Å and a resolution $\Delta\lambda/\lambda$ of 0.0035, much greater than is required for small angle scattering. The profile of the beam is determined by a set of remotely controllable slits operating in vacuum. Each slit consists of four jaws of a tungsten aluminium composite. This gives a final beam profile at the sample of about 3mm X 0.5mm and a flux of 5×10^5 photons s^{-1} mm^{-1} when the SRS is running at 2 GeV and 200m A. Because the current gradually reduces with time in the storage ring, the incident intensity was repeatedly monitored with an ionization detector before the sample. An evacuated aluminium flight tube with beryllium windows, two metres long was used between the sample and the detector, giving a final sample to detector distance of 217cm.

Both the area detector and the single wire detector, were used. Both have a much greater spatial resolution (typically a fraction of a mm) than the detector of D11. This enables spacings up to 1300Å to be resolved which is almost equivalent to D11, despite the much shorter wavelength of the Xrays. The Q range covered at a fixed detector distance was greater than D11, this is the main advantage of the small angle Xray facility at Daresbury compared with the D11 camera at the I.L.L. Both detectors are linked via sophisticated processing electronics to a dedicated PDP11 computer.

Experimental Details

The small angle Xray sample holder was similar to the neutron sample holder described previously. The main component is a brass block containing two soldering iron heaters connected to a temperature controller. The block contains two window slits approximately 2mm X 8mm glazed with thin strips (10μm) of mica. Specimen sample thickness of 0.1 - 0.2mm were used, this thickness gives an optimum transmission-absorbtion ratio. Chlorine having an appreciable absorbtion of X-rays (in the solution chlorinated polyethylene). Films of the SCPE/PMMA blends were taped onto thin brass plates over another 2mm X 8mm slit. The brass plates were attached to a circular wheel which rotated around in a step fashion sliding the brass plates into and out of the brass block. During an experiment the brass plate holding the sample was held rigidly

in alignment with the X-ray beam. The length of the block was long enough to maintain an isothermal region in the centre.

Experiments were performed on two separate dates using on the first occasion the linear wire detector and on the second occasion the area detector. The linear wire detector was used first because initially there was no idea of the time scale of the phase separation process and the linear detector offered the advantage of more rapid data acquisition since the time to dump the data to disc was shorter and there was less chance of saturating the linear detector. On the second experimental day the area detector was used because by now there was a good idea of the rate of phase separation and it was hoped to follow the early stages of the phase separation process where the intensity of the scattering is weaker and the statistics can be improved considerably by utilising an area detector.

Treatment of SAXS Data

Treatment of Linear Wire Detector Data

Both static and real time experiments were performed using the linear wire detector. Unfortunately, the time slicing facility for controlling the real time experiments was not available and the timing had to be carried out manually resulting in a large error in the time of the runs.

This complicated the subsequent subtraction of parasitic scattering from the scattering pattern which is particularly pronounced at small Q vectors.

Static quenched samples were run for 60s so the timing error is minimal control blends of the same composition and thickness were run for an identical time and used as subtraction runs to correct for absorption by the chlorine atoms present and parasitic scattering, after correction for any change in the flux of the beam. No attempt was made to correct for slit smearing as the geometry of the beam is not drastically slit like and there is considerable debate as to how slit smearing corrections should be made. Finally, the quality of the data is not sufficient to warrant slit smearing corrections. No attempt was made to correct for multiple scattering, or the counting efficiency of the detector. The efficiency of the detector was however measured and found to exhibit an approximately even response along its entire length. Any correction would be small, much less than $\pm$ 5%.

Real time data was treated in a similar fashion. The first time slice during which no appreciable phase separation occurred was used as the sample background and subtracted from subsequent runs in the series. Small corrections for variations in the period of the time slice were made according to the number of counts in the first channel. This channel corresponds to a Bragg spacing of 3000Å and it is assumed that scattering from the sample

contributes a negligible number of counts to this channel. The data from SAXS and SANS experiments are in reasonable agreement suggesting the methods of data analysis are satisfactory.

Treatment of Area Detector Data

Cells giving spuriously high or low readings were masked out by placing pieces of lead sheet over the relevant areas of the detector, prior to collecting data. Data was radially summated from segments of the detector containing no masks. Time slicing was carried out automatically so no correction for the time period of the run was required. The first run of each series was again used as a background for subsequent runs in the series.

CHAPTER 10

RESULTS AND DISCUSSION

Polystyrene/Polybutadiene Oligomers

Cloud points were determined by placing coverslip encapsulated films in the sample holder of the small angle light scattering instrument at 120°C. The scattered intensity was measured over an angular range of 32° as the sample was cooled at ≈0.5°C min^{-1}. In all cases the scattering curve remained approximately constant until suddenly the scattered intensity started to rise dramatically, particularly at small angles. This is illustrated in Fig. 20a. The onset of the increase in the scattered intensity was taken as the cloudpoint temperature. However, occasionally over a limited composition range the development of a scattering maximum was observed. This is illustrated in Fig. 20b. A nucleation and growth mechanism would not be expected to give rise to a sharp scattering maximum, unless a large number of identical nucleii were present. In contrast spinodal decomposition will always give rise to a scattering maximum.

Scattering maxima were observed from 30% PS to 71% PS in PS 4500/PB 960 mixtures and at 70% PS in a PS 1460/PB 2660 mixture. The cloudpoint

curves are shown in Fig. 21 for these two systems.

The PS/PB oligomers have low molecular weights and are unentangled, their diffusion coefficients will be high and this will favour the observation of nucleation and growth as the samples are cooled into the two phase region. The amount of nucleation and growth that takes place in a given sample will depend on how long the sample takes to transverse the metastable region and how fast the oligomer molecules diffuse.

From the cloudpoint data it might be expected that the spinodal lies close to the binodal in the PS 4500/PB 960 system, whilst the spinodal strikes the cloudpoint sharply near 70% PS in the PS 1460/PB 2660 system. Pulse induced critical scattering (PICS)[152,153] can be used to determine the spinodal around the critical point in oligomeric mixtures. This technique involves measuring the light scattered from a sample in both stable and metastable states at 30 and 90°. By extrapolating a plot of the reciprocal of the intensity (I) against temperature to the point where 1/I is zero, an accurate estimate of the spinodal is obtained. Spinodal data collected using PICS by Atkin et al[154] for the PS 1460/PB 2660 system is shown in Fig. 22 and it can be seen that the 70 weight percent composition indeed lies fairly close to the critical composition. The sharpness of the spinodal curve around the maximum indicates that it was extremely fortuitous to make a composi-

tion lying close to the critical composition prior to having the PICS data. The spinodal for an almost identical system to the PS 4500/PB 960 system has recently been determined[155] (Fig. 21). Here the spinodal is broader and lies close to the cloudpoint curve over a comparatively large range of compositions.

This data provides strong evidence for the development of a scattering maximum only arising within the spinodal, and nucleation and growth giving rise to no scattering maximum.

KINETICS

The PS 4500/PB 960 System

It proved impossible to follow the early stages of spinodal decomposition in this system. Over no time period was the correlation length (Dm) time independent and not surprisingly plots of Ln (scattered intensity) against time were non linear, even for very shallow quenches into the spinodal Typical I(Q) plots are shown in Fig. 23 and a typical scattering pattern in Fig. 24. Although the initial time invariant correlation length must be shorter than the first correlation length observed, it is unlikely to be much shorter. The indication is that it must be much larger than predicted by van Aartsen[64].

$$Dm = 2\pi\ell \left[3 \frac{T_s - T}{T_s}\right]^{-\frac{1}{2}}$$

The value of ℓ will be approximately 25Å for this system giving an expected value of Dm of 720Å at 88°C.

Russel et al[86] have also studied phase separation in oligomers. They demonstrated using real time SAXS experiments that the scale of phase separation was greater than 897Å and in fact occurred on a range accessible to SALS. A plot of the correlation length against log time is shown in Fig. 25. At no stage is the plot linear. Similar results were found by Snyder et al[108] with polystyrene/poly(vinylmethylether) mixtures. They claimed their results demonstrated that no distinct coarsening mechanism was taking place during the late stages.

The PS 1460/PB 2660 System

Two small angle techniques NS and SALS were used to study the demixing process. The SANS samples contained a small proportion (less than 10%) of a deuterated polybutadiene. Deuteration is known to affect the phase boundaries in these mixtures[118]; however the small proportion of deuterium added had no significant effect on the measurement of cloudpoint curve.

Preliminary SALS studies demonstrated that off critical quenches just into the spinodal could not be performed quickly enough to prevent significant nucleation and growth taking place, particularly with mixtures containg less than 70% by weight PS. Nucleation and growth is presumably aided by the large metastable gap between the binodal and spinodal arising from the sharpness of the spinodal curve, as well as the high mobility of the system.

For these reasons only quenches at 70% PS and deep quenches at 80% PS were studied. The cloudpoint curve for this system is at a much lower temperature than the PS 4500/PB 960. Furthermore, the critical composition is towards the PS component with the higher glass transition temperature. Applying the Fox equation[156] as below and assuming glass transition temperatures of 80°C and -60°C for polystyrene

$$\frac{1}{Tg_{AB}} = \frac{\phi_A}{Tg_A} + \frac{1-\phi_A}{Tg_B}$$

ϕ_A = weight fraction polymer A

Tg_A = the glass transition temperature polymer A

Tg_B = the glass transition temperature polymer B

Tg_{AB} = the glass transition temperature of the mixture.

and polybutadiene gives a glass transition for the 70% PS composition of 21°C. This value is close to spinodal temperature suggesting that

the mobility of this mixture may be low within the spinodal and enable the study of the early stages of phase separation. The glass transition is plotted as a function of composition in Fig. 21.

SALS Experiment

The SALS study was carried out with the 70% PS composition only. At early times the scattering maximum was at a fixed angle and the scattered intensity grew exponentially in agreement with predictions of the C/H theory. A typical plot of LnI(Q) against time is shown in Fig. 26.

The time period over which the plot is linear is sufficiently long to be able to neglect the temperature jump time (5-10s) and to get a large number of points on the linear portion. At later times the intensity no longer grew exponentially and the peak position moved to smaller angles and became sharper (Fig. 27). The initial correlation length (Dm) is clearly the order of a micron and also temperature dependent, decreasing with increasing quench depth into the spinodal (see Table 11). The correlation length is clearly much larger than predicted by van Aartsen's expression. Despite this the observed temperature dependence is qualitatively predicted by the theory. Values for $R(Qm)\ Qm$ and $\bar{D}$ are also listed in Table 11. The order of magnitude of $\bar{D}$ ($\simeq 10^{-13} cm^2 s^{-1}$) compared with values for high molecular weight blends of PS/PVME[106,108,89] ($\tilde{D} \simeq 10^{-10} - 10^{-13} cm^2 s^{-1}$) seems too small. However,

these latter measurements were taken at much higher temperatures and well above the glass transition temperature of the system. Comparison with measurements of diffusion coefficients of polystyrene oligomers[27] at similar temperatures suggest the magnitude of $\overline{D}$ is reasonable. Russel et al[86] found $\overline{D}$ also to be about $10^{-13}cm^2s^{-1}$ for an oligomeric PS/PB system but at much higher temperatures and well above the glass transition. It seems likely that Russel et al[86] were therefore not following the early stages of phase separation, especially as they were only observing the high Q portion of the scattering pattern.

Cahn[44] predicted that the plot of the Cahn-Hilliard diffusion coefficient ($\overline{D}$) against temperature should be linear and extrapolate to the spinodal at $\overline{D} = 0$ enabling the spinodal to be determined from the two phase region of the phase diagram. Such a plot is shown in Fig. 28 and is not linear. The decrease in $\overline{D}$ for deep quenches is suspected to arise from a reduction in the interdiffusion coefficient as the glass transition is approached since:

$$\overline{D} = M \frac{\partial^2 G}{\partial \phi^2}$$

Cahn assumed M to be independent of temperature.

An alternative method for determining the spinodal is to plot Qm^2 against temperature the plot should be linear with an intercept at Qm^2

= 0 corresponding to the spinodal. Despite the fact the Qm cannot be determined precisely a plot of Qm^2 against temperature is shown in Fig. 29. The plot does not extrapolate to zero at the spinodal. This could be explained by:

1. The radius of gyration of the component oligomers being temperature dependent;
2. The thermodynamics of miscibility not being modelled accurately by Flory-Huggins theory.

The cut-off wavevector Qc is byond the resolution of the SALS instrument, but is greater than $\sqrt{2}$.Qm, the predicted value from the C/H theory.

Plots of the correlation length (Dm) against log (time) are shown in Fig. 30. At no time does Dm follow any power law behaviour typical of the coalescence or Ostwald ripening mechanism, nor does it grow exponentially as predicted by Mcmaster[56].

SANS experiments

Sharp temperature jumps could not be performed with the large mass of sample and thick walled quartz cells used in SANS experiments. A typi-

cal temperature-time profile for a deep quench is shown in Fig. 19. For this reason only deep quenches with the 80% by weight polystyrene composition were studied. A scattering maximum was observed (Fig. 31) at low Q corresponding to a correlation length of 1230Å. The peak became sharper and moved slowly to smaller angles with time. Plots of Ln scattered intensity against time were non-linear. This is not surprising considering the thermal history of the sample. The correlation length is approximately that predicted by the van Aartsen expression assuming the interaction length ℓ to have an identical value to the previously studied 70% PS composition.

The cut-off wavevector Qc is approximately $1.71 \times 10^{-2} Å^{-1}$. Clearly this value is greater than $\sqrt{2}.Qm$. Using the expression below first derived by Park[49], that takes into account the thermal fluctuations considered by Cook[48]

$$\frac{Qm}{Qc} = \left[\frac{Ts-T}{2Ts}\right]^{-\frac{1}{2}}$$

and taking Ts as 313K and T as 273K gives a predicted ratio of 0.255 for Qm/Qc, compared with the actual value of 0.275. The agreement is surprisingly good considering the poor thermal quench. Russel et al[86] found values of Qc in their SAXS experiments on a very similar PS/PB oligomer system that were apparently temperature dependent. This is in contradiction to the modified expression of Park. The values found by

Russel et al were in the range 2.4-3.3 x $10^{-2}Å^{-1}$. Our value of 1.71 x $10^{-2}Å^{-1}$ is smaller but for a slightly lower molecular weight mixture.

ETHYLENE VINYL-ACETATE COPOLYMER/SOLUTION CHLORINATED POLYETHYLENE (EVA/SCPE)

DETERMINATION OF PHASE BOUNDARIES

Originally an attempt was made to study phase separation in commercial chlorinated poly(ethylene)/ethylene vinyl-acetate copolymer mixtures. Homogeneous blends could not be obtained; partial phase separation occurred during solvent casting and crystal spherulites roughly 0.5μm in size were observed by light microscopy. Phase separation in these inhomogeneous blends appeared to take place by two mechanisms (Fig. 32). The structure of the solvent cast blends was very variable and had an influence on the phase separation process. The study of phase separation in these blends was terminated and laboratory prepared SCPE/EVA blends were investigated instead.

Cloudpoint curves for $SCPE^{50}/EVA^{45}$ and $SCPE^{50}/EVA^{40}$ were determined using the turbidimeter. These are shown in Fig. 33 and agree with previously published results. Subsequent SALS experiments demonstrated these blends to have undergone partial phase separation, particularly with the lower vinyl-acetate content copolymer, EVA^{40} at high SCPE

weight fractions. The EVA and the SCPE both have a broad molecular weight distribution and it was thought that a small amount of high molecular weight polymer could be causing the partial phase separation. Molecular weight fractionation was carried out in order to overcome this problem, as well as other potential problems associated with a polydisperse system. Homogenous blends across the whole composition range could only be formed with the lowest molecular weight fraction of the $SCPE^{50}$. This was the fifth fraction obtained and is therefore labelled $SCPE^{50}/^{5}$. All the subsequent studies were carried out using this fraction with $EVA^{45}/^{3}$.

The phase boundary was measured using the SALS instrument and carrying out isothermal experiments as described in Chapter 9. The phase boundary is shown in Fig. 34. In contrast to the PS/PB oligomers, in all cases where phase separation took place a scattering maximum was observed. The implication of this is that the experimentally determined phase boundary corresponds to the spinodal and not the binodal. Nucleation and growth is probably strongly suppressed in this system because of (1) the low mobility due to the highly branched EVA, (2) the closeness of the phase boundary to the glass transition temperature of the SCPE, at high SCPE weight fractions. The phase boundary has a lower LCST than the polydisperse system from which it was fractionated, despite the reduced molecular weight of both components. There are two possible explanations for this:

1. Previously determined phase boundaries are kinetically shifted to higher temperatures, because the higher average molecular weight in the unfractionated blends reduces the mobility.
2. The fractionation procedure has fractionated not only the basis of chain length, but also on the polarity of the polymers, thus on the chlorine content of the SCPE[50] or the vinyl-acetate content of the EVA[45]. This could only occur if the chlorine and vinyl-acetate are non-randomly distributed among the polymer chains. This seems unlikely for the SCPE but potentially possible for the EVA.

A careful elemental analysis was carried out on both the SCPE fractions and the EVA fractions. The results are presented in Tables 12 and 13 and show no evidence of fractionation on the basis of vinyl-acetate or chlorine content. Thus there appears to be a strong kinetic effect on the phase diagram determined previously for the unfractionated blends.

The minimum of the phase diagram is at high SCPE weight component as expected on the basis of the combinatorial entropy terms. The phase boundary of this system is very similar to that of poly(vinylchloride) /EVA blends that always exhibit greater miscibility at high EVA weight fractions.

KINETIC EXPERIMENTS

Preliminary studies by SANS and SALS showed this blend system to phase separate only in the Q range accessible by light scattering so phase separation was followed using the purpose-built light scattering instrument described in Chapter 8. Kinetic experiments were carried out as outlined in the experimental section. Within the phase boundary plots of Ln (Intensity) against time were initially linear (Fig. 35) providing the rate of phase separation was fairly slow and the early stages could be followed. At high SCPE concentrations ℓn (Intensity)-time plots were initially linear over a 20°C temperature range. This data confirms that the measured phase boundary is the spinodal.

Unlike studies on PS/PVME blends[106,107] a temperature dependence of the initial correlation length was found in this polymer mixture for compositions high in EVA. Compositions containing large amounts of SCPE had initial correlation lengths that were independent of temperature. Temperature dependence of the initial correlation length has been found in studies of spinodal decomposition in UCST systems and is normally called quench depth dependence. It is the theoretically expected behaviour since:

$$Q_m^2 \propto \left[\frac{\partial^2 G}{\partial \phi^2}\right]$$

The $\partial^2G/\partial\phi^2$ term would be expected to increase the further you go into the spinodal. Thus the initial correlation length reflects $\partial^2G/\partial\phi^2$, the thermodynamic driving force for phase separation. The initial correlation length does decrease as T-Ts increases for EVA concentrations greater than 46% EVA. Data for the quench depth dependence of Dm for several concentrations is shown in Figs. 36 and 37. van Aartsen's equation (equation 15, p. 29) fits the observed data well providing a value for ℓ, the interaction length is arbitrarily chosen. The exact mathematical definition of ℓ is unclear, but it should be the order of the radius of gyration of the polymer molecules. The values of ℓ required to fit the experimental data are much larger than even the radius of gyration of the highest molecular weight component, the EVA. Values for ℓ are given in the caption of Fig. 36. The magnitude of ℓ does however increase as the EVA content of the blend increases. Nishii et al[89] also used a value for ℓ much greater than the radius of gyration in their study of phase separation in PS/PVME blends.

It has been postulated that phase separation in many polymer blends is brought about by the dissociation of a specific chemical interaction and a subsequent reduction in the favourable enthalpy of mixing term. A Fourier transform infra red study of the carbonyl stretching frequency in EVA/SCPE blends provides evidence for a hydrogen bond specific interaction that dissociates as the temperature is raised[135]. The data taken from this study is shown in Fig. 11. As the phase boundary

is crossed the carbonyl stretching frequency shifts dramatically. However, above 100°C there is no further change indicating that the hydrogen bonds have completely dissociated.

Heat of mixing measurements with oligomer analogues show a marked reduction in the enthalpy of mixing as the temperature is raised[114]. This data is shown in Fig. 10 and provides further evidence for the dissociation of a specific interaction.

The quench depth dependence is only observed from about 95°C upwards (Figs. 36 and 37) indicating that the effect of temperature on the ΔS term is now the most likely driving force for phase separation. The concept of entropy driving the phase separation in an LCST phase diagram implies that the entropy must be unfavourable towards mixing, i.e. it must be negative. This is disturbing at first sight. However, the following expression is routinely used[125] for the entropy term in the equation of state approach to modelling phase boundaries.

$$-T\Delta S_M = RT(n_1 \ln\phi_1 + n_2 \ln\phi_2) + 3\bar{r}Nv^*\{\phi_1 P_1^* \bar{T}_1 \ln \cdot$$

$$[(\bar{v}^{1/3}-1)/(\bar{v}^{1/3}-1)] + \phi_2 P_2^* \bar{T}_2 \ln[(\bar{v}_2^{1/3}-1)] - \bar{r}Nr^*$$

$$+ \phi_1\phi_2 TQ_{12}$$

The last term is included in the entropy of mixing term in order to fit the experimental data, where Q_{12} is the empirical interaction entropy parameter that reflects the change in entropy due to the interaction of unlike segments during mixing. Q_{12} is therefore very unlikely to be negative resulting in ΔS being negative.

There are four possible reasons why no quench depth dependence of the initial correlation length is observed in blends with a high SCPE content. They are:

(1) The specific interaction in this blend could dissociate over a narrow temperature range resulting in a large reduction in the enthalpy of mixing. In this case the phase separation will be driven not by the entropy term, but by the enthalpy of mixing term. No prediction can then be made as to how the initial correlation length will vary as a function of temperature.

(2) There is some structure in these blends or on the surface of the coverslip that preferentially favours a given particle size.

(3) The value for the interaction length l which is related to the radius of gyration is temperature dependent. Studies of polymer/liquid systems have shown[157] that the radius of gyration of polymer molecules reduce as the co-existence curve is approached

and the liquid becomes a poorer solvent for the polymer. The calculated amount χ would have to change by as a function of temperature within the spinodal is shown in Fig. 38 assuming the phase separation is entropically driven.

(4) The phase boundary could possibly be at a much lower temperature than shown in Fig. 34. At large values of ΔT, i.e. for a deep quench the initial correlation length will be almost insensitive to temperature.

Since there appears to be a smooth transition on going from quench depth behaviour to no quench depth behaviour the second explanation seems unlikely. The phase boundary would have to be at 20°C for the fourth explanation to be valid which is not credible. Neutron scattering studies[158,159] of the radius of gyration of polymer molecules in polymer mixtures have so far only demonstrated a slight coil expansion or contraction with respect to the homopolymer melt. It seems unlikely therefore that such a large change in the radius of gyration could occur to account for the third explanation. The most probable explanation is therefore the first one.

Growth rates of the fastest growing wavevector, R(Qm) obtained from the slope of ln intensity against time plots are given in Tables 14 to 18. Also shown are the values of Qm and the calculated values of the Cahn-Hilliard diffusion coefficient, $\overline{D}$. If the mobility of the polymers

does not change significantly with temperature and the phase separation is brought about by the entropy term, the plot of $\overline{D}$ should be linear and extrapolate to the spinodal at $\overline{D} = 0$. This has recently been demonstrated by Snyder et al[108] and by Hashimoto et al[106] for PS/PVME blends. Plots of $\overline{D}$ against temperature are shown in Figures 39 and 40 for EVA/SCPE blends. The extrapolation back is reasonable for EVA rich compositions 55% EVA and 59% EVA. Least square fits giving values for the intercepts of 100°C and 116°C compared with the temperature of the spinodal at 95°C and 113°C respectively. The data for the SCPE rich compositions give nonlinear plots. For example the 24% EVA composition is shown in Figure 40 and a least squares fit gives an intercept of 70°C compared with 53°C. The nonlinearity probably results from two causes:

(1) The quench depth dependence is not modelled by equation 15, p.19, the wavevector maximum will therefore be larger than expected for small values of ΔT and since $\overline{D}$ is calculated by

$$\overline{D} = \frac{2R}{Qm^2}$$

This will lead to a lower value of $\overline{D}$ being obtained for small ΔT values.

(2) As the temperature increases the mobility term M also increases and since

$$\frac{\partial^2 G}{\partial \phi^2} = 2B \left(\frac{Ts-T}{Ts}\right)$$

where B is a constant

and

31. $$\overline{D} = 2BM \left(\frac{Ts-T}{Ts}\right)$$

Equation 31 is analogous to the proposed scaling relationship for $\overline{D}$ i.e.

$$\overline{D} \alpha \left(\frac{Ts-T}{Ts}\right)^{\gamma^*}$$

Snyder et al found γ^* to be approximately equal to one for PS/PVME blends as predicted by the linearized Flory-Huggins/Cahn-Hilliard model despite observing no quench depth dependence of Dm. These results are in stark contrast to the exponential WLF behaviour found normally for polymer diffusion where γ^* would not be a constant and to the results shown earlier on PS/PB oligomers.

The correlation length was always found to be time independent during the period that LnI against time was linear. In most cases the wavevector cut-off, Qc was beyond the range of the instrument; in all cases Qc $> \sqrt{2}$xQm as was found in PS/PB oligomer mixtures. For shallow quenches into the spinodal and particularly around 20-40% EVA, the scattering maximum was very broad, probably as a result of Qc $>>$ Qm and possibly the very low mobility of the system.

EVA rich compositions near to the spinodal have a wavevector cut-off Qc within the range of the instrument, this is shown in Fig. 41. Qc $>$ $\sqrt{2}$.Qm but not as large as predicted by Park[49]. If the phase separation is entropy driven and thermal fluctuations are also included then Park showed that Qc should remain fixed whilst only Qm should alter. In contrast neglect of thermal fluctuations results in both Qc and Qm changing with temperature since their ratio is fixed. Slightly deeper quenches into the spinodal result in Qc moving to higher Q and out of range of the instrument in contradiction to Park's expression. A study of the temperature dependence of Qc by SANS in conjunction with a SALS

study of Qm might be useful in deciding whether thermal fluctuations should be included in the theory.

Plots of $R(Q)/Q^2$ against Q^2 should be linear according to C/H theory (equation 6) and extrapolate to the apparent diffusion coefficient of the system at $Q^2 = 0$. Such plots are shown in Figures 42 and 43. In all cases there is a marked deviation from linearity, as found for many other systems. During the late stages the correlation length increases and the scattering peak sharpens. Typical I(Q) plots are shown in Figs. 44 and 45. It was noted that the correlation length grew more rapidly for the polymer mixtures with high proportions of SCPE. This is clearly seen when Figs. 46 and 47 are compared. The 13% EVA composition shows a much faster growth of Dm than the 46% EVA composition for similar quench depths and temperatures. It appears that the SCPE is much more mobile than the EVA despite its much higher glass transition temperature, presumably the greater mobility arises from the lower molecular weight of the SCPE and the branched nature of the EVA. The higher proportion of SCPE in the 13% EVA composition results in Dm growing more rapidly than in the 46% EVA composition.

The late stages of spinodal decomposition are normally regarded as being entirely separate from the early stages. Distinctly different mechanisms are believed to take place such as Ostwald ripening, coalescence and viscous flow, most of which predict power law behaviour. No

evidence of any power law behaviour was found for Dm at any temperature or composition. Typical plots are shown in Figs. 46 to 48. This could indicate that Ostwald ripening coalescence and viscous flow mechanisms do not take place, or that they all take place with no one mechanism dominating.

LIGHT MICROSCOPY

Differential interference microscopy was used to study the blends before and after heat treatment. An interconnected morphology with a diffuse interface was observed at early times (Figs. 49 to 50). Later the wavelength of the system becomes longer and the interface sharper. An interconnected structure has often been cited as evidence for spinodal decomposition having taken place; however interconnected structures can arise from nucleated systems, the additional presence of a diffuse interface provides much stronger evidence for spinodal decomposition. At temperatures very close to the spinodal at high temperatures, for example compositions with 59% and 62% EVA, a dispersed phase with a sharp interface was observed intermingled with an interconnected morphology (Fig. 50). It appears therefore that significant nucleation and growth takes place close to the spinodal at very high temperatures where the system is fairly mobile. Points where an interconnected morphology with a diffuse interface were observed are plotted on the phase diagram and provide additional evidence for the measured boundary

being the spinodal. Unfortunately, close to the phase boundary at low temperatures there was insufficient contrast to observe any morphology by microscopy.

One surprising observation was that the interconnected morphology was still seen during the time period that the correlation length grew dramatically (Fig. 51) explaining why the power law behaviour expected from Ostwald ripening and coalescence mechanisms was not found.

Deep inside the spinodal nucleation and growth could still take place providing a suitable nucleus is present. Nucleation can be seen in Fig. 53 and has clearly initiated from a heterogenous particle. Fig. 52 shows the same sample at a point well away from the heterogenous particle; the interconnected morphology typical of spinodal decomposition can be seen. Note the large size of the domains formed by nucleation and growth compared with the small domains formed by spinodal decomposition.

POLY(METHYLMETHACRYLATE)/SOLUTION CHLORINATED POLYETHYLENE MIXTURES

Introduction

A full analysis of the dynamics of phase separation in poly(methylmethacrylate)/solution chlorinated polyethylene blends is hindered at present because of insufficient data. Experimental time for SAXS and SANS was limited because of the high demand for these techniques. The data analysis is complicated by the polydispersity of the SCPE ($\overline{M}w/\overline{M}n \simeq 6.5$), that may give rise to a range of diffusion coefficients and interaction lengths. Molecular weight fractionation is presently being carried out to eliminate these complexities in future experiments. Despite the limited data, particularly for the early stages, the results are of interest because the scale of phase separation is much smaller than has been previously observed in any other polymer mixture. For this reason the results will be presented here.

Two different chlorinated polyethylenes were studied because fully deuterated poly(methylmethacrylate) was not available initially and in order to get reasonable contrast with neutrons the level of chlorination of the polyethylene had to be increased (see Table 2).

Determination of Phase Boundaries

Both SAXS and SALS were used to determine the phase boundary of PMMA/SCPE mixtures. Small angle light scattering determinations using the

turbidimeter did not show a sharp discontinuity in the plot of the scattered intensity at 45° as a function of temperature. This resulted in a large error in the cloudpoint curve. The ill-defined cloudpoint was thought to arise from the poor refractive index difference between the component polymers. However, it was later found that the phase separation initially occurs on a scale smaller than can be observed by light scattering. The phases slowly grow to light scattering dimensions, resulting in a gradual increase in the scattered intensity. The experimentally determined phase boundaries for PMMA/SCPE^{67} and PMMA/SCPE^{72} are shown in Figs. 54 and 55.

Small angle X-ray scattering was used to study phase separation in this blend and showed the initial scale of phase separation to occur on a submicron level. Because both component polymers have almost identical glass transition temperatures the phase boundary cannot be determined by any method that involves measurement of a glass transition. Small angle X-ray scattering was therefore used to determine phase boundaries. A Kratky camera was used and the procedure is outlined in the Techniques section. This was a rapid though not ideal method for determining phase boundaries, becuse of the limited range of the Kratky camera ($d_{max} \cong 300Å$), poor resolution at such large spacings and slit smearing. Samples heat treated at high temperatures frequently exhibited almost no small angle scattering compared with samples heat treated at a lower temperature for an identical time period. Studies on the

same samples at the SRS (Daresbury) where the small angle camera has a resolution of about 1300Å showed this effect to be due to the correlation length increasing with time faster at higher temperatures and the peak going out of the range accessible to the Kratky camera.

The SAXS measured phase boundaries are lower than those determined by SALS indicating that the initial domains take a long time to grow to light scattering dimensions. Both phase boundaries are close to the glass transition temperature of the blend. The glass transition temperature as a function of composition is calculated according to the Flory-Fox equation and shown on Figs. 54 and 55. Because the observed phase boundaries are so close to the glass transition temperature they can only be regarded as an upper limit to the phase boundary. The fact that PMMA/SCPE^{67} and PMMA/SCPE^{72} blends showed partial miscibility was surprising since Chai[160] claimed that SCPE with 62% by weight chlorine was completely miscible with PMMA. Originally it was thought that Chai's conclusion was wrong since he utilized differential scanning calorimetry to show only a single glass transition and there is only a small difference in the glass transitions of the two polymers. However, subsequent studies of PMMA/ SCPE^{65} blends using both SAXS and SANS showed this system to be completely miscible. Thus there appears to be a window of complete miscibility of PMMA with SCPEs having a degree of chlorination of about 62%.

The phase boundary for the PMMA/SCPE^{72} system determined using the small angle Kratky camera is shown in Fig. 55. Unfortunately, homogenous blends could not be cast at high PMMA weight fractions, so the phase boundary is ill-defined in this region. The phase boundary appears to be slightly higher than that for PMMA/SCPE^{67} blends; this could be real or a kinetic effect due to the higher glass transition temperature of the SCPE^{72}.

It is clear from these results that there has to be another term besides that of the specific interaction term emphasised by Chai[123] which is of importance in determining the miscibility of PMMA and SCPE, particularly at high degress of chlorination.

Deuterating the poly(methylmethacrylate) appears to have very little effect on the observed phase boundary in contrast to polystyrene/poly-(vinylmethylether) blends. Deuteration would be expected to move the phase boundary to higher temperatures, the slight movement to lower temperatures observed may well result from the slightly higher molecular weight of the PMMA and a small change in its tacticity. For example, the miscibility of poly(vinylchloride)/PMMA blends is heavily dependent on the tacticity of the PMMA[161], isotactic PMMA being completely immiscible whilst syndiotactic is fully miscible.

Preliminary Studies

Preliminary studies showed the original polymer blend films prior to heat treatment to exhibit very little small angle scattering by light X-rays or neutrons and they were therefore assumed to be homogenous blends. Occasionally a very small peak at very low Q ($\simeq 10^{-3}$ Å^{-1}) was observed by SANS (Fig. 58). However its intensity was low and since it was not in the Q-range where phase separation initially took place it can be safely ignored. It is thought to result from microvoids in the solvent cast film.

Confirmation that small angle neutron and X-ray scattering were observing phase separation and not void formation due to solvent left over from the preparation could not be obtained by conventional methods of determining two distinct glass transitions, since both polymers have almost identical glass transitions. However, poly(methylmethacrylate) /solution chlorinated polyethylene blends where the chlorinated polyethylene has a lower degree of chlorination, 54.5%, show two distinct glass transition temperatures[162] as well as a short correlation length[163] after heat treatment in the two phase region. Transmission electron microscopy of some of the phase separated samples studied by SANS was undertaken. Although both polymers are not very stable to irradiation by the electron beam and the contrast was poor, phase separation was clearly seen and the size of the domains observed agreed approximately with the peaks in the appropriate I(Q) plots. Typical

micrographs are shown in Figs. 56 and 57. The I(Q) plot for the sample shown in Fig. 56 is Fig. 58.

Further evidence that a phase separation of the component polymers was being observed is that blends of PMMA/SCPE^{65} were found not to phase separate at all by SAXS and SANS. If voiding due to residual solvents was causing the apparent phase separation then there is no reason why it should not also occur in PMMA/SCPE^{65} blends prepared in an identical manner.

COMPARISON OF SAXS AND SANS

Data was obtained both by SAXS at Daresbury and SANS at Grenoble on phase separation of PMMA/SCPE blends. One quenched sample was studied by both techniques, the intensity against Q plots obtained are shown in Fig. 78. There is reasonable agreement between the two techniques, particularly at the maximum and on the low Q side of the maximum. There is however a small significant difference between the two techniques at high Q, which could arise from:

1. Errors in the subtraction of a large background from the SAXS scattering pattern;

2. Errors in the Q calibration of the detector using the Bragg diffraction peaks of collagen;

3. The fact that the SAXS instrument has a much smaller beam area than the D11 camera and thus a small atypical part of the sample was viewed by the X-ray beam.

It is hoped to test this latter point when further time for SAXS becomes available at the Daresbury SRS.

The maximum wavevector Qm of Fig. 58 corresponds to approximately 600Å or 0.06μm; this is interesting because the scale of phase separation is much smaller than predicted by van Aartsen (equation 15, p19). Previous studies of phase separation in high molecular weight polymer mixtures have demonstrated the phase separation to occur only on a scale of approximately 1.0μm. Very recently phase separation in two high molecular weight systems PS/PVME[164] and poly(ethylacrylate)/poly (vinylidenefluoride)[165] has been studied by SAXS. In both cses there was no evidence of a scattering maximum.

There are several possible explanations for observing a short correlation length.

1. This polymer blend is a mixture of two glassy polymers in contrast to most polymer blends studied that are mixtures of two rubbers or a glass with a rubber. Just above the glass transition temperature of the blend, where phase separation occurs, the interaction length, ℓ, is not the order of the radius of

gyration, but much smaller because segments of the polymer chain are effectively immobile.

2. The specific interaction consisting of a hydrogen bond is still important in the two phase region and acts as a physical cross-link preventing large scale phase separation.

3. The thermodynamic driving force for phase separation, the $\partial^2 G/\partial\phi^2$ term is extremely large and since:

$$Qm^2 \propto \frac{\partial^2 G}{\partial \phi^2}$$

a small correlation length results. It is conceivable that this arises in part from the phase boundary being considerably below the glass transition temperature and in part from the enthalpy of mixing term becoming rapidly unfavourable as the hydrogen bonds between the two polymers dissociate.

4. The scale of phase separation is constrained by entanglements and influenced by reptation. Theoretical studies by Binder, de Gennes and Pincus all predict short correlation lengths, the order of the radius of gyration for high molecular weight entangled polymers undergoing spinodal decomposition.

5. There is some structure within the polymer blend or on its surface that causes the preferential heterogenous nucleation of a short correlation length.

The first explanation cannot be valid because mixtures of PMMA/SCPE[54], where the SCPE has a lower degree of chlorination and lower glass transition temperature, also phase separate with a short correlation length. No evidence for or against the other explanations is available at present. The fifth explanation will be readily eliminated if the initial correlation length can be shown to be temperature dependent.

SMALL ANGLE X-RAY SCATTERING STUDIES

Linear Wire Detector Data

Figures 59 and 60 show a series of I(Q) plots at different times. The peak position moves to lower Q vectors, whilst the intensity increases, and the peak becomes sharper, particularly on the high Q side.

Data for the growth of the correlation length as a function of log time for different compositions is shown in Figs. 61 to 65. At no stage is the correlation length time invariant so the early stages only last for a very short time even at temperatures just above the glass transition temperature of the blend.

Because of the short correlation length, the polymer molecules have to diffuse much shorter distances (≈300Å) than in, for example, PS/PVME blends where the correlation length is typically ≈10,000Å and thus approach equilibrium much faster. It is also possible that the mechanism of translational diffusion in polymer melts is different over the two different distance scales involved. Unfortunately, the fact that the early stages are not realised considerably hinders the interpretation of the data and particularly makes any observation of the quench depth dependence of the initial correlation length impossible since the correlation length is never time invariant.

There is however some circumstantial evidence for a quench depth dependence. Figs. 62 and 63 do appear to show that the higher temperature data would extrapolate back to a shorter correlation length. Furthermore, samples containing 27% and 13% SCPE[67] (Figs. 63 ad 64) do exhibit a significantly larger correlation length than do samples containing 70% and 55% SCPE[68] (Figs. 62 and 61) at a given time and temperature. At a set temperature the quench depth (ΔT) is smaller for samples containing 27% and 13% SCPE[67] because the spinodal is higher at low SCPE weight fractions. This could reflect a quench depth dependence or a composition variation due to the low molecular weight tail of the SCPE.

As the temperature is raised the correlation length grows more rapidly, presumably as a result of the effect of temperature on the viscosity

and on diffusion. Over no time period does the correlation length exhibit any power law behaviour, as might be expected from Ostwald ripening, coalescence or viscous flow mechanisms. The 80% $SCPE^{72}$ blend shows a significantly shorter correlation length at a given time and temperature (Fig. 65) than any of the PMMA/$SCPE^{67}$ blends. The growth of the correlation length is also slower at a given temperature, thus the shorter correlation length could arise from viewing the phase separation at an earlier stage. The slower growth of the correlation length probably results from the higher glass transition of the $SCPE^{72}$ compared with the $SCPE^{67}$.

Area Detector Data

Unfortunately most of the data obtained using the area detector and automatic time slicing was invalid because of the high count rate saturating the detector. However, two runs using an identical sample and temperature did give a low enough count rate to get valid data. The sample used was a PMMA/$SCPE^{72}$ mixture containing 80% $SCPE^{72}$ at 126°C. I(Q) plots at different times are shown for both runs and are scaled to the intensity of the maximum intensity of the first run (Fig. 66). There is very good reproducibility between the two runs. However, despite the fact that the temperature is very close to the apparent spinodal for this composition, the peak position is never time invariant and the intensity does not grow exponentially. It is possible that the phase boundary is much lower than originally thought and that

the measured phase boundary corresponds to the onset of appreciable mobility above the glass transition. Thus there could be a very large thermodynamic driving force for phase separation resulting in a very short time period for the early stages where the scattered intensity grows exponentially.

SMALL ANGLE NEUTRON SCATTERING STUDIES

Quenched Sample Experiments

Quenched sample experiments were carried out with a PMMA/SCPE^{72} blend containing 80% SCPE^{72}. Statistics were poor during the early stages due to poor contrast. The samples were not of identical thickness, so corrections to the data had to be carried out, and these were very inaccurate because of uneven film thickness. It was also suspected that some rehomogenisation of the phase separated blends occurred during quenching to room temperature. Fig. 67 shows a series of I(Q) plots for films of PMMA/SCPE^{72} heated at 127°C for different times. Fig. 68 shows a plot of LnI(Q) against time. Clearly the quenched sample technique is not very satisfactory.

Real Time Experiments

In order to do real time experiments fully deuterated poly(methylmethacrylate) (PMMA(D)) was used. Only one composition was studied due to

limited amounts of PMMA(D) being available. This composition was 55% SCPE[67] by weight.

Fig. 69 shows the correlation length as a function of log time for this sample at different temperatures. There is clearly a quench depth dependence of the initial correlation length, which remains approximately constant for a short time period at the lowest temperature studied. This demonstrates that the short correlation length is not originating from any structure in the solvent cast blends. Unfortunately the statistics at high Q vectors are not sufficient to be able to observe the wavevector cut-off Qc directly at these temperatures. It is suspected that at high temperatures the quench depth dependence is present, but cannot be observed because the time period over which the correlation length remains constant is shorter than the time slicing period of 10s.

Data for the growth of the correlation length as a function of log time for the equivalent undeuterated PMMA composition studied by SAXS is shown in Fig. 61. Compare Figs. 61 and 69. The growth process is faster at a given temperature in the PMMA(D)/SCPE[67] than in the PMMA/SCPE[67] despite the slightly higher molecular weight of the PMMA(D). This difference probably arises from the slightly deeper quenches into the spinodal for the deuterated system compared with the hydrogenous system at a given temperature and suggests that during the growth stage observed phase separation is still being driven by the $\frac{\partial^2 G}{\partial \phi^2}$ term. The

classical view assumes that distinct coarsening processes are taking place when the correlation length starts to increase and there is no further phase separation. The data here suggests that this is not the case since the total integrated scattered intensity is still increasing during the observed coarsening providing strong evidence for the continued creation of new phase. Not surprisingly at no stage does the correlation length grow in a manner predicted by coalescence or Ostwald ripening theories.

Typical I(Q) plots are shown in Figs. 70 to 72 for the deuterated sample. The dominant features are the shift of the maximum in Q to lower values of Q with increasing time and the sharpening of the scattering peak. The movement of the peak to lower Q and its sharpening apparently result initially from high Q vectors, small wavelength fluctuations ceasing to grow exponentially in intensity. This arises because the short wavelength fluctuations approach equilibrium faster than longer wavelengths and the nonlinear terms neglected by Cahn become important sooner.

Guinier plots of LnI against Q^2 were plotted and were not linear during the early stages. An example is shown in Fig. 73a. The nonlinearity could reflect the absence of distinct particles and therefore provide evidence against a nucleation and growth mechanism, or reflect a polydisperse distribution of particles or aggregation of particles, or a spinodally decomposed structure.

During the late stages however Guinier plots were linear (Fig. 73b). This could be a result of the smaller particles in a nucleated system disappearing at the expense of larger particles and therefore the particle size distribution becoming more monodisperse. Alternatively, the sinusoidal concentration gradients in a spinodally decomposed system could cause this effect by becoming more square wave-like with time as predicted by Hillert[166].

Only at the lowest temperature studied (113°C) where the correlation length was initially time invariant did the scattered intensity grow exponentially. Typical LnI(Q) against time plots are shown in Fig. 74. Plots of LnI(Q) against time at 117°C are shown in Fig. 75. The initial slope of this plot was taken to obtain a lower estimate for R and $\overline{D}$. Values for Qm, R(Qm) and $\overline{D}$ are listed in Table 19. The values for the Cahn-Hilliard diffusion coefficient in Table 19 are very low compared with published values[89,90,102] for the PS/PVME blends that are in the range 10^{-10}-10^{-13} cm^2s^{-1}. However, the values seem respectable considering the high molecular weight of both components and the close proximity of both temperatures to the glass transition.

The diffusion coefficient of poly(methylmethacrylate) has recently been estimated by Jud[167] from fracture toughness studies of crack healing in compact tension specimens. Jud gives a value for PMMA ($\overline{M}w$ = 1.23x10^5, $\overline{M}w/\overline{M}n$ = 1.86) of 2.35 x 10^{-16} cm^2s^{-1} at 117°C. This value is comparable

to the Cahn-Hilliard diffusion coefficient obtained here for blends of PMMA and SCPE at 113°C and 117°C.

A plot of R(Q) against Q for the deuterated sample at 113°C is shown in Fig. 76. The cut-off wavevector cannot be precisely defined, but is greater than $\sqrt{2}$ Qm.

A plot of $R(Q)/Q^2$ against Q^2 should be linear and extrapolate to D_{app}. Clearly this plot (Fig. 77) exhibits marked curvature and is in disagreement with the Cahn-Hilliard theory. This could arise from a wave vector dependent diffusion coefficient as proposed by de Gennes[62] and Pincus[63], or be due to polydispersity. However, such curvature was also found for EVA/SCPE blends and PS/PVME blends where the correlation length is vastly in excess of the distance between entanglements. Small molecule systems, e.g. glasses, also show such curvature and it therefore appears that this discrepancy arises from a deficiency in the original Cahn-Hilliard theory, possibly as a result of assuming regular solution behaviour.

One of the faults of all the studies of spinodal decomposition is the analysis of the data assumes a sinusoidal concentration fluctuation, thus effectively assuming that spinodal decomposition is taking place. Analysis of the data in terms of a particle model (thus assuming a nucleation and growth model) ideally should be carried out as well.

Programs[168],[169] are readily available for the deconvolution of I(Q) into S(Q) and P(Q). These programs were originally developed for charged micelles[170],[171] and have been used in a SANS study of the nucleation and growth of ceramics[172]. Deconvolution of the scattering curve I(Q) was attempted for PMMA/SCPE kinetic data obtained by SANS. This approach was not very successful because a large range of particle diameters could be fitted to the experimental data for the following reasons:

1. Poor statistical accuracy of I(Q) scattering pattern particularly during the early stages.

2. Broad diffuse peaks not being covered by the comparatively small Q range of D11.

3. The loss of the low Q data particularly for the late stages when the statistics are good and the peak in I(Q) is sharper.

These problems cannot be overcome using the D11 camera without resorting to quenched samples and measuring I(Q) over two adjacent Q ranges.

Deconvolution of the SALS data was not undertaken because of the limited number of experimental points and the lack of high Q data. The SAXS data covers a wide Q range, but is not in a suitable format for

carrying out deconvolution readily and the subtraction of the large amount of parasitic scattering will distort I(Q) at very low Q. This approach of analysing the data in terms of a particle model is still felt to be worthwhile for good quality SAXS data or SANS data collected over a wider Q range.

CHAPTER 11

DISCUSSION

Unlike small molecule mixtures, notably the extensively studied aluminium/zinc alloy system, the polymer mixtures studied here exhibit a well defined spinodal. The sharp spinodal boundary has been predicted theoretically by de Gennes and Binder. Binder also predicts that homogenous nucleation and growth will be suppressed in high molecular weight mixtures and this is indeed found to be the case in these experiments. In the absence of any heterogenous nucleii, measured phase boundaries for the two high molecular weight blends studied (EVA/SCPE and PMMA/SCPE) correspond to the spinodal, whilst the measured phase boundary corresponds to the binodal in oligomeric mixtures of PS/PB.

EARLY STAGES

The early stages of the spinodal decomposition process cannot be followed in polymer mixtures as readily as might be first expected. However, with the systems studied here the mobility of the blends could be reduced by moving the phase boundary to lie close to the glass transition temperature of the mixture (PS/PB and PMMA/SCPE) or by using a blend where diffusion by reptation is suppressed by chain branching (EVA/SCPE). In this way the early stages could be followed.

During the early time period the following features predicted by the C/H theory were observed for the three systems studied.

1. Development of a scattering maximum.
2. Exponential growth of the most rapidly growing wavevector.
3. An approximately time invariant correlation length.
4. Observation of an interconnected structure with a diffuse interface.

However, the C/H theory does not satisfactorily predict the wavevector dependence of the growth rate, nor the observed ratio of Qc/Qm which is always greater than the predicted value of $\sqrt{2}$.

These deficiencies of the theory could arise from neglect of the non-linear terms, neglect of thermal fluctuations, or the invalid assumption of the free energy/composition diagram being adequately described by regular solution theory.

TEMPERATURE DEPENDENCE OF THE INITIAL CORRELATION LENGTH

Cahn[44], assuming a regular solution theory description for the free energy composition diagram and a purely entropic driving force for phase demixing, predicted that the wavevector maximum Qm would be given by:

$$Qm \propto \left[\frac{Ts-T}{Ts}\right]^{\frac{1}{2}}$$

This relationship was not found to be valid for the PS/PB system and most of the EVA/SCPE mixtures studied.

The possibility that the observed results could be explained by an increase in the dimensions of the polymer coils with increasing quench depth can be discounted because only slight coil expansion or contraction has been observed[158,159] in polymer mixtures with respect to the corresponding polymer melt.

The assumption of a regular solution theory description for the free energy of mixing is questionable for polymers. Other descriptions for the free energy such as Flory-Huggins and Equation-of-State theories again assume an entropy driven phase separation and give rise to identical behaviour to that proposed by Cahn. Most high molecular weight polymer mixtures have thermodynamic behaviour dominated by specific chemical interactions and it is the dissociation of these interactions that is likely to drive the phase separation process.

Even with the PS/PB oligomer system that many workers regard as being modelled well by Flory-Huggins theory, evidence is emerging from neutron scattering studies that the $\partial^2G/\partial\phi^2$ term has a temperature dependence much less than the 1/T expected on entropic grounds. This is in agreement with the data presented in this thesis on PS/PB oligomers.

PREDICTION OF THE SIZE SCALE OF PHASE SEPARATION

None of the current theories for predicting the initial time invariant correlation length are satisfactory. The van Aartsen expression (equation 19) fails to predict the initial correlation length found for PS/PB oligomers where no chain entanglements can exist.

One of the two high molecular weight systems studied, PMMA/SCPE phase separates on a very small scale, which is in agreement with the theoretical predictions by de Gennes, Pincus and Binder that take into account the entangled nature of polymers. Whether the short correlation length arises, in this system, from the presence of entanglements cannot be ascertained with certainty due to the limited data and the polydispersity in molecular weight of the SCPE. A second prediction of the theoreticians is that the Cahn-Hilliard diffusion coefficient should be the same order of magnitude as the reptation diffusion coefficient of the mixture. The value for the Cahn-Hilliard diffusion coefficient of this system is indeed close to that for the reptation diffusion coefficient of poly(methylmethacrylate) calculated by Jud[167], thus providing some additional support for the entanglement theories.

The other high molecular weight polymer system studied EVA/SCPE phase separates on a scale comparable to that predicted by van Aartsen. In many respects this system is similar to the PS/PVME mixtures studied by

Snyder et al[88,90,107]. Both systems exhibit quenched depth dependence of the initial correlation length at some compositions, but not at others. In each of these systems one component is close to the entanglement molecular weight and in the case of EVA/SCPE, the EVA is branched, therefore translational motion by reptation would not be favoured and the entanglement theories need not apply. However, the PS/PVME mixture studied by Hashimoto et al[106] has both component polymers above their entanglement values, yet the initial correlation length is still the same magnitude as the system studied by Snyder et al. It is possible that Hashimoto et al are observing the late stages of phase separation and the early stages where the correlation length is the same order of magnitude as that found in the PMMA/SCPE mixture only last a few tenths of a second.

It is also likely that the failure of the current theories to predict the size scale of phase separation arises again from the assumption of inadequate thermodynamic models for the phase behaviour. For example the small scale of phase separation observed in PMMA/SCPE mixtures could result from the sudden dissociation of the specific interaction resulting in a very negative $\partial^2 G/\partial\phi^2$ term, whilst it is assumed in modelling the phase behaviour of this system that the enthalpy of mixing associated with the specific interaction is independent of temperature. Conversely, the larger than predicted correlation length in PS/PB oligomer mixtures could arise from χ the thermodynamic interaction parameter

having a temperature dependence much less than the 1/T expected from Flory-Huggins theory.

LATE STAGES

As phase separation proceeds the Cahn-Hilliard theory starts to breakdown very rapidly for two reasons:

1. Failure of the theory to take into account the nonlinear terms.
2. The $\partial^2 G/\partial\phi^2$ term is unlikely to be constant during the phase separation process and if it has any meaning once phase separation has occured, it would be expected to become less negative as equilibrium is approached.

This results in the scattered intensity failing to continue to grow exponentially and the wavevector maximum moving to smaller angles. An interconnected morphology was still observed during the late stages for EVA/SCPE and PMMA/SCPE mixtures in contradiction to the theory proposed by Siggia[58] and emphasised by Snyder et al[39]. These authors have emphasised that separate mechanisms occur during the late stages, that start with the breakup of the interconnected structure into dispersed and matrix phases. The results of Snyder et al[88,90,107] may well be influenced by the thin films used. Studies on mixtures of small molecules and of polymers[56] indicate that the interconnected structure breaks down when the correlation length approaches the film thickness.

Siggia emphasises the idea that the interconnected morphology breaks down, because mathematically the Cahn-Hilliard theory cannot be readily extended to late times. Mcmaster's model for the late stages is qualitatively correct in that it assumes an interconnected structure. However, the data for the three systems studied does not agree with the predicted exponential growth. Hillert[166] extended the C/H theory by including more of the nonlinear terms and predicts that the correlation length will grow and the concentration fluctuations will become less sinusoidal and more square wave in nature. This prediction is in better agreement with the results found for the three systems studied here.

POSSIBLE THEORETICAL DEVELOPMENTS

The linearized Cahn-Hilliard theory is a good first approximation in analyzing spinodal decomposition of polymer melts. The main deficiency in predictions of early stage behaviour of this theory and those theories based on it is the assumption of an entropy driven phase separation. It is hard to suggest simple ways of improving the C/H theory in a way that would be applicable to all systems. It might be useful to try and model a system in thermodynamic terms without resorting to using an entropy driving force to produce demixing. The current equation of state theories for modelling polymer-polymer miscibility utilize a non-combinatorial entropy term in order to achieve phase separa-

tion, whilst neglecting the fact that the heat of mixing term in most cases is not constant, but temperature dependent.

The C/H theory could be improved by replacing the regular solution description of the free energy of mixing with a more accurate description, in which the phase separation was brought about by a reduction in the heat of mixing. Comparing kinetic data with predictions of the modified theory could then be carried out to see if any improvement had been made.

REFERENCES

1. Olabisi, O., Robeson, L.M. and Shaw, M.T. "Polymer-Polymer Miscibility", Academic Press N.Y. (1979).
2. Paul, D.R. and Newman, S. eds. "Polymer Blends", Vols. 1 and 2, Academic Press N.Y. (1978).
3. Sanchez, I.C. Ann. Review Mater. Sci. 13, 387 (1983).
4. Gibbs, J.W. "Scientific Papers", p.105-252, Dover N.Y. (1961).
5. Flory, P.J., J. Chem. Phys. 10, 51-60 (1940).
6. Huggins, M.L. Ann. N.Y. Acad. Sci. 43 (1942).
7. Flory, P.J. J. Chem. Phys. 9, 660 (1941).
8. Flory, P.J. Discuss. Faraday Soc. 49, 7 (1970).
9. Flory, P.J., Orwoll, R.A. and Vrij, A. J. Am. Chem. Soc. 86, 3515 (1964).
10. Flory, P.J. J. Am. Chem. Soc. 87, 1833 (1965).
11. Zhikuan, C. and Walsh, D.J. Die Macromol. Chem. 184, 1459 (1983).
12. Doubé, C.P. and Walsh, D.J. Polymer 20, 1115 (1979).
13. Walsh, D.J., Higgins, J.S., Rostami, S. and Weeraperuma, K. Macromolecules 16, 391 (1983).
14. Walsh, D.J. and Cheng, G.L. Polymer 25, 499 (1984).
15. Ferry, J.D. "Viscoelastic Properties of Polymers", 3rd Ed., Wiley N.Y. (1980).
16. Tirrel, M. Rubber Chemistry and Technology 57, 523 (1984).

17. de Gennes, P.G. "Scaling Concepts in Polymer Physics", Cornell University Press, Ithaca (1979).

18. de Gennes, P.G. Physics Today 33, 416 (1983).

19. Edwards, S.F. Proc. Phys. Soc. London 92, 9 (1967).

20. Klein, J. Nature 271, 143 (1978).

21. Klein, J. and Briscoe, B.J. Proc. Roy. Soc. London A 365, 53 (1979).

22. Klein, J. and Briscoe, B.J. J. Polym. Sci. Phys. Ed. 15, 2065 (1977).

23. Leger, L., Hervet, H. and Rondelez, F. Macromolecules 14, 1732 (1981).

24. Klein, J. Macromolecules 14, 460 (1981).

25. Doi, M. and Edwards, S.F. J. Chem. Soc. Faraday Trans. 2, 1789.

26. Rouse, P.E. J. Chem. Phys. 21, 1273 (1953).

27. Bachus, R. and Kimmich, R. Polymer 24, 964 (1983).

28. Fleischer, G. Polym. Bull. 9, 152 (1983).

29. Smith, B.A. Samulski, E.T., Yu, L.P. and Winnik, M.A. Phys. Rev. Lett. 15, 45 (1984).

30. Klein, J. Nature 304, 526 (1983).

31. de Gennes, P.G. J.Phy. 36, 1199 (1975).

32. Richter, D., Baugartner, A., Binder, K., Ewen, B. and Hayter, J.B.

33. Higgins, J.S. and Roots, J. Unpublished Paper.

34. Boué, F., Nierlich, M., Jannink, G. and Ball. R. J. Phys. Paris Lett. 43, L585 (1982).

35. Gilmore, P., Falabella, R. and Lawrence, R.L. Macromolecules 13, 880 (1980).

36. de Gennes, P.G., C.R. Seances Acad. Sci. Ser. 2 292, 1505 (1981).

37. Binder, K. and Stauffer, D. Phys. Rev. Lett. 33, 1006 (1974).

38. Goldburg, W.I. and Huang, J.S. in "Fluctuation Instabilities and Phase Transitions", ed. T. Riste (1975).

39. Snyder, H.L. and Meakin, P. J. Chem. Phys. 79, 5588 (1983).

40. Cahn, J.W. and Hilliard, J.E. J. Chem. Phys. 28, 258 (1958).

41. Cahn, J.W. and Hilliard, J.E. J. Chem. Phys. 31, 688 (1959).

42. Cahn, J.W. Acta Metall. 9, 795 (1961).

43. Cahn, J.W. Trans. Metall. Soc. AIME 242, 166 (1968).

44. Cahn, J.W. J. Chem. Phys. 42, 93 (1965).

45. Langer, J.S. "Fluctuations and Instabilities", Ed. T. Riute, Plenum New York (1975).

46. Hilliard, J.E. Phase Transformations, Ed. Aaronson, H.I. Am. Soc. Met. Metals Park Ohio (1970).

47. Binder, K. Phys. Rev. B15 nom 4425 (1977).

48. Cook, H.E. Acta Metall. 18, 297 (1970).

49. Park, M.W., Cooper, A.R. and Hener, A.H. Scripta. Met. 9, 321 (1975).

50. Langer, J.S. Ann. Phys. 65, 53 (1971).

51. Langer, J.S. Actal. Metall. 21, 1649 (1973).

52. Langer, J.S., Bar-on, M. and Miller, H.D. Phys. Rev. All, 1417 (1975).

53. Kawasaki, K. and Ohta, T. Progr. Theor. Phys. 59, 362 (1978).

54. Jain, S.C. and Huges, A.E. J. Mat. Sci. 13, 1611 (1978).

55. Lifshitz, I.M. and Slyozo, V.V. J. Phys. Chem. Solids 19, 35 (1961).

56. Mcmaster, L.P. Adv. Chem. Ser. 43, 142 (1975).

57. Tomotika, S. Proc. Roy. Soc. London 150, 332 (1935).

58. Siggia, E.D. Phys. Rev. A20, 595 (1979).

59. Binder, K. J. Chem. Phys. 79, 6287 (1983).

60. Joanny, J.F. and de Gennes, P.G. J. Chem. Phys. All, L117 (1978).

61. de Gennes, P.G. J. Phys. Lett. (Paris) 38, L441 (1977).

62. de Gennes, P.G. J. Chem. Phys. 72, 4756 (1980).

63. Pincus, P. J. Chem. Phys. 75, 1996 (1981).

64. van Aartsen, J.J. Eur. Polym. J. 6919 (1970).

65. de Gennes, P.G. Journal de Physique 42, 735 (1981).

66. Kerker, M. "Scattering of Light and Other Electromagnetic Radiation", Academic Press New York (1969).

67. Stein, R.S. and Rhodes, M.B. J. Appl. Phys. 31, 1873 (1960).

68. Huglin, M.B. "Light Scattering from Polymer Solutions", Academic Press London (1972).

69. Chu, B. "Laser Light Scattering", Applied Science London (1974).

70. Maconnachie, A. and Richards, R.W. Polymer 19, 739 (1978).

71. Higgins, J.S. in "Neutron Scattering in Material Science", Ed. G. Kostorz (1978).

72. Stuhrmann, H.B. "Small Angle X-ray Scattering of Macromolecules in Solution", Chap. 15 (1980).

73. Glatter, O. and Kratky, O. "Small Angle X-ray Scattering", Academic Press N.Y. (1982).

74. Rundman, K.B. and Hilliard, J.E. Acta. Metall. 15, 1025 (1967).

75. Walker, C.B. and Guinier A. Acta. Metall. 1, 568 (1953).

76. Guinier, A. Ann. Phys. 12, 161 (1939).

77. Wright, A.F., Nunn, S. and Brett, N.H. Proc. of Conference "Zirconia 83", Stuttgart 1983. Advances in Ceramics, American Ceramic Society.

78. Wright, A.F., McMillan, P.W. and Brett, N.H. "The Structure of Non Crystalline Materials", Proc. of the 2nd Intnl. Conf. Physics and Chemistry of Glasses Conference Volume (1982).

79. Rundman, K.B. and Hilliard, J.E. Scr. Metall. 1, 37 (1967).

80. Agarwal, S. and Herman, H. Scr. Metall. 7, 503 (1973).

81. Nielsen, G.F. Phys. Chem. Glasses 10, 54 (1969).

82. Srinivivasan, G.R., Colletta, R. and Macebo, P.B. Phys. Chem. Glasses 14, 90 (1973).

83. Acuna, R.J. and Craivich, A.F. J. Non Crystalline Solids 24, 13 (1982).

84. Pines, E. and Prins, W. Macromolecules 6, 888 (1973)

85. Nojima, S. and Nose, T. Polymer J. 14, 269 (1982).

86. Russel, T.P., Hadziioanou, G. and Warburton, M. Macromolecules 18, 78 (1985).

87. Smolders, C.A. and van Aartsen, J.J. Eur. Polym. J. 6, 1105 (1970).

88. Snyder, H.L. and Meakin, P. J. Chem. Phys. 79, 5588 (1983).

89. Nish, T., Wang, T.T. and Kwei, T.K. Macromolecules 8, 227 (1975).

90. Snyder, H.L. and Meakin, P. J. Polym. Sci. Macromol. Rev. (in press).

91. Goldburg, M.S. J. Chem. Phys. 68, 484 (1978).

92. Knobler, C.M. and Wang, T.T. J. Chem. Phys. 66, 4707 (1977).

93. Chou, Y.C. and Goldburg, W.I. Physical Review A20, 2105 (1979).

94. Debye, P. J. Chem. Phys. 31, 680 (1959).

95. Ditchek, B. and Schwartz, L.H. Ann. Rev. Mater. Sci. 9, 219 (1979).

96. Gerold, V. and Kostorz, G. J. Appl. Cryst. 11, 376 (1979).

97. Gerold, V. and Merz, W. Scr. Metall. 1, 33 (1967).

98. Junqua, A., Mimault, J. and Delaford, J. Acta. Metall. 24, 779 (1976).

99. La slaz, G., Kostorz, G., Roth, M., Guyot, P. and Stewart, R.J. Phys. Stat. Sol. 41, 577 (1977).

100. La slaz, G., Guyot, P. and Kostorz, G. J.P. Phys. C7, 406 (1977).

101. Cartraud, M., Guillot, J., Mimmault, J. and Grillné, J. Scripta Metall. 13, 281 (1979).

102. Nojima, S., Tsutsumi, K. and Nose T. Polymer J. 14, 225 (1982).

103. Nojima, S. Okyami, Y., Yamaguchi, M. and Nose, T. Polymer J. 14, 907 (1982).

104. Gelles, R. and Frank, C. Macromolecules 15, 1481 (1982).

105. Gelles, R. and Frank C. Macromolecules 16, 1448 (1983).

106. Hashimoto, T., Kumaki, J. and Kawai, H. Macromolecules 16, 641 (1983).

107. Snyder, H.L. Personal Communication.

108. Snyder, H.L. and Meakin, P. Macromolecules 16, 753 (1983).

109. Stein, R.S., Gilmer, J. and Goldstein, N. J. Polym. Sci. Phys. Ed. 20, 2219 (1982).

110. Higgins, J.S. Personal Communication.

111. Tripathi, S. PhD Thesis, Department of Chemical Engineering, Imperial College London (1981).

112. Koningsveld, R. and Kleintjens, L.A. Br. Polym. J. 10, 170 (1978).

113. Tomlins, P.E. and Higgins, J.S. Accepted for publication in Polymer.

114. Rostami, S. PhD Thesis, Department of Chemical Engineering, Imperial College London (1983).

115. Higgins, J.S. Personal Communication.

116. Yip, W. Unpublished work.

117. Chong, C.L. PhD Thesis, Department of Chemical Engineering, Imperial College London (1981).

118. Kleintjens, L.A. PhD Thesis, University of Essex, Colchester (1979).

119. Stehling, F.S., Ergas, E. and Mendelkern, L. Macromolecules 4, 672 (1971).

120. Strazielle, C. and Benoit, H. Macromolecules 8, 203 (1975).

121. Yang, H., Hadziianou, G. and Stein, R.S. J. Polym. Sci. Phys. Ed. 21, 159 (1983).

122. Buckingham, A.D. and Hertschel, H.G.E. J. Polym. Sci. Phys. Ed. 18, 853 (1980).

123. Zhikuan, C., Ruona, S., Walsh, D.J. and Higgins, J.S. Polymer 24, 263 (1983).

124. Rostami, S. PhD Thesis, Department of Chemical Engineering, Imperial College London 1983.

125. Chai, Z., Ruona, S., Walsh, D.J. and Higgins, J.S. Polymer 24, 283 (1983).

126. Rostami, S. and Walsh, D.J. Macromolecules 17, 315 (1984).

127. Chai, Z. and Higgins, J.S. Unpublished work.

128. Higgins, J.S. and Walsh, D.J. J. Polym. Eng. Sci. 24, 555 (1984).

129. Zhikuan, C. Unpublished work.

130. Zhikuan, C. PhD Thesis, University of London (1982).

131. Chai, Z. and Walsh, D.J., Makromol. Chem. 184, 1549 (1983).

132. Rostami, S. and Walsh, D.J. To appear in Macromolecules.

133. Walsh, D.J., Higgins, J.S. and Rostami, S. Macromolecules 16, 387 (1983).

134. Walsh, D.J. and Rostami, S. Adv. Polym. Sci. In press.

135. Coleman, M.M., Moskola, E.J., Painter, P.C., Walsh, D.J. and Rostami, S. Polymer 24, 1410 (1983).

136. Brydson, D. "Rubber Chemistry", Appl. Sci. (1978).

137. Walsh, D.J., Higgins, J.S. and Zhikuan, C. Polymer Communications 23, 336 (1982).

138. Zhikuan, C., Lianghe, S. and Sheppard, R.N. Polymer 25, 369 (1984).

139. Koningsveld, R. Adv. Polym. Sci. 7.

140. Small, P.A. Adv. Polym. Sci. 18.

141. Fetters, L.J. and Morton, M. Rubber Revs. 48, 359 (1973).

142. Kratky, O. and Skala, Z. Z. Electrochem. 62, 75 (1958).

143. Prentice, P. and Hashemi, S. J. Mat. Sci. 19, 519 (1984).

144. Billmeyer, F.W. "Textbook of Polymer Science", 2nd Edition, J. Wiley & Sons London (1971).

145. "Polymer Handbook", Interscience London (1966).

146. Ibel, K. J. Appl. Cryst. 9, 296 (1976).

147. Timmins, P.A. and May, R.P. "D11 Operating Manual", ILL, November (1981).

148. Ghosh, R. "A Computing Guide for Small Angle Scattering Experiments", ILL 81GH29T.

149. Helliwell, J.R. J.Phys. E. 201, 175 (1982).

150. Helliwell, J.R. J. Phys. E. 15, 1363 (1982).

151. Nave, C. "Facilities for Solution Scattering and Fibre Diffraction at the Daresbury SRS" (Unpublished paper).

152. Derham, K., Goldsbrough, J. and Gordon, M. Pure Appl. Chem. 38, 97 (1974).

153. Kennedy, J.W., Gordon, M. and Alvarez, G.A. Polymery. Warsaw 20, 463 (1975).

154. Atkin, E.L., Kleintjens, L.A., Koningsveld, R. and Fetters, L.J. Makromol. Chem. 185, 377 (1984).

155. Tomlins, P.E. Unpublished results.

156. Fox, T.G. and Flory, P.J. J. Appl. Phys. 21, 581 (1950).

157. Eskin, L. J. Polym. Sci. C16, 1619 (1967).

158. Hadziioannou, G. and Stein, R.S. Macromolecules 17, 567 (1984).

159. Higgins, J.S. and Tomlins, P.E. Unpublished work.

160. Chai, Z. Unpublished work.

161. Grosse, G. and Riess, K.F. Unpublished work quoted by Kiess, K.F. in Plast Kaut 12, 90 (1965).

162. Rueda, G., PhD Thesis, Department of Chemical Engineering, Imperial College London (in prep.).

163. Rueda, G. and Hill, R. (unpublished results).

164. Russel, T. Personal Communication.

165. Endres, B., Garbella, R.W., Hermann, O. Klemmer, N., Werdorff, J.H., Zietz, R. and Koch, M.H.J. HASYLAB Jahresbericht (1984)

166. Hillert, M. Acta. Metall. 9, 525 (1961).

167. Jud. K. These 413, Ecole Federale de Lausanne (1982).

168. Hayter, J.B. and Penfold, J. "A Fortran Package to Calculate S(Q) from Macroion Solutions", ILL Report (1982).

169. Hayter, J.B. "Trogs", A program for Fast Bidirectional Transforms between G(r) and S(Q), Ill Report No. 79HA48S.

170. Hayter, J.B. and Penfold, J. Colloid and Polymer Science Prepr. SA83-64.

171. Hansen, J.P. and Hayter, J.B. Molecular Physics 46, 651 (1982).

172. Wright, A. "Microstructure Control by Thermal Treatment", to be published.

173. Erb. D. PhD Thesis, Northwestern University, Evanston, Ill (1969).

174. Hilliard, J.E. Phase Transformations, Ed. Aaronson, H.I. Am. Soc. Met. Metals Park, Ohio, p. 497 (1970).

Table 1a Neutron Scattering Lengths for Carbon, Hydrogen, Deuterium, Oxygen and Chlorine

Element	$\bar{b} \times 10^{-12}$ cm
^{1}H	-0.374
^{2}H	0.667
^{12}C	0.665
^{16}O	0.580
Cl	0.960

Table 1b Summed Scattering Lengths (B)

$B = \Sigma\bar{b}$

Polymer	$B \times 10^{-12}$ cm
Deuterated PMMA (D)	9.82
Hydrogenous PMMA	1.49
$SCPE^{72}$	3.02
$SCPE^{67}$	2.38
$SCPE^{61}$	1.73
$SCPE^{57}$	1.53
$SCPE^{50}$	1.08

Table 2 Relative cross-sections (contrast) and time to obtain a scattering pattern for hydrogenous and fully deuterated Poly (methylmethacrylate)s with a range of solution chlorinated polyethylenes

SCPE	Contrast with PMMA	Time	Contrast with PMMA(D)	Time
$SCPE^{72}$	2.33	60s	46.25	3.1s
$SCPE^{67}$	0.79	180s	55.36	2.6s
$SCPE^{61}$	0.06	2400s	65.46	2.2s
$SCPE^{57}$	0.0013	30Hrs	68.74	2.1s
$SCPE^{50}$	0.17	840s	76.40	1.9s

Table 3 Characteristics of Chlorinated Polyethylenes

Description	Code	Source	$\overline{M}w$	$\overline{M}n$	Weight % Cl	Tg	RFI
Commercial Chlorinated Polyethylene	H48	Dupont	-	-	48.0	-	1.49
Solution Chlorinated Polyethylene	$SCPE^{50}$	Laboratory Prepared	$9.0x10^5$	$1.4x10^5$	50.0	30°C	1.51
Fractionated Solution Chlorinated Polyethylene Fifth Fraction	$SCPE^{50}/5$	Laboratory Prepared	$1.3x10^4$	$1.1x10^4$	50.0	30°C	1.51
Solution Chlorinated Polyethylene	$SCPE^{67}$	Laboratory Prepared	$8.0x10^5$	$1.2x10^5$	67.5	121°C	1.51
Solution Chlorinated Polyethylene	$SCPE^{72}$	Laboratory	$8.8x10^5$	$1.3x10^5$	72.0	144°C	1.51

Table 4 Characteristics of Ethylene Vinyl-acetate Copolymers

Description	Code	Source	$\overline{M}w$	$\overline{M}n$	Weight % vinylacetate	Tg	RFI #
Ethylene vinyl acetate copolymer	EVA^{45}	ICI	1.2×10^6	8.0×10^4	45	-20°C	1.42
Fractionated Ethylene vinyl acetate copolymer	$EVA^{45/3}$	ICI	4.0×10^5	1.5×10^5	45	-20°C	1.42
Ethylene vinyl acetate copolymer	EVA^{40}	ICI	-	-	40	-20°C	1.40

refractive indices calculated assuming mixture of Polyethylene and Polyvinylacetate

Table 5 Characteristics of Poly(methylmethacrylates)

Description	Code	Source	$\bar{M}w$	$\bar{M}n$	Tg	RFI
Atactic Poly(methylmethacrylate)	PMMA	Polysciences	8.4×10^4	3.5×10^4	107°C	1.47
Atactic Deuterated Poly(methylmethacrylate) (> 98%)	PMMA(D)	Laboratory Prepared	9.6×10^4	7.4×10^4	107°C	-

Table 6 Characteristics of Polystyrene Oligomers

Description	Code	Source	$\bar{M}w$	$\bar{M}n$	Tg	RFI
Oligomeric Polystyrene	PS1460	Polymer Lab.	1460	1340	80°C	1.59
Oligomer Polystyrene	PS4500	Polymer Lab.	4500	4090	80°C	1.59

Table 7a Characteristics of Polybutadiene Oligomers

Description	Code	Source	$\bar{M}w$	$\bar{M}n$	Tg	RFI
Oligomeric Polybutadiene	PB960	Polymer Lab.	960	1340	-60°C	1.50
Oligomer Polybutadiene	PB2600	Polymer Lab.	2660	2354	-60°C	1.50
Deuterated Polybutadiene 98%	PB(D)	L.Fetters Laboratory Prepared	3260	2810	-60°C	1.50

Table 7b Microstructure Polybutadienes

Code	%CIS	% TRANS	% VINYL
PB2660	41±2	49±2	10±2
PB960	39±2	50±2	11±2
PBD	36±4	54±4	10±2

Table 8 Diode Characteristics

Parameter	Typical Value
Sensitivity	60mV/μW/cm^2
Rise time	50μs
Fall time	50μs
Dark level Temperature coefficient	150μV/°C
O/P Noise Voltage	1mV rms

Table 9 Stability of Laser Light Sources

He/Ne				He/Cd			
5s readings		100s readings		5s readings		100s readings	
Mean	S.D. n=10	Mean	S.D. n=10	Mean	S.D. n=10	Mean	S.D. n=10
1007	13	994	21	1002	33	1001	45

Table 10 Errors in Diode Normalisation

Diode Number	He/Ne Laser Mean	He/Ne Laser S.D	He/Cd Laser Mean	He/Cd Laser S.D
1	530	21	773	38
2	537	12	775	29
3	508	9	744	31
4	593	39	837	22
5	594	23	844	41
6	598	21	850	19
7	601	33	857	35
8	614	12	662	21
9	489	19	705	43
10	553	23	765	27
11	555	17	794	41
12	573	41	807	23
13	598	23	842	41
14	537	17	752	39
15	571	18	800	53
16	537	26	757	17

Table 11 R(Qm), $\overline{D}$, Dm (Initial) and Qm as a function of temperature for a mixture of PS 1460/ PB 2660 containing 70% PS

Temperature 5°C	R(Qm) ($x10^{-3}s^{-1}$	$\overline{D}$ ($x10^{-13}cm^2s^{-1}s$)	Dm(initial) (μm)	Qm ($x10^{-4}Å^{-1}$)
46.2*	-	-	-	-
43.4	0.85	-3.1	0.85	7.38
42.25	3.0	-10.8	0.65	9.66
42.0	3.75	-9.7	0.71	8.85
38.8	1.05	-2.2	0.65	9.66
35.2	1.10	-2.1	0.61	10.30

*The mixture does not phase separate at this temperature

Table 12 Elemental Analysis of $SCPE^{50}$ Fractions

Code	$\overline{Mn}$	% Cl (Estimated error±1%
$SCPE^{50}$	$1.4x10^5$	50.4
$SCPE^{50}/1$	$9.0x10^4$	49.6
$SCPE^{50}/2$	$5.3x10^4$	49.1
$SCPE^{50}/5$	$1.0x10^4$	51.8

Table 13 Elemental Analysis of EVA^{45} Fractions

Code	$\overline{Mn}$	% Oxygen Estimated error±0.5%
EVA^{45}	$8.0x10^4$	18.9
$EVA^{45}/2$	$4.0x10^5$	18.4
$EVA^{45}/3$	$1.5x10^5$	18.3
$EVA^{45}/5$	$2.8x10^4$	19.4

Table 14 Values for R(Qm), Qm and $\overline{D}$ for a mixture of $EVA^{45}/^{3}/SCPE^{50}/^{5}$ containing 13% EVA

Temperature °C	R(Qm) ($x10^{-3}s^{-1}$)	Qm ($x10^{-4}Å^{-1}$)	$\overline{D}$ ($x10^{-12}cm^{2}s^{-1}$)
54.4	2.38	9.13	-0.57
64.9	9.75	9.13	-2.33
70.1	21.0	9.13	-5.04
83.9	51.6	9.13	-12.24

Table 15 Values for R(Qm), Qm and $\overline{D}$ for a mixture of $EVA^{45}/^{3}/SCPE^{50}/^{5}$ containing 24% EVA

Temperature °C	R(Qm) ($x10^{-5}s^{-1}$)	Qm ($x10^{-4}Å^{-1}$	$\overline{D}$ ($cm^{2}s^{-1}$)
55.3	5.5	10.18	$-1.06x10^{-14}$
63.8	32	10.63	$-5.66x10^{-11}$
73.8	86	8.81	$-2.22x10^{-10}$
86.0	71	9.73	$-1.50x10^{-9}$
99.3	3900	9.73	$-8.24x10^{-9}$
99.9	5800	10.18	$-1.11x10^{-8}$

Table 16 Values for R(Qm), Qm and $\bar{D}$ for a mixture of $EVA^{45/3}/SCPE^{50/5}$ containing 55% EVA

Temperature °C	R(Qm) ($x10^{-3}s^{-1}$)	Qm ($x10^{-4}Å^{-1}$)	$\bar{D}$ ($\times cm^2s^{-1}$)
95.6	1.94	2.48	$-6.30x10^{-12}$
100.4	5.5-6.0	3.63-4.58	$-5.72-8.34x10^{-12}$ #
105.2	2.92-40.8	3,89-5.30	$-5.39-20.7x10^{-12}$
106.0	10.9	2.66-3.14	$-3.08-2.21x10^{-11}$
107.7	67.5	5.54	$-4.39-x0^{-11}$
112.1	43.1	3.63-4.11	$-5.10-6.54x10^{-11}$
116.0	130	6.01	$-7.19x10^{-11}$
118.1	250	6.49	$-11.87x10^{-11}$

Experimental range of values

Table 17 Values for R(Qm), Qm and $\bar{D}$ for a mixture of $EVA^{45}/3/SCPE^{50}/5$ containing 59% EVA

Temperature °C	R(Qm) ($x10^{-3}s^{-1}$)	Qm ($x10^{-4}Å^{-1}$)	$\bar{D}$ ($x10^{-12}cm^2s^{-1}$)
117.6	5.9	1.77	-3.75
126.2	14.6	1.70	-10.1
128.0	55	2.48	-17.9
129.7	30-44	3.63	-4.5-6.7
130.9	46.9	4.58	- 4.41

Table 18 Values for R(Qm), Qm and $\bar{D}$ for a mixture of $EVA^{45/3}/SCPE^{50/5}$ containing 62% EVA

Temperature °C	R(Qm) ($x10^{-3}s^{-1}$)	Qm ($x10^{-4}Å^{-1}$)	$\bar{D}$ ($x10^{-12}cm^2s^{-1}$)
138.1	4.25	1.21	-5.81
#143.3	> 7.0	1.70	>-4.84

Ln(I) time plot not very linear early stages very short at this temperature

Table 19 Values for R(Qm), Qm and $\bar{D}$ for a PMMA(D) $SCPE^{67}$ mixture containing 55% SCPE

Temperature °C	R(Qm) ($x10^{-3}s^{-1}$)	Qm ($10^{-2}Å^{-1}$)	$\bar{D}$ ($x10^{-15}cm^2s^{-1}$
113	16.8	1.76	-1.1
117	32.3	2.20	-13.3

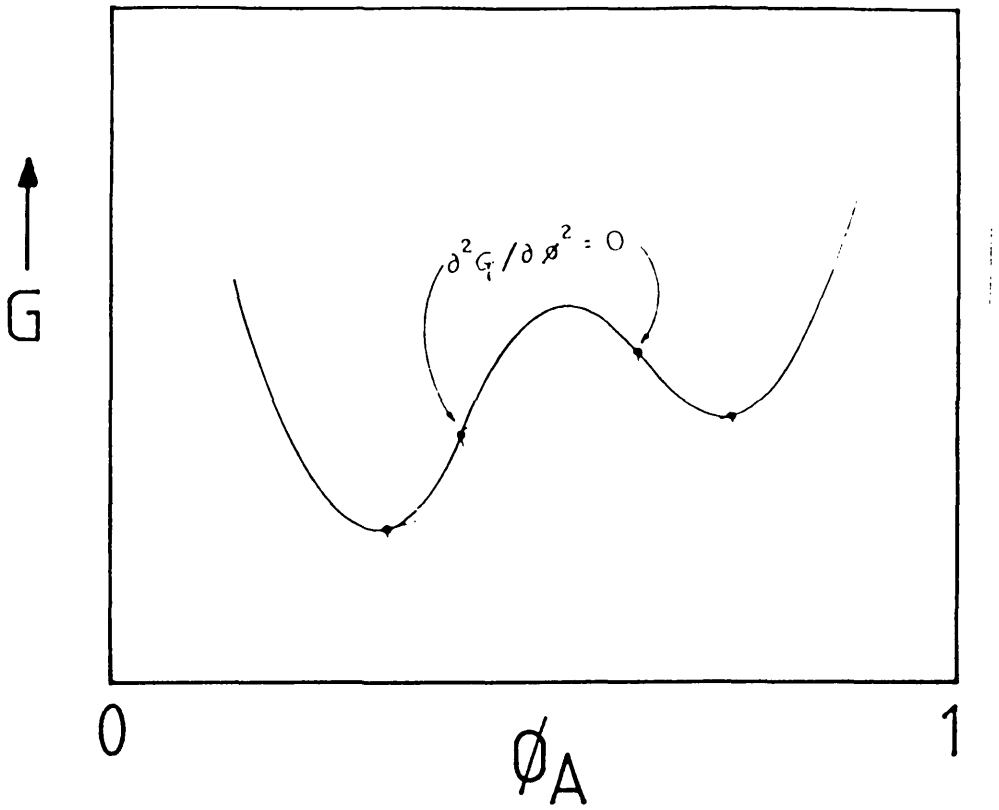


Fig.1 Plot of the free energy of mixing as a function of composition.

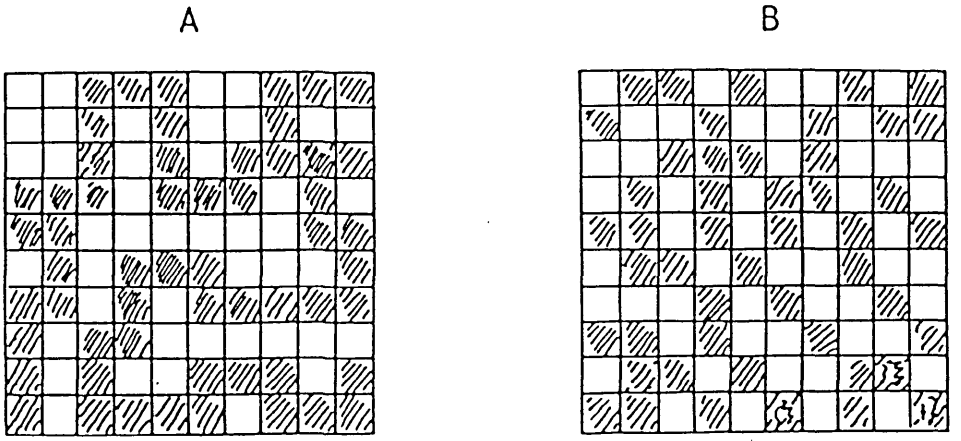


Fig.2 Illustration of the Lattice Model showing the arrangement of small molecules on the Lattice (B) and the arrangement of polymer molecules (A).

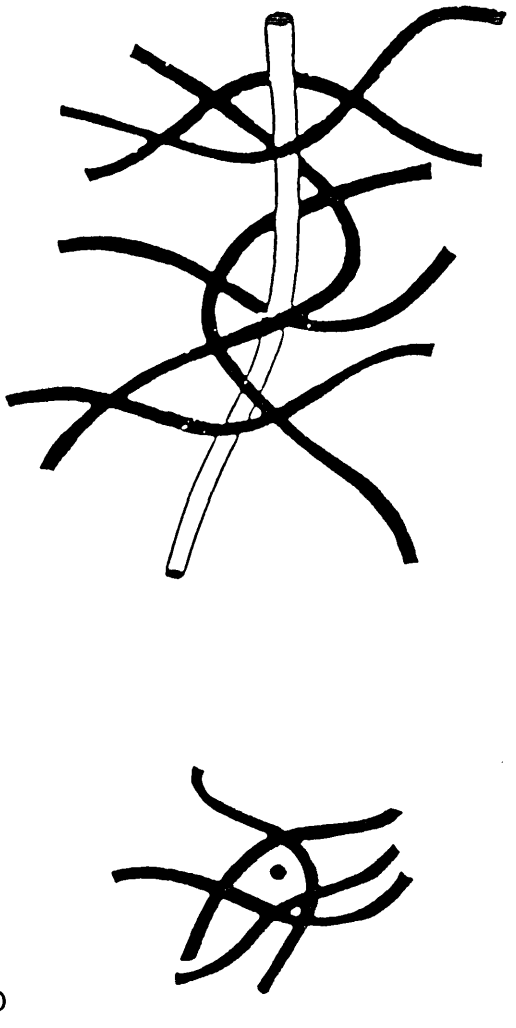


Fig.3 Schmatic illustration of the Reptation entanglement model of Polymer diffusion showing a polymer chain trapped within its tube.

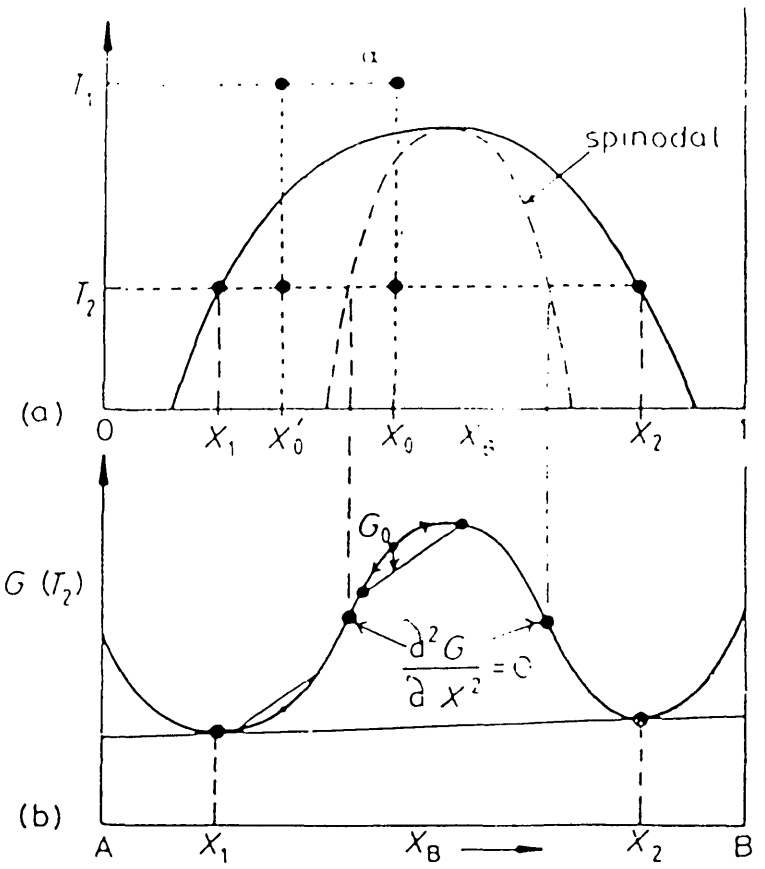


Fig.4 Polymer mixtures between spinodal points are unstable and can decompose into two phases χ_1 and χ_2 without overcoming an activation energy barrier. Polymer mixtures between the binodal and spinodal decompose by nucleation.

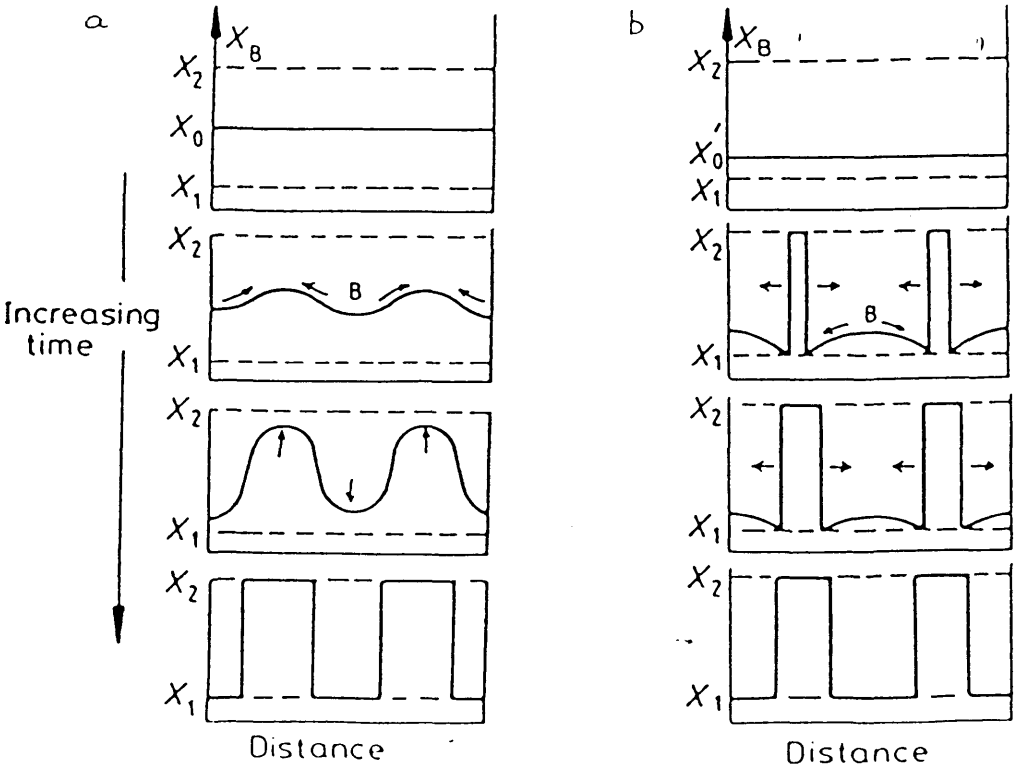


Fig.5 Schematic composition profiles at increasing times in a polymer mixture (a) quenched into the spinodal region (Xo in Fig.4), (b) quenched into the metastable region (Xó Fig.4).

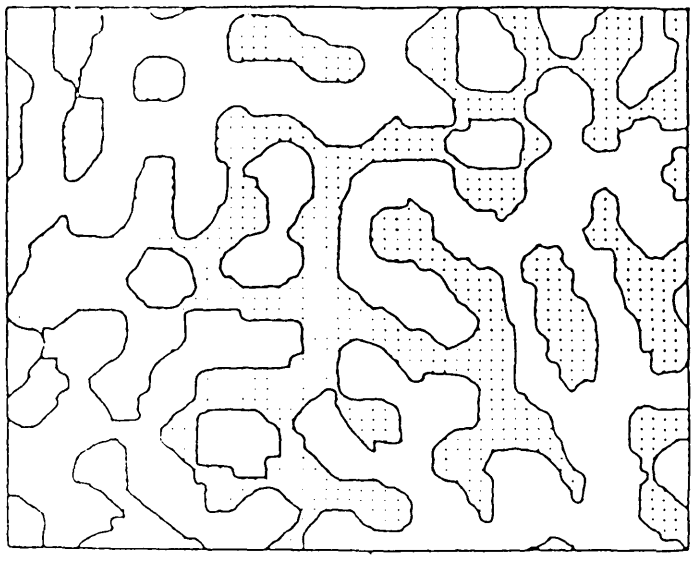


Fig.6 Computer simulation of an interconnected structure taken from Cahn.

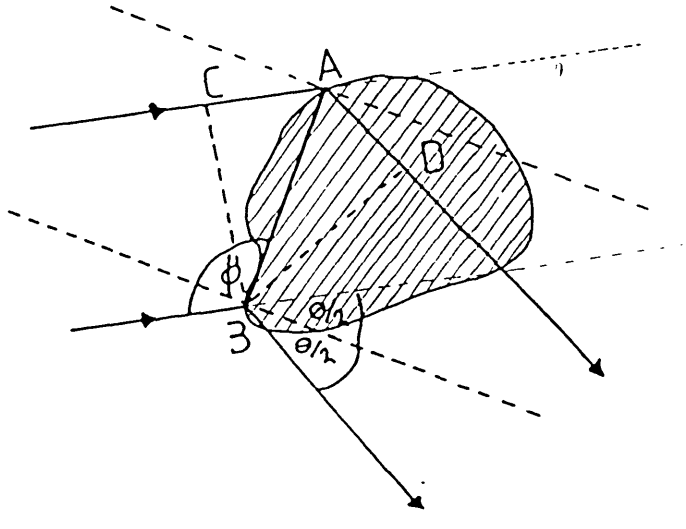


Fig.7 Scattering diagram

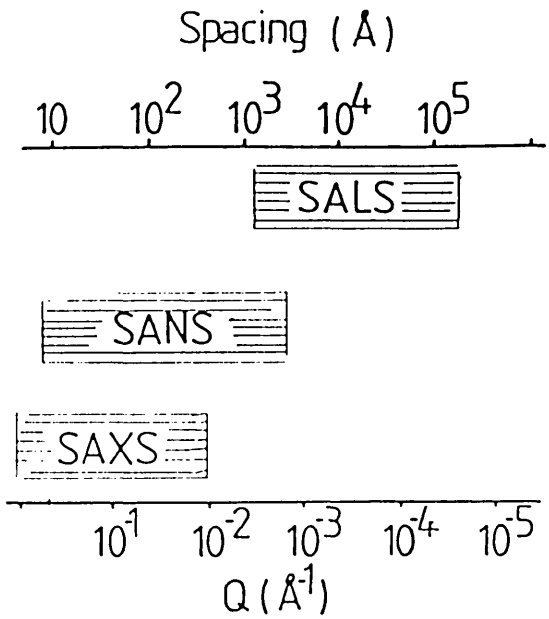


Fig.8 Range Accessible to SANS, SAXS and SALS.

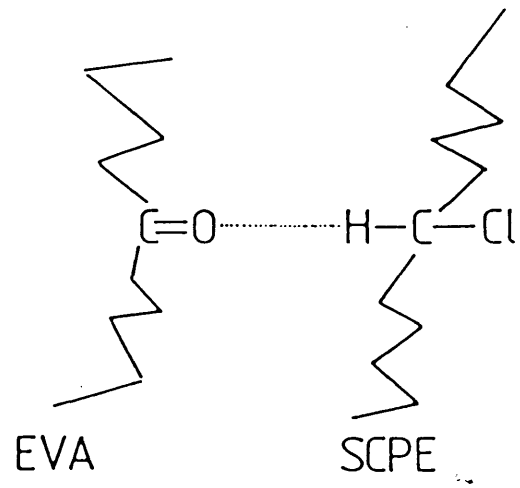


Fig.9 Illustration of a hydrogen bond specific interaction in an EVA/SCPE mixture.

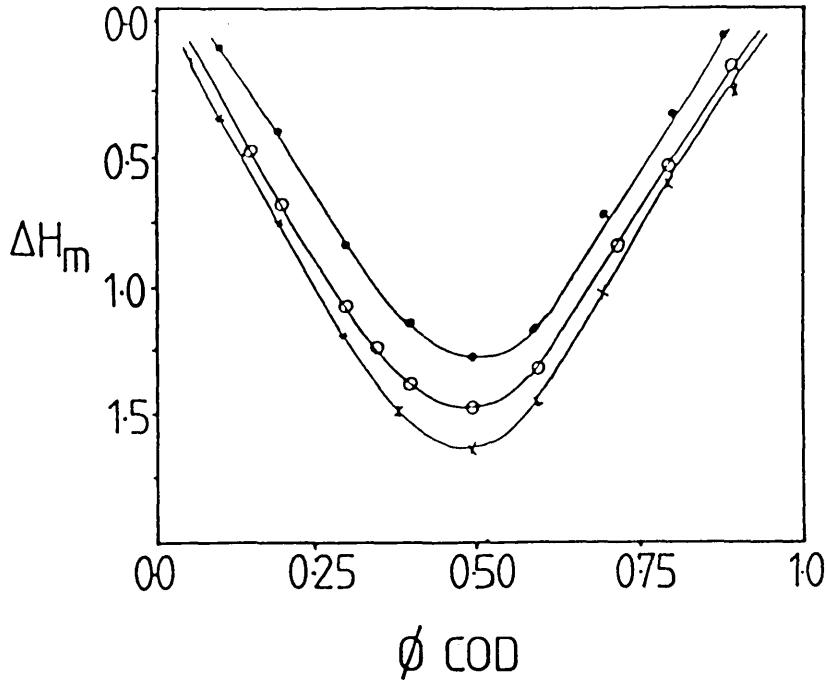


Fig.10 Heat of mixing of sec octylacetate and chlorinated octadecane at three temperatures.

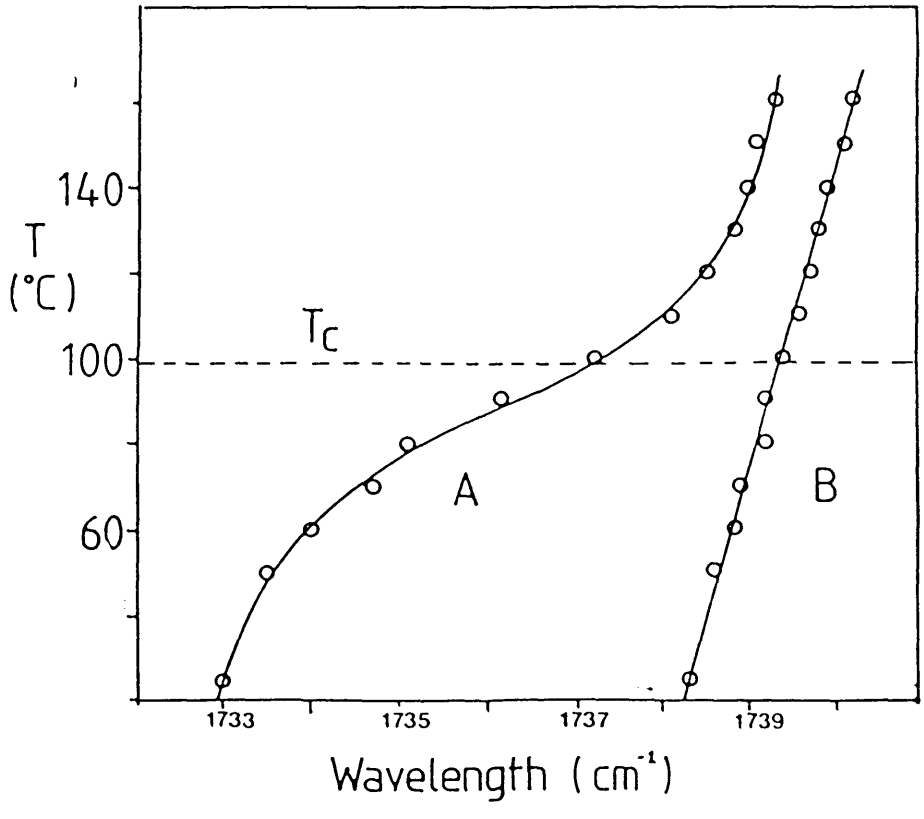


Fig.11 Shift of the carbonyl group stretching frequency in EVA. A is an 80/20EVA/SCPE blend and B is pure EVA. The stretching frequency shifts back to that of pure EVA on phase separation.

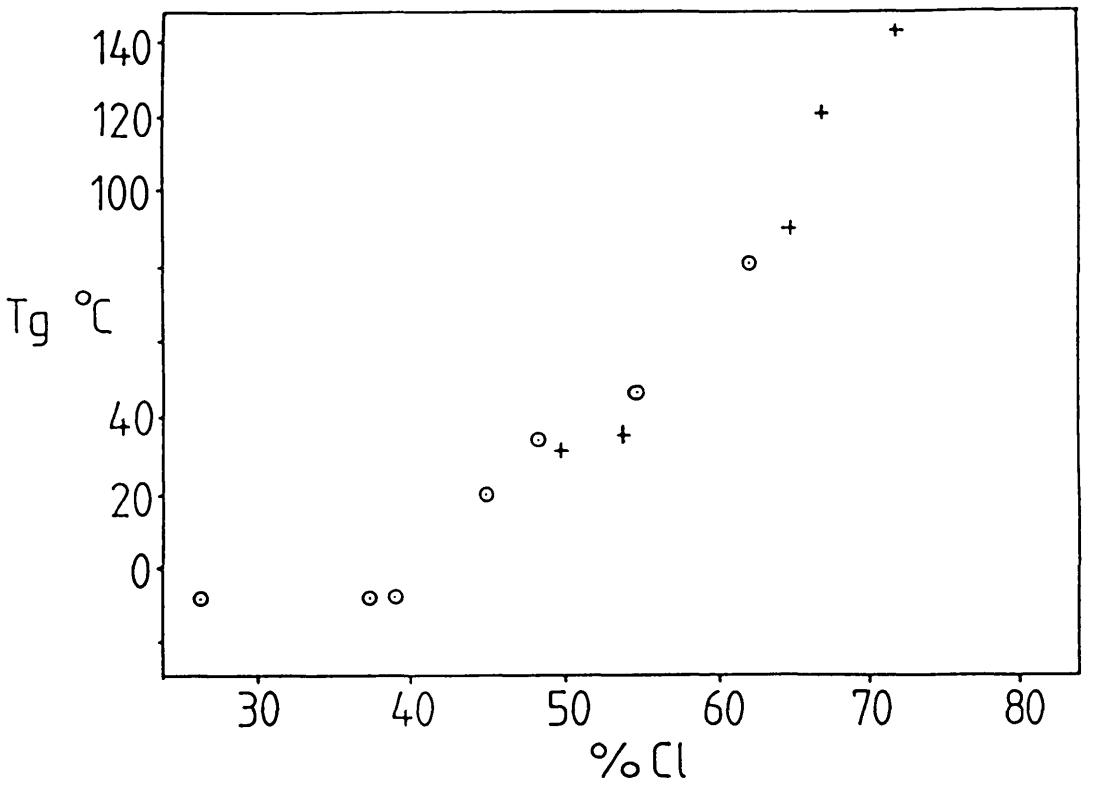


Fig.12 Plot of glass transition temperature against percentage chlorination polyethylenes.

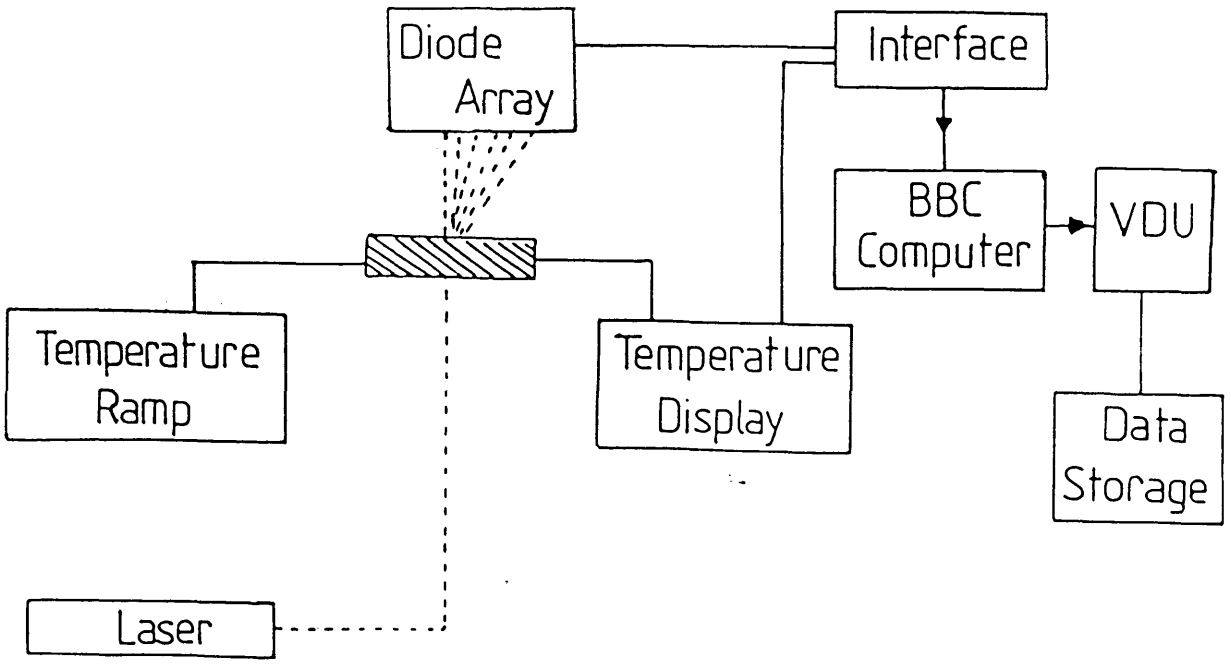


Fig.13 Schematic illustration of the small angle light scattering instrument.

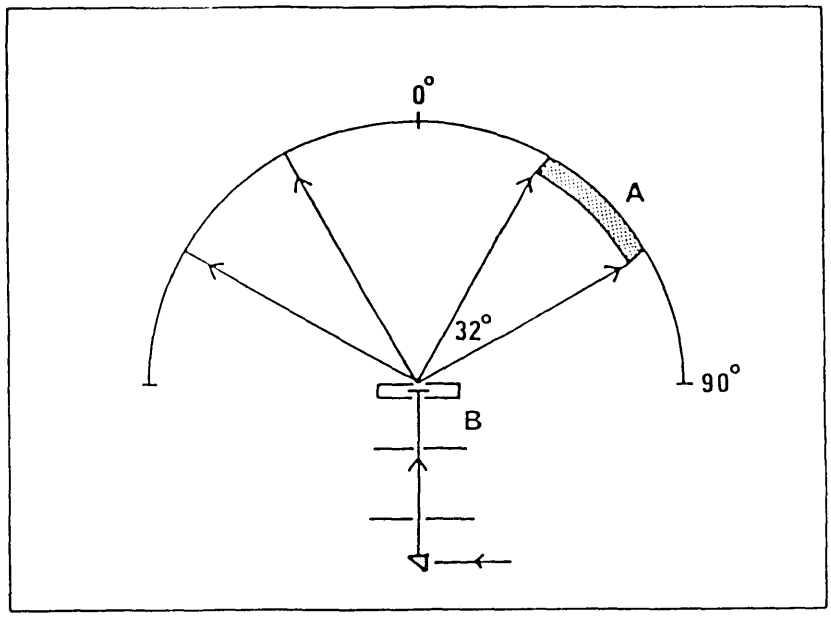


Fig.14 Optical arrangement of small angle light scattering Instrument B = Sample Block.

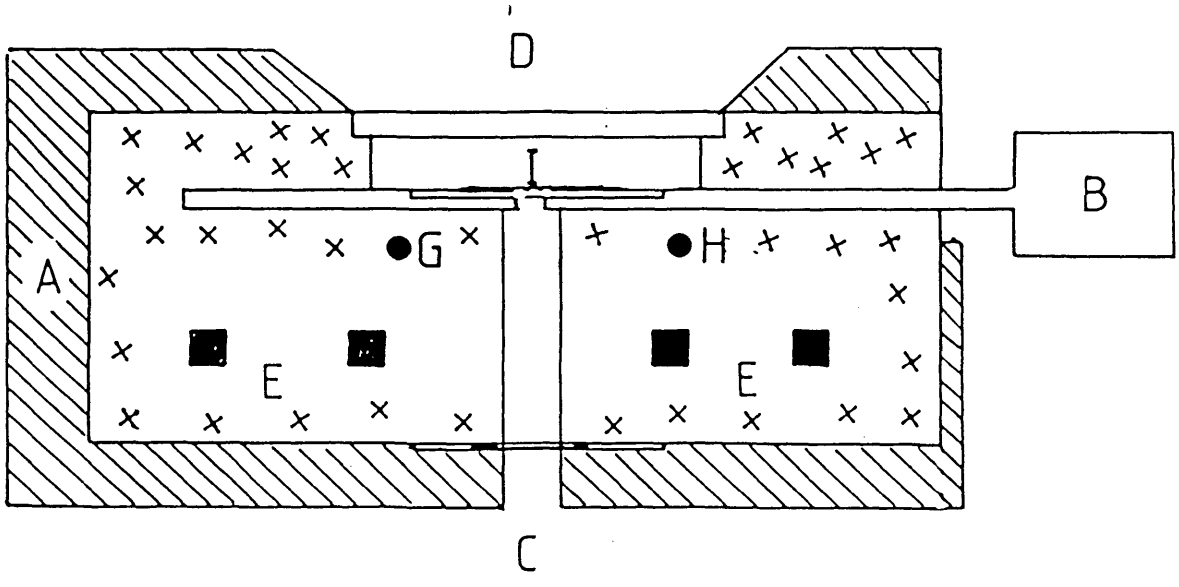


Fig.15 Cross-section through sample block showing A = insulating Jacket, B = Sample Holder C = Entry Window, D = Exit window, E = Heaters, G = Thermocouple H = Probe for temperature control, I = Sample.

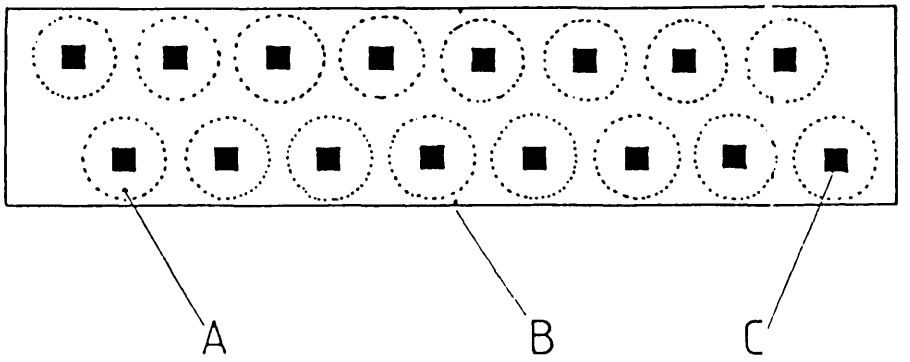


Fig.16 Diode Array showing staggered arrangement of diodes. A = diode B = centre mark. C = active area of diode.

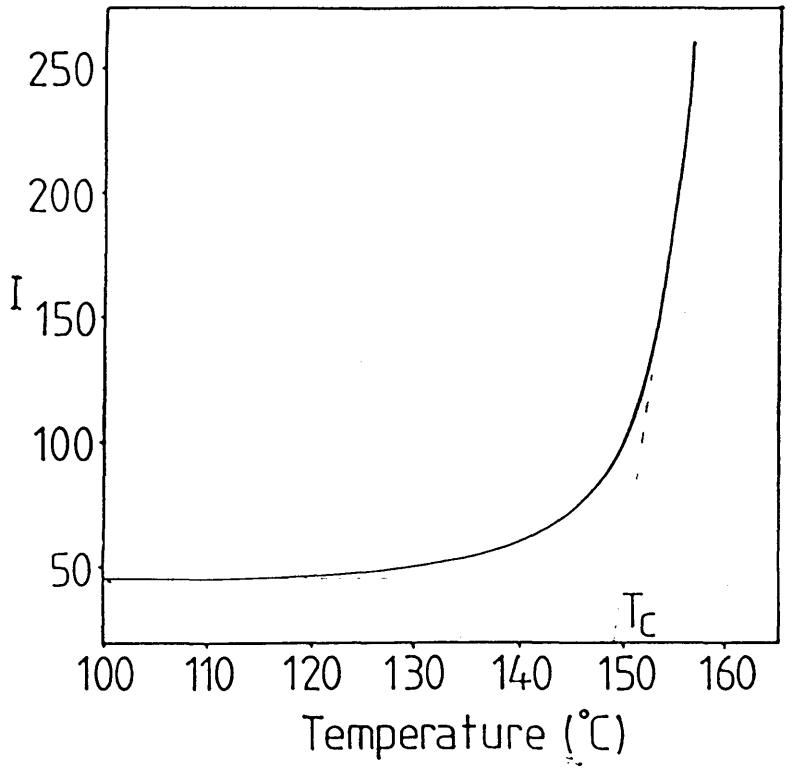


Fig.17 Typical cloud point transition obtained using the Turbidimeter.

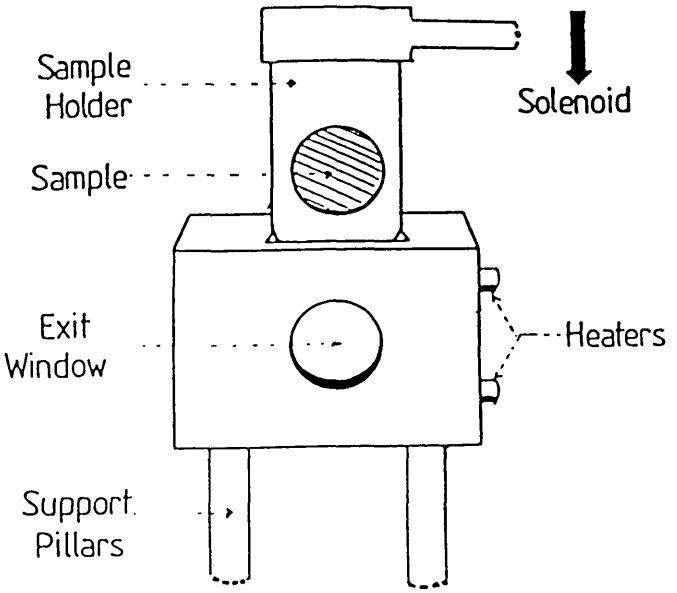


Fig.18 Sample Holder for Real time SANS experiments.

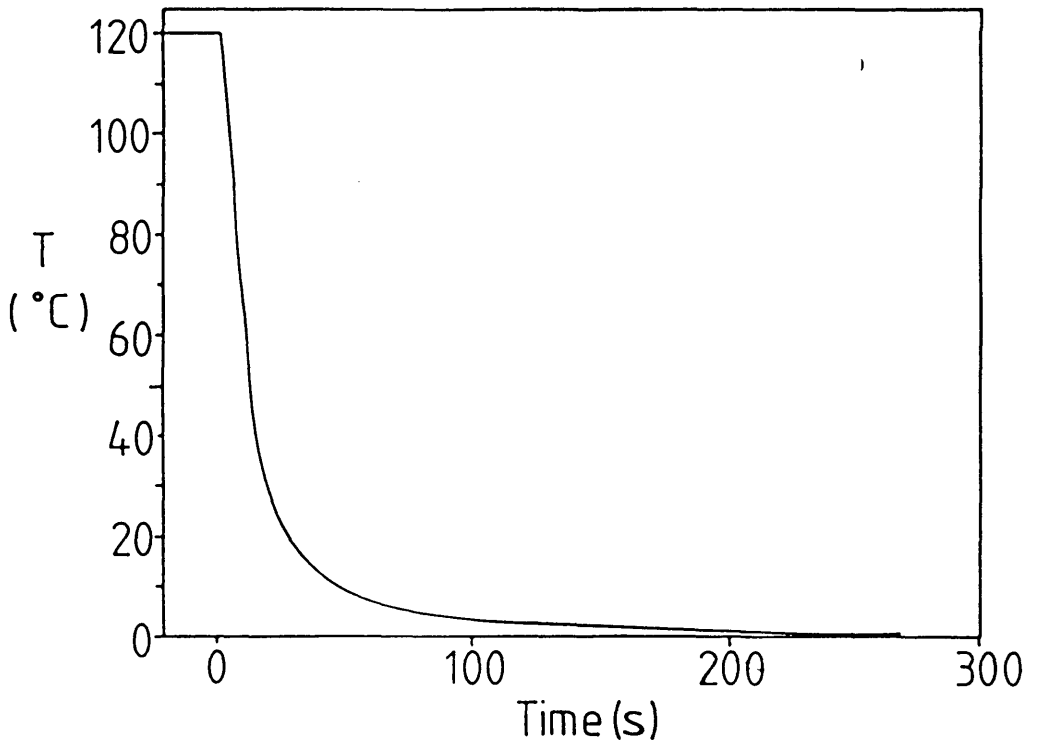


Fig.19 Typical Temperature quench profile for PS/PB SANS experiments.

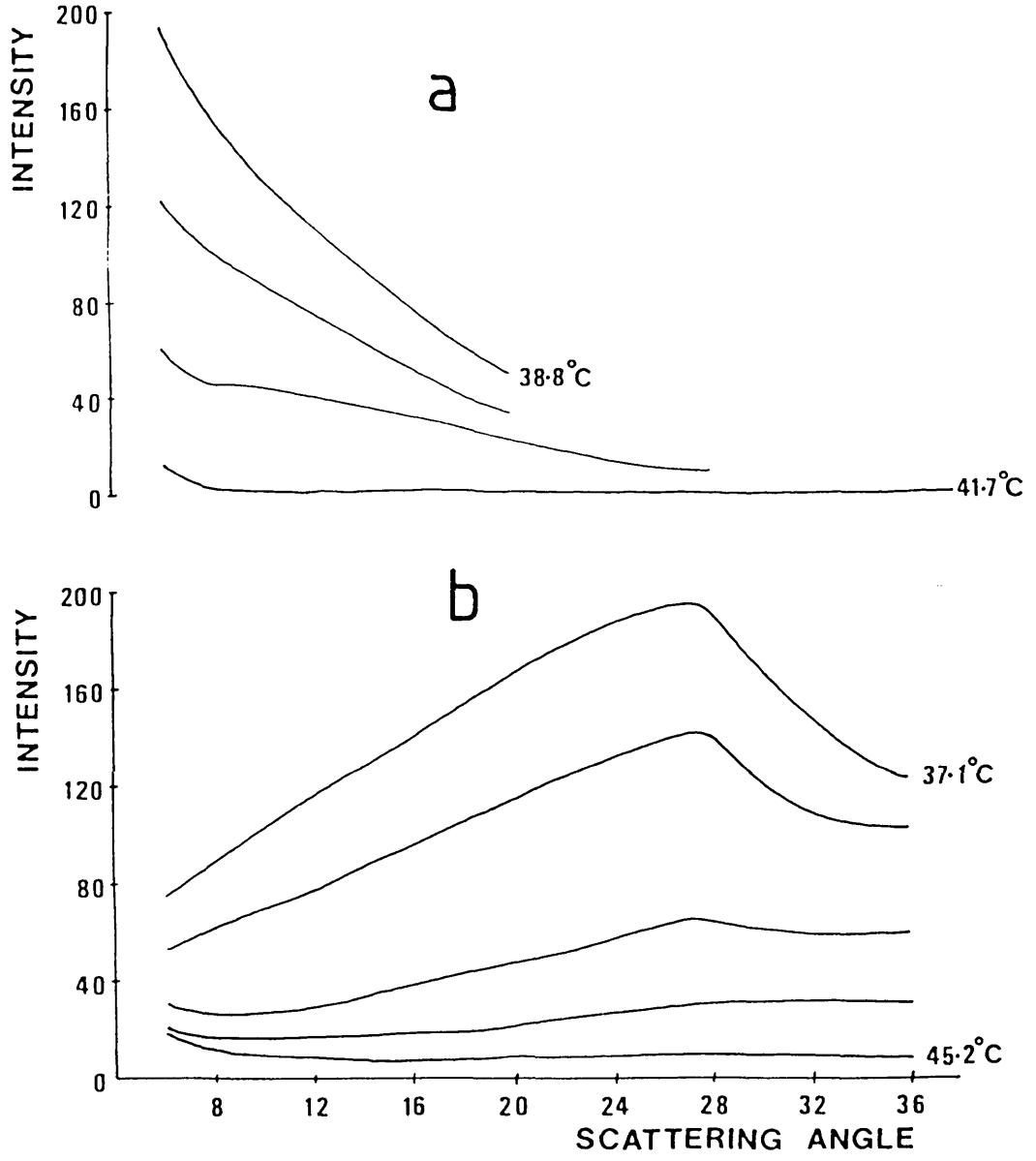


Fig.20 Scattered intensity as a function of angle for compositions P and Q shown in Fig. 22 during cooling at $0.5^{0}c$ Min^{-1}.

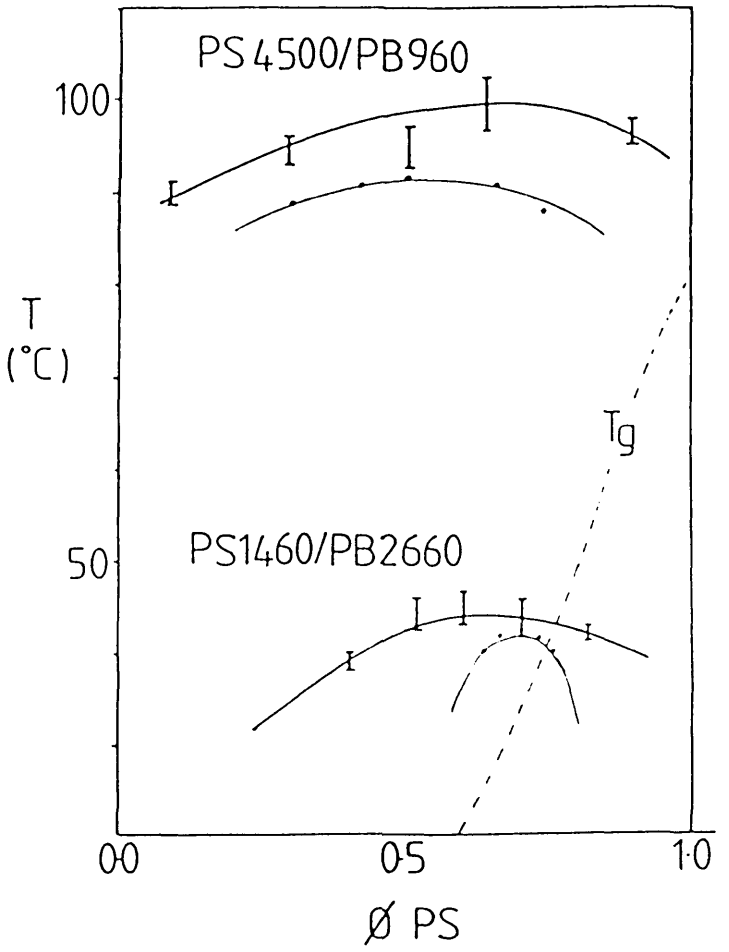


Fig.21 Cloud point curves-spinodals – and glass transition temperatures ···· for PS/PB oligomers.

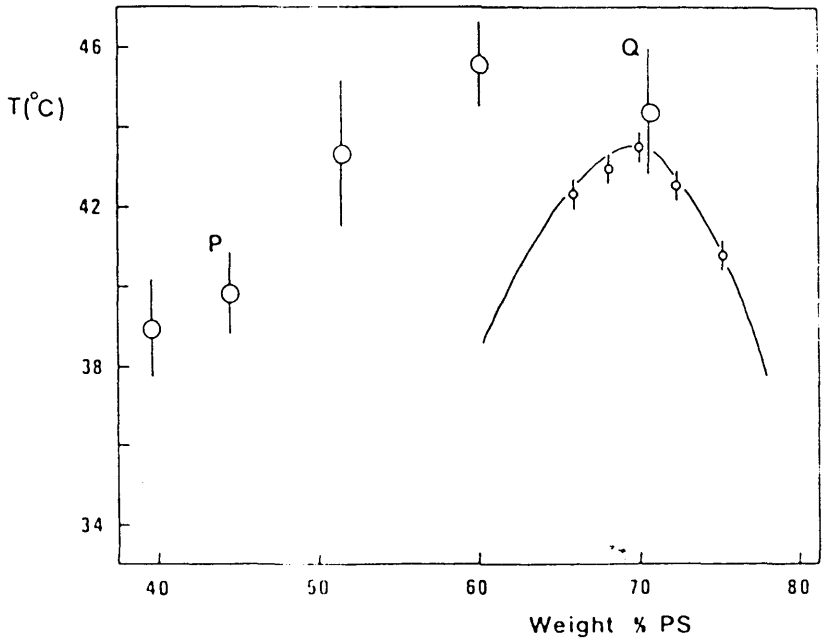


Fig.22 Cloud point curve and spinodal locus for the PS 1460/ PB 2660 system. The spinodal has been redrawn from Atkin et al.

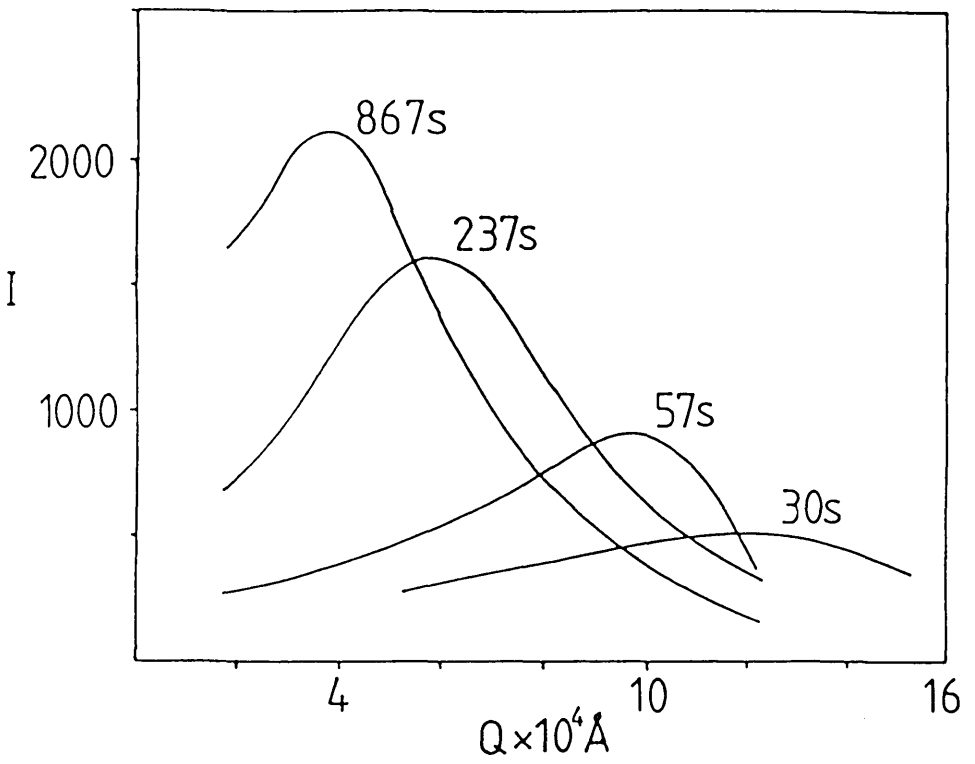


Fig.23 A typical series of I(Q) plots at different times within the spinodal for a PS 4500/PB.960 mixture, 64% PS composition at 99°C .

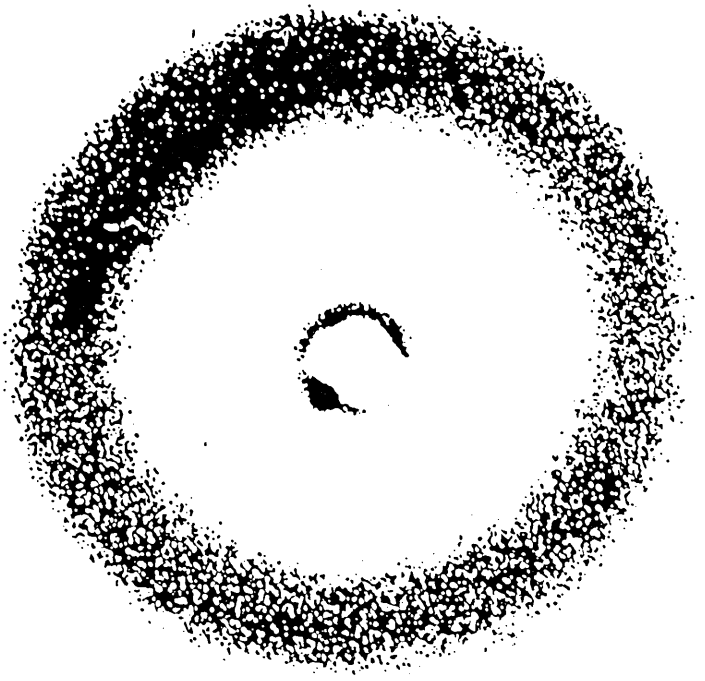


Fig.24 Typical scattering pattern sometimes referred to as a "spinodal ring".

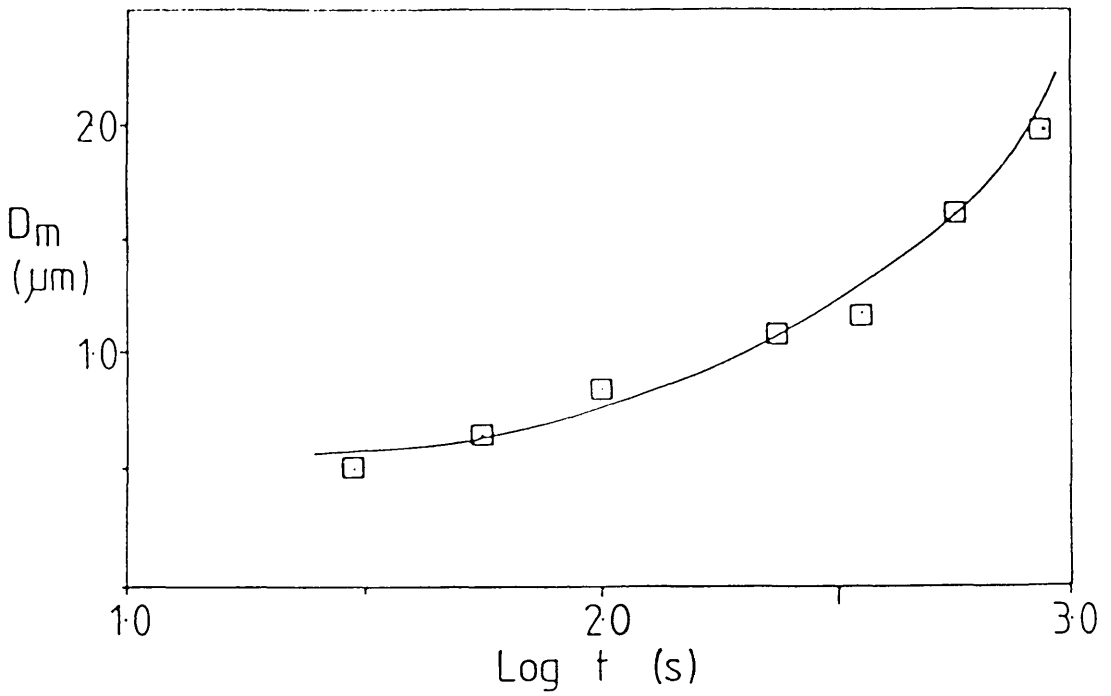


Fig.25 The correlation length (Dm) as a function of log (time) for the PS 4500/PB 960 system.

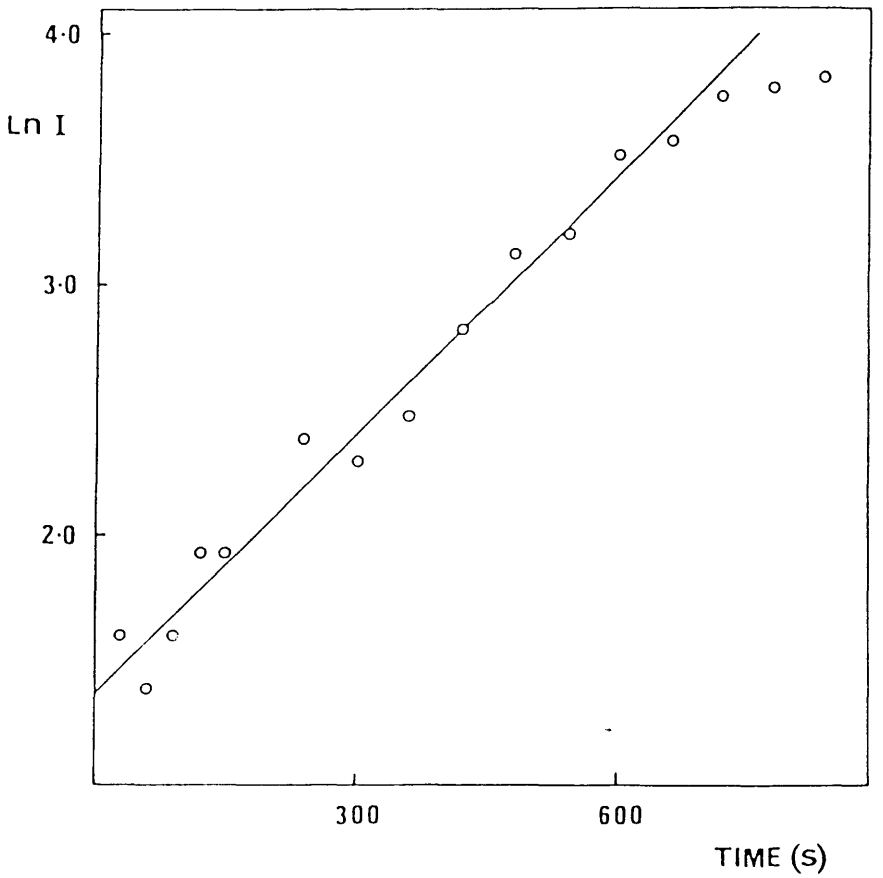


Fig.26 Ln I as a function of time for the fastest growing wavevector (Qm) at 43.5^{0}C.

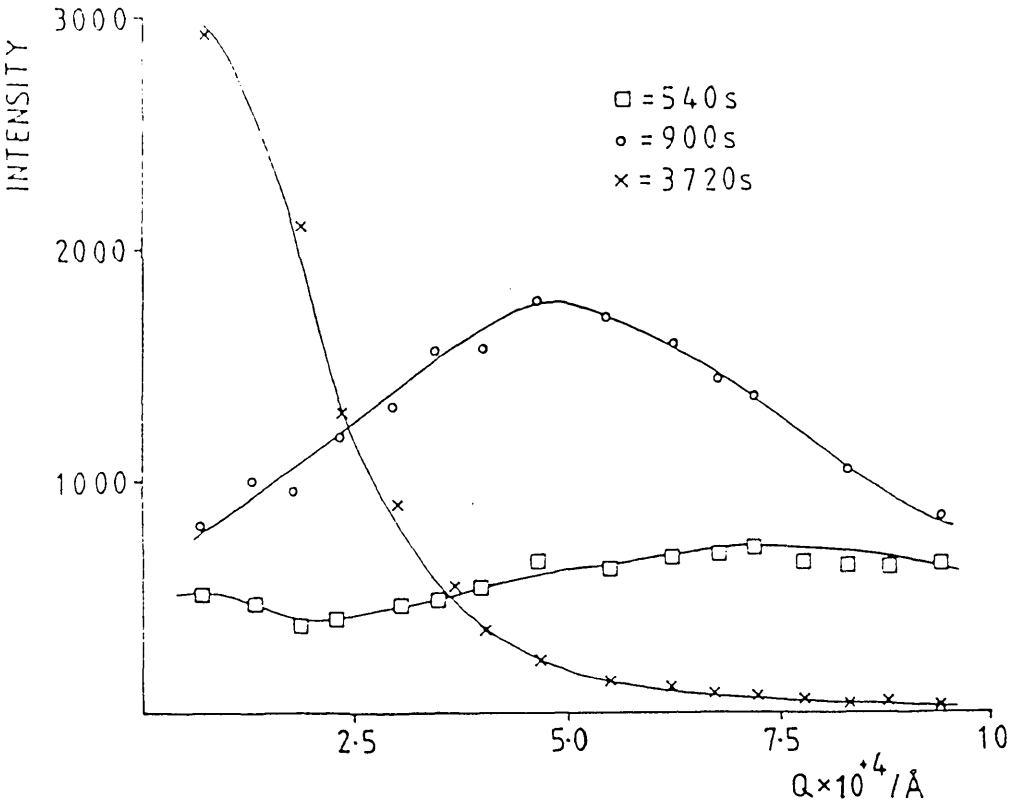


Fig.27 Intensity against Q at various times after jumping into the unstable region.

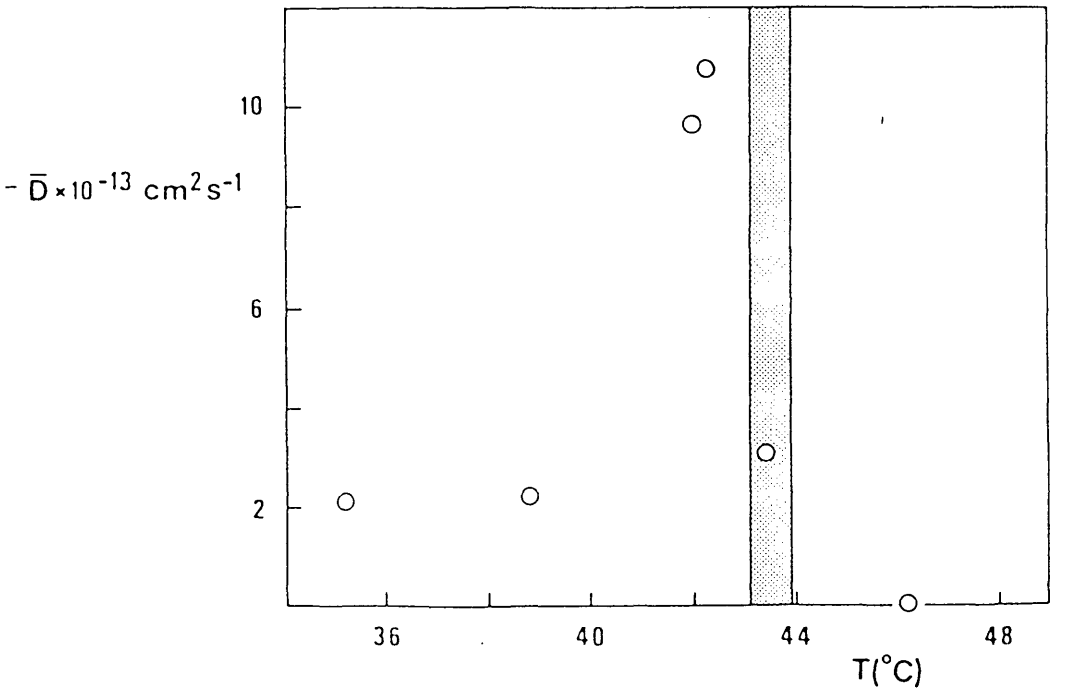


Fig.28 Effect of temperature on $\bar{D}$. Normally at temperatures away from the spinodal $\bar{D}$ is primarily dependent on the value of $\delta^2G/\delta\phi^2$, i.e. it should drop to zero at the spinodal temperature (marked by the vertical bar on the figure). However, as the temperature approaches the blend Tg (33^0C) $\bar{D}$ falls again because of decreasing chain mobility.

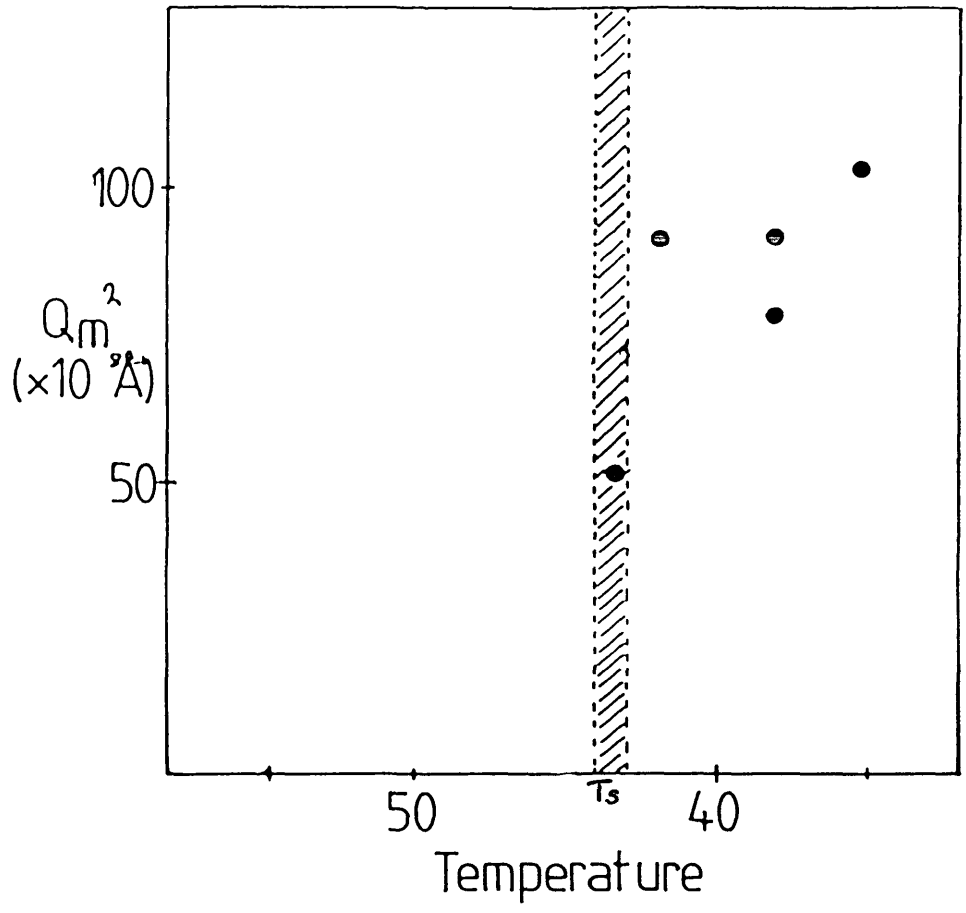


Fig.29 A plot of Qm^2 against temperature for the critical composition in the PS.1460 PB 2660 system.

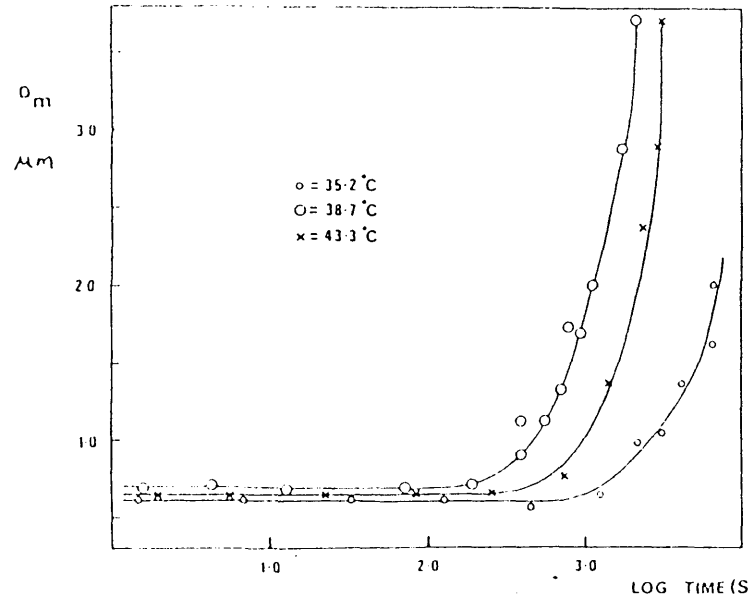


Fig.30 Time dependence of the correlation length, Dm for a PS 1460/PB2660 mixture containing 70% PS.

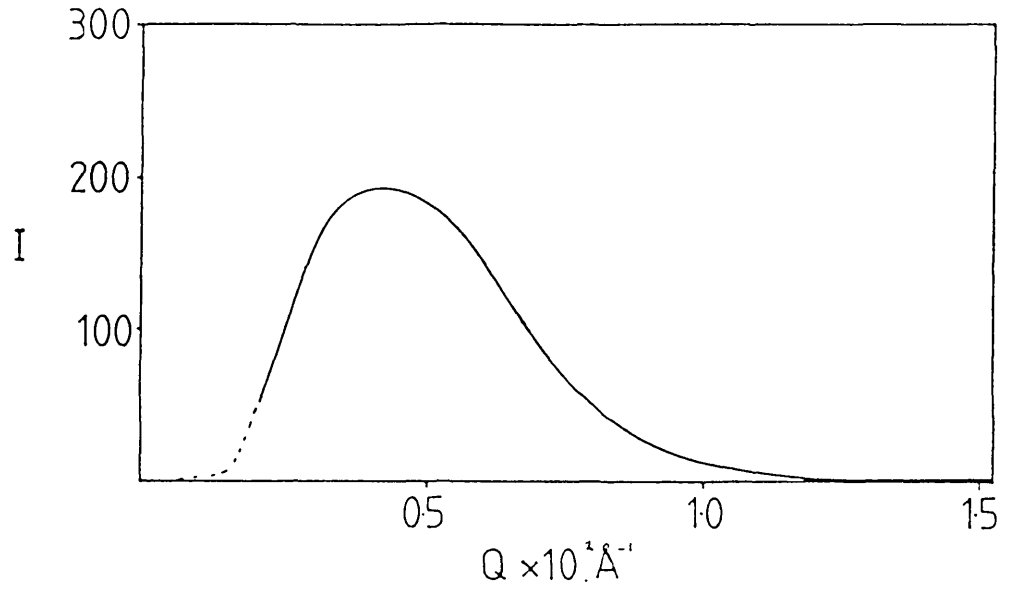


Fig.31 Typical I(Q) plot obtained by SANS for a PS 1460/PB 2660 mixture, 80% composition quenched to 0^0C.

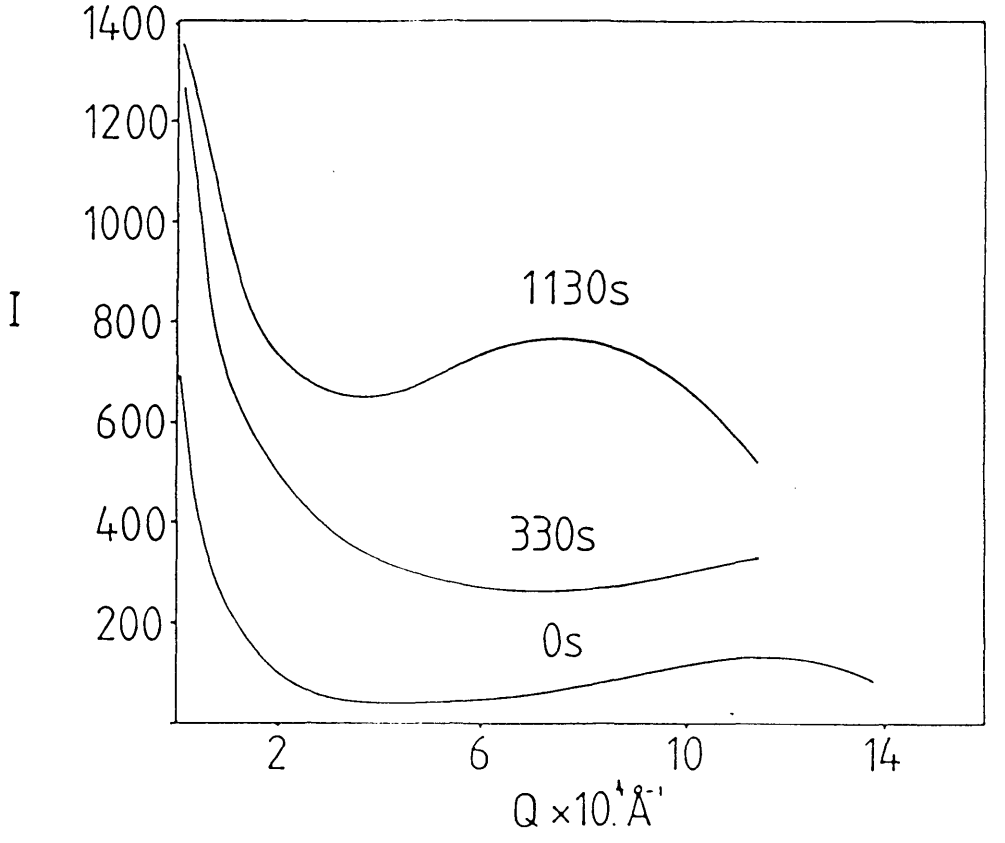


Fig.32 Typical scattering patterns for EVA/SCPE. Note the maximum present in I(Q) at zero time.

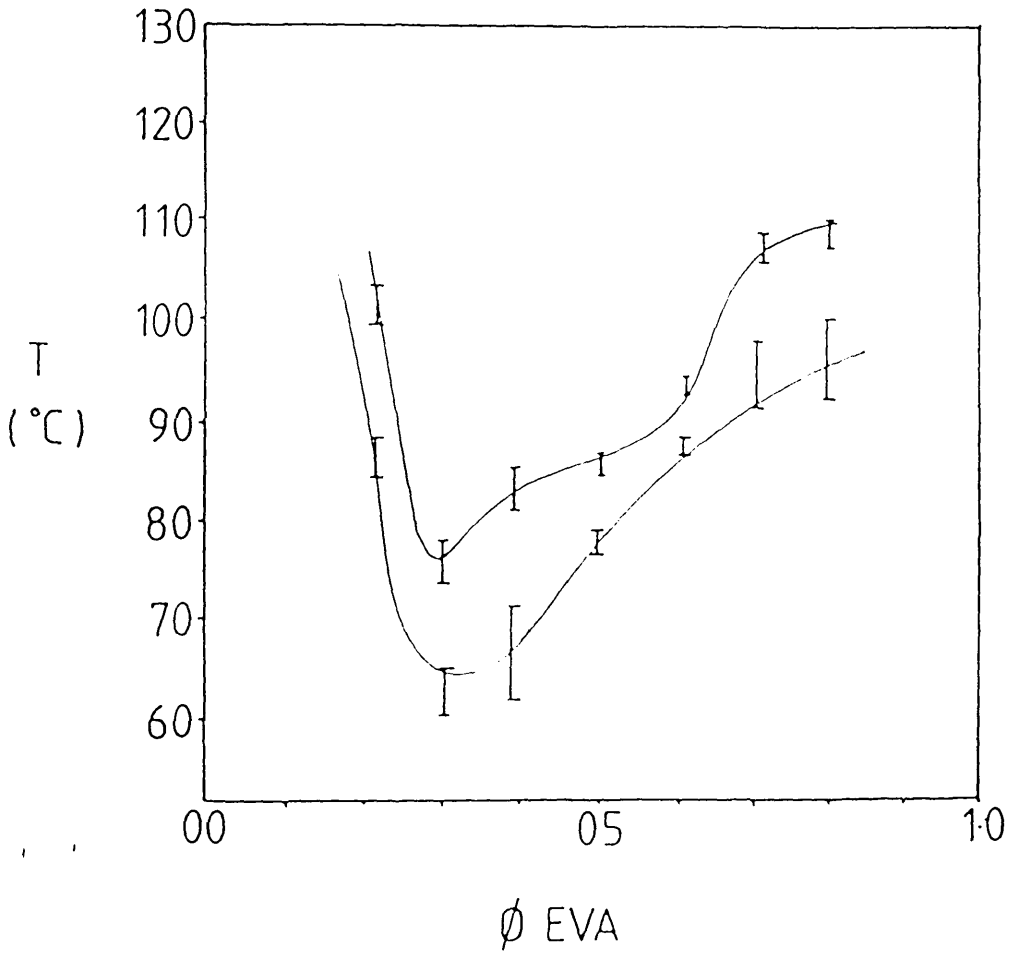


Fig.33 Cloud point curves for $EVA^{45}/SCPE^{50}$ upper curve and $EVA^{40}/SCPE^{50}$ lower curve obtained using the Turbidimeter.

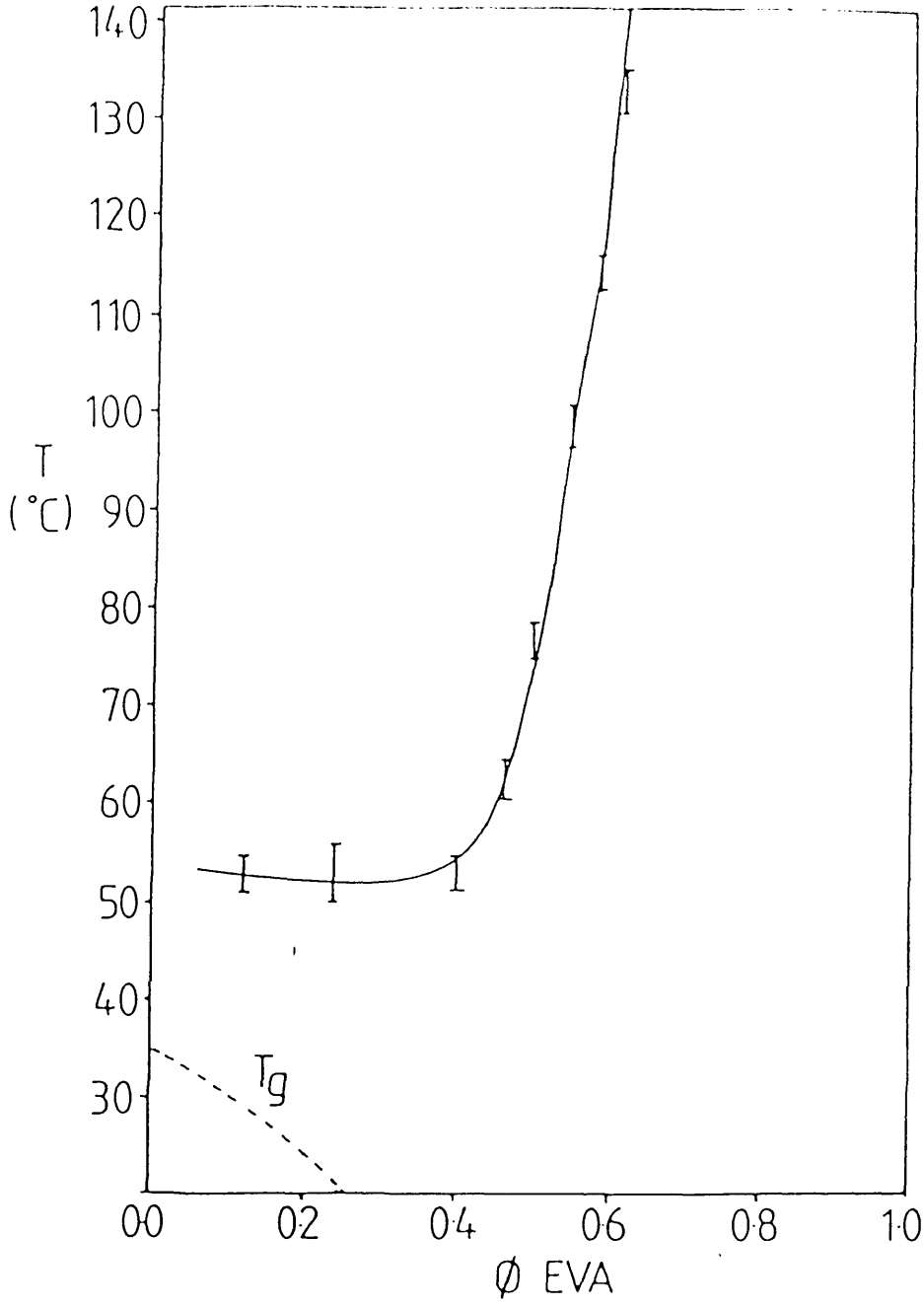


Fig.34 Phase boundary and glass transition for $EVA^{45/3}/SCPE^{50/5}$ blends determined using the SALS instrument.

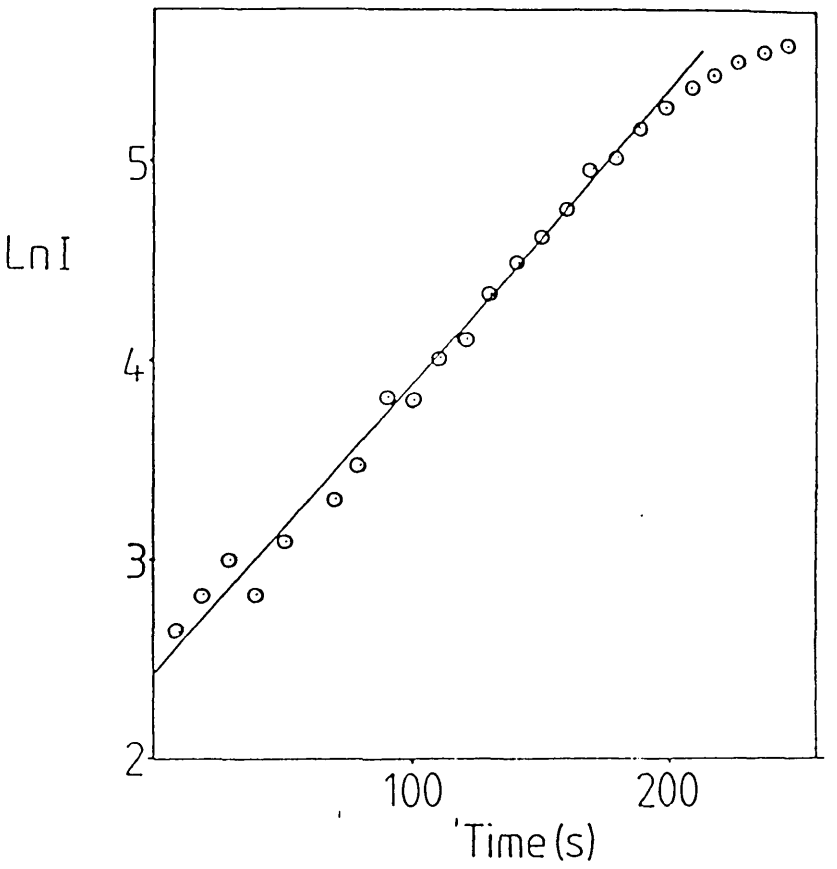


Fig.35 Plot of Ln (Intensity) against time for an EVA/SCPE blend containing 53% EVA at 106°C

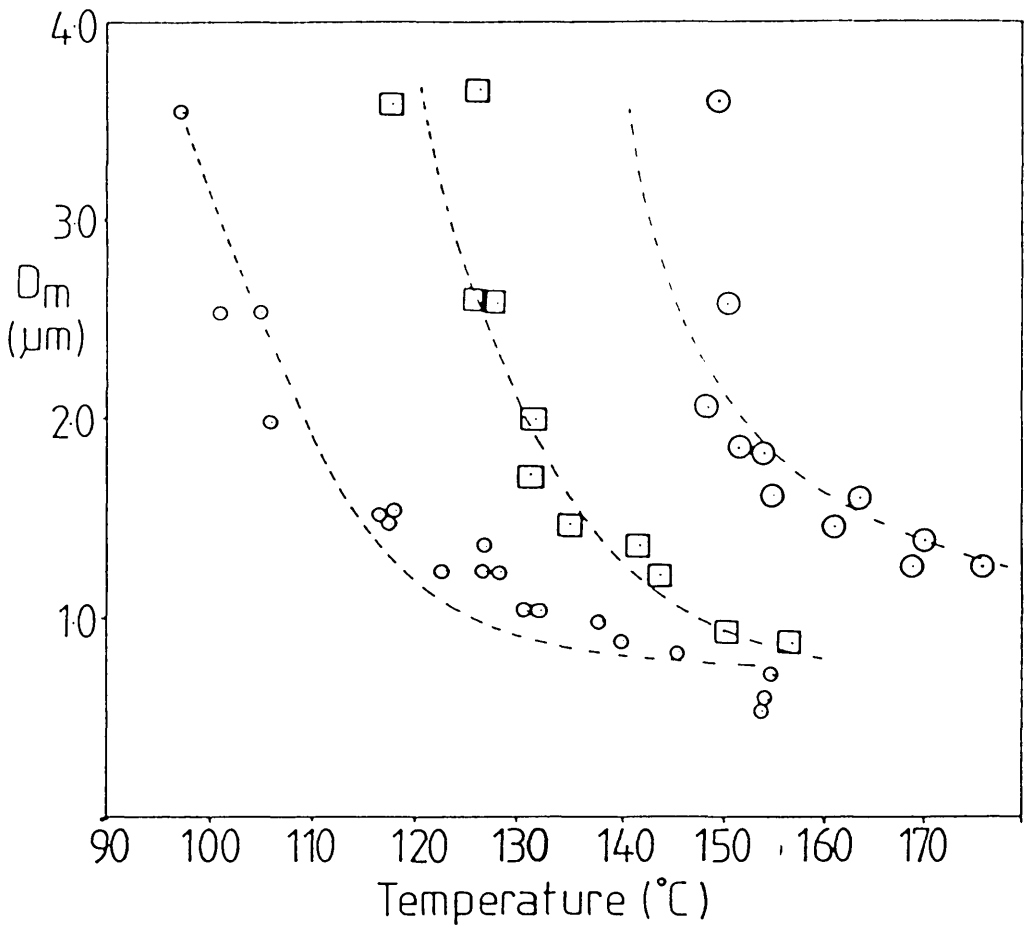


Fig.36 The initial correlation length as a function of temperature for $EVA^{45/3}/SCPE^{50/5}$. o = 55% EVA ⊡ = 59% EVA = 62% EVA. The dashed lines are the predicted initial correlation lengths using van Aartsens equation $Dm = 2\pi L\left[\frac{(3T-Ts)}{TS}\right]^{-\frac{1}{2}}$ l = 800Å 55% EVA l = 1000Å 59% EVA and l = 1400Å 62% EVA.

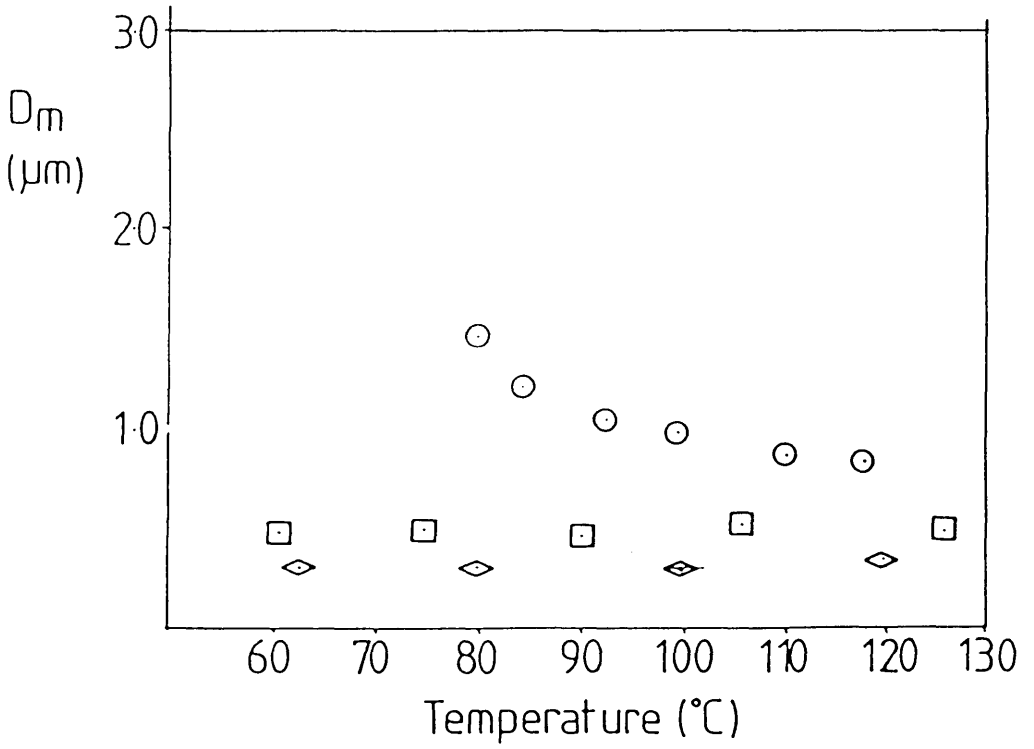


Fig.37 The initial correlation length as a functon of temperature for $EVA^{45/3}/SCPE^{50/5}$ o = 50% EVA ⊡ = 46% EVA ◇ = 24% EVA.

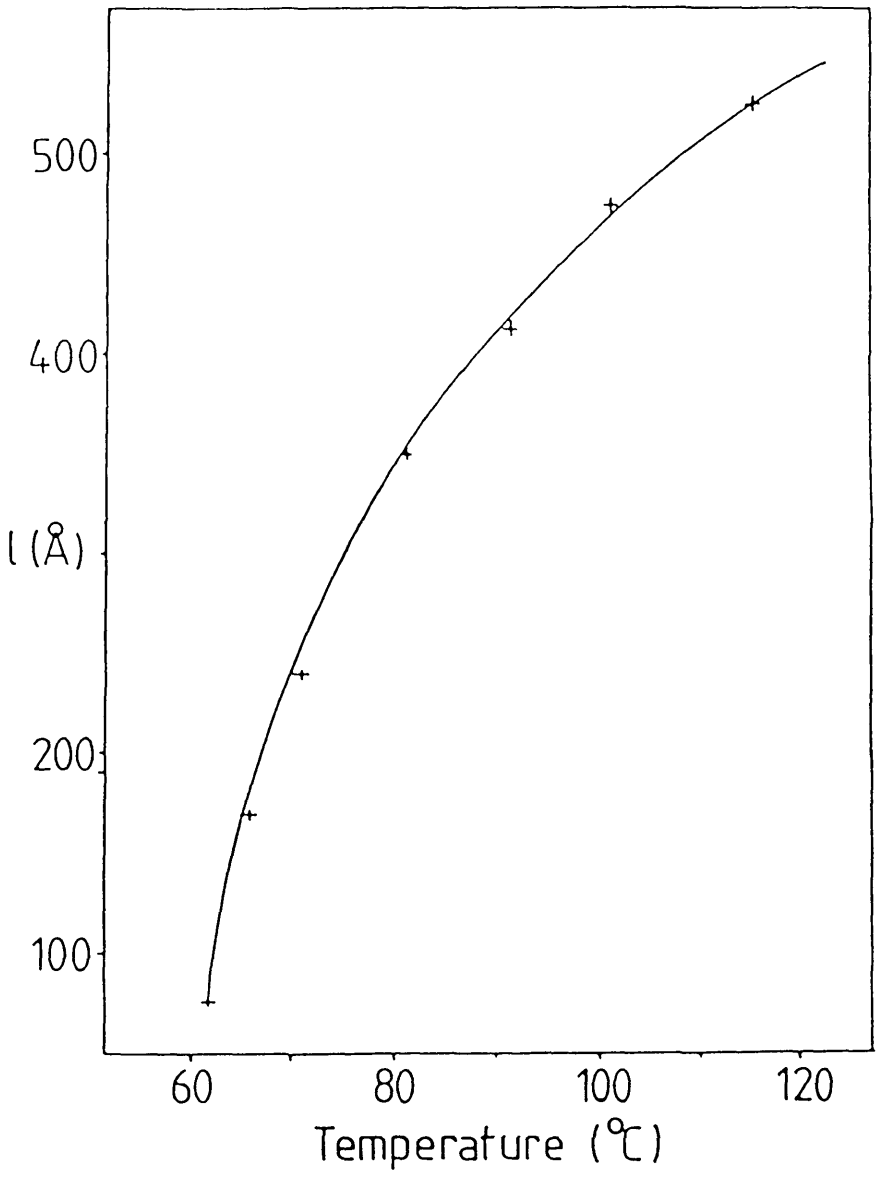


Fig.38 Plot of the value of the interaction length l needed to fit the initial correlation length data for a mixture containing 24% EVA to the van Aartsen equation.

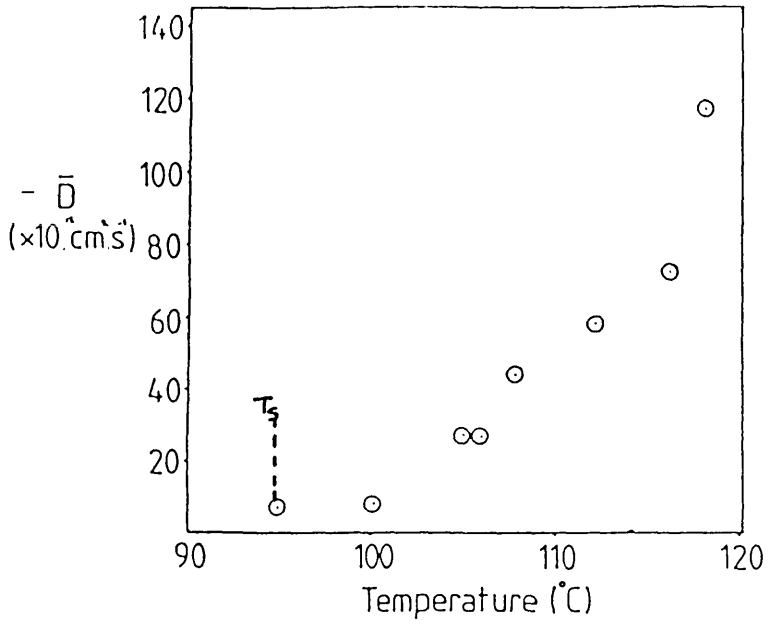


Fig.39 The Cahn-Hilliard diffusion coefficient plotted against temperature for an $EVA^{45/3}/SPCE^{50/5}$ mixture containing 55% EVA.

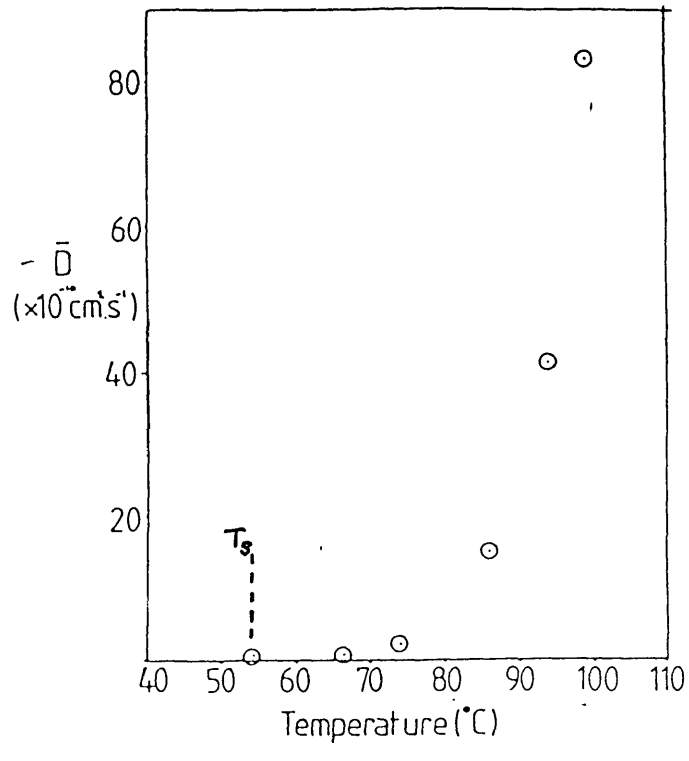


Fig.40 The Cahn-Hilliard diffusion coefficient plotted against temperature for an $EVA^{45/3}/SCPE^{50/5}$ mixture containing 24% EVA.

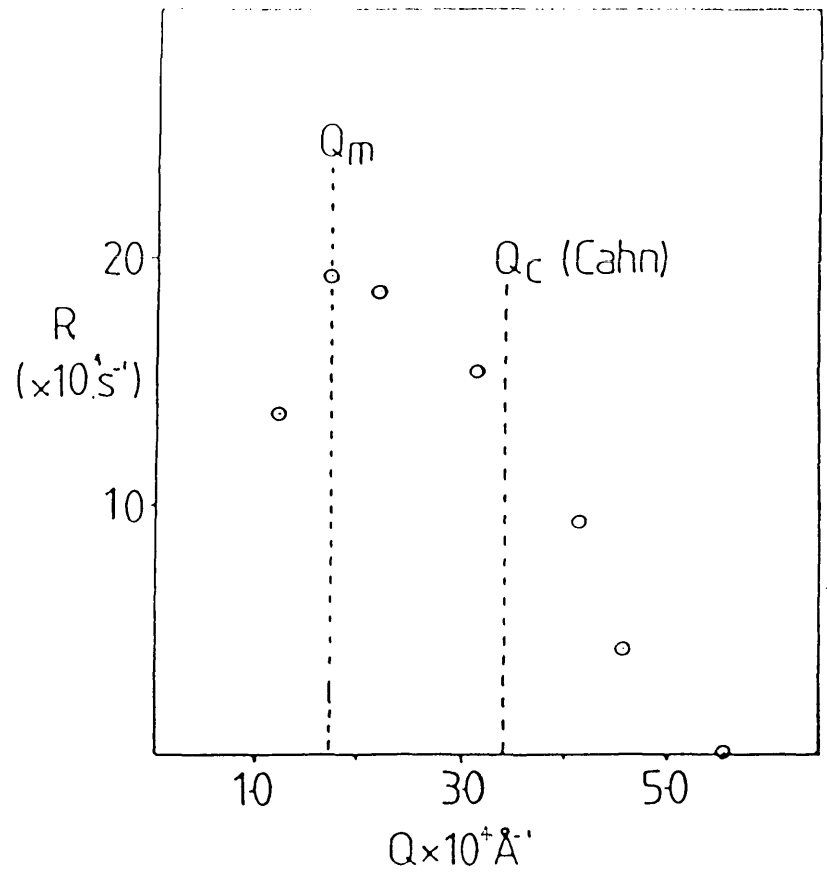


Fig.41 Plot of the growth rate (R) against wavevector (Q) for an EVA $^{45/3}$/SCPE$^{50/5}$ mixture containing 55% EVA at 96 °C.

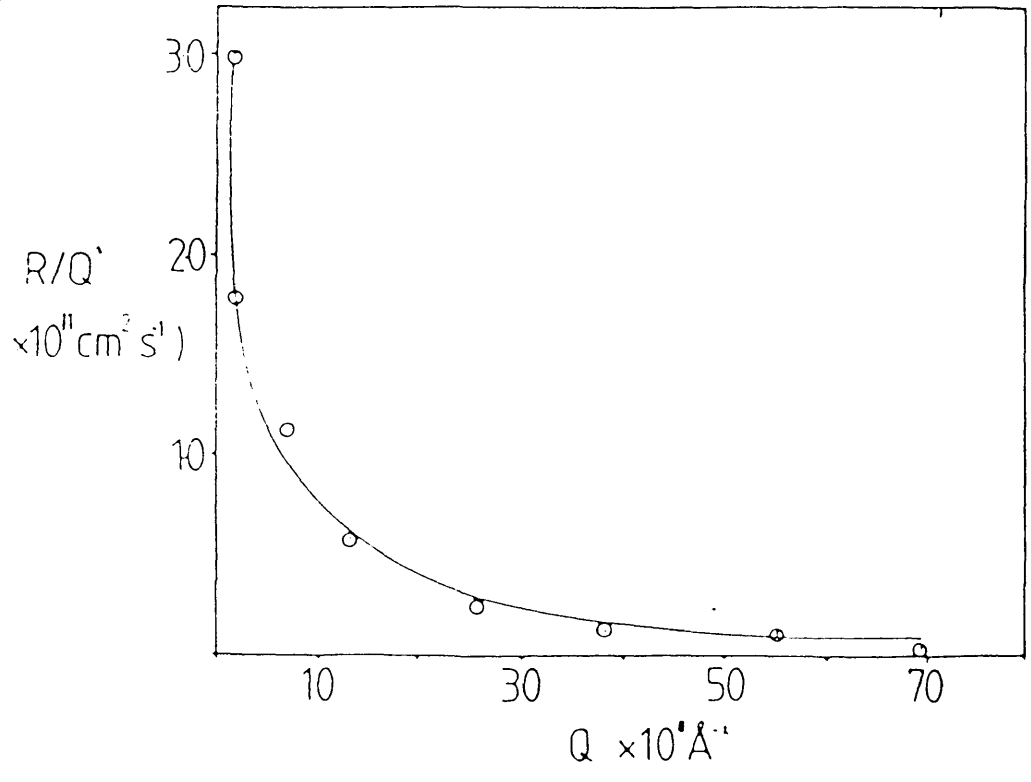


Fig.42 Plot of R/Q^2 against Q^2 for an EVA$^{45/3}$/SCPE$^{50/5}$ mixture containing 55% EVA at 100 °C.

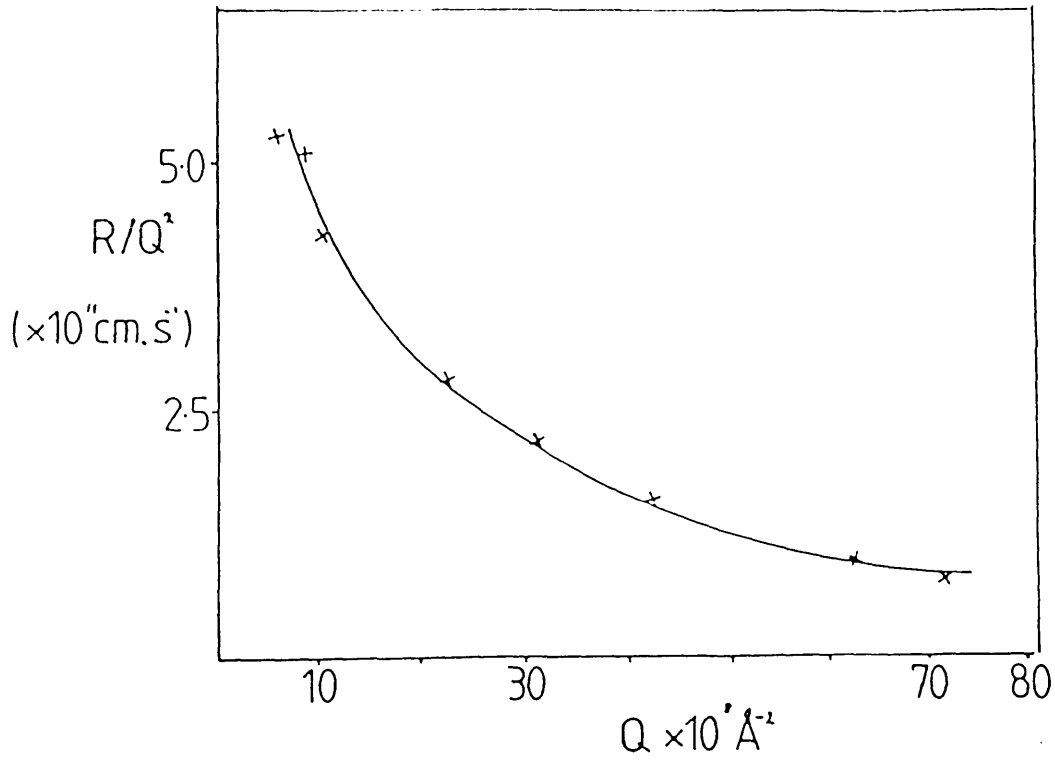


Fig.43 Plot of R/Q^2 against Q^2 for an $EVA^{45/3}$/ $SCPE^{50/5}$ mixture containing 55% EVA at 107.7 ^{0}C.

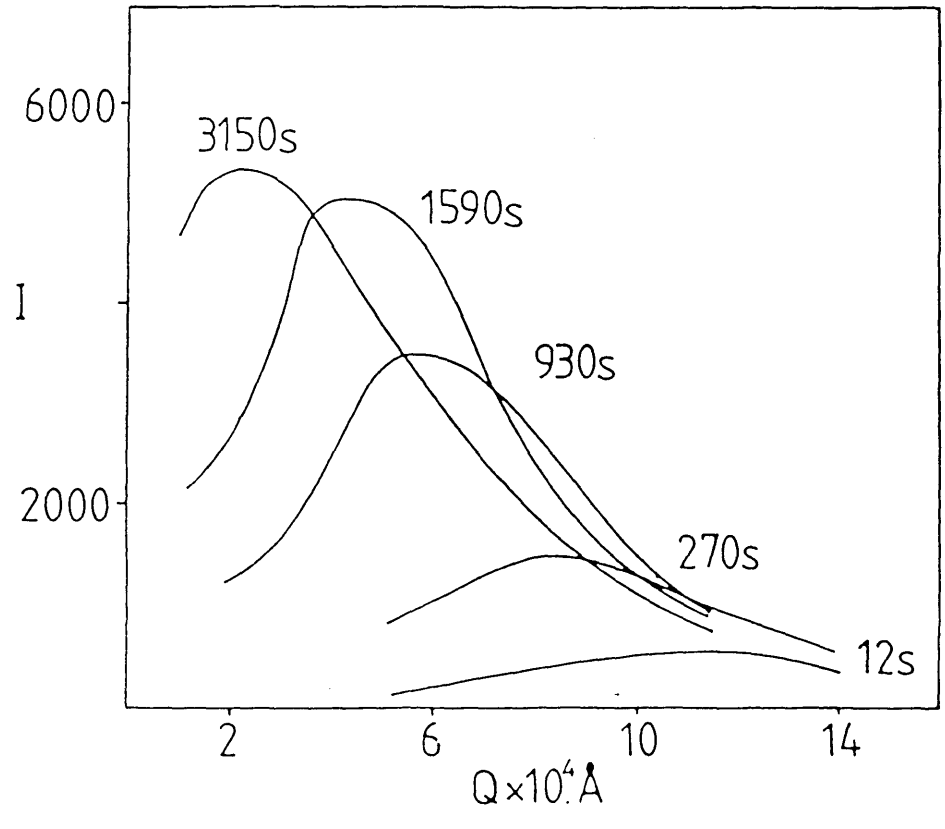


Fig.44 I(Q) plots at different times from an $EVA^{45/3}$/$SCPE^{50/5}$ blend containing 55% EVA at 153.5 ^{0}C.

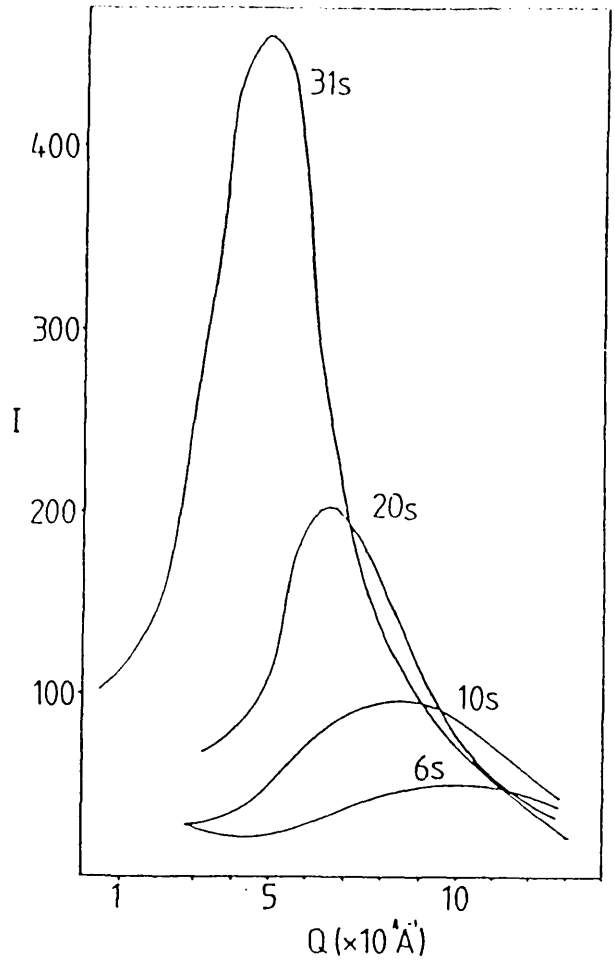


Fig.45 I(Q) plots at different times from an EVA$^{45/3}$/ SCPE$^{50/5}$ blend containing 13% EVA at 83·3°C.

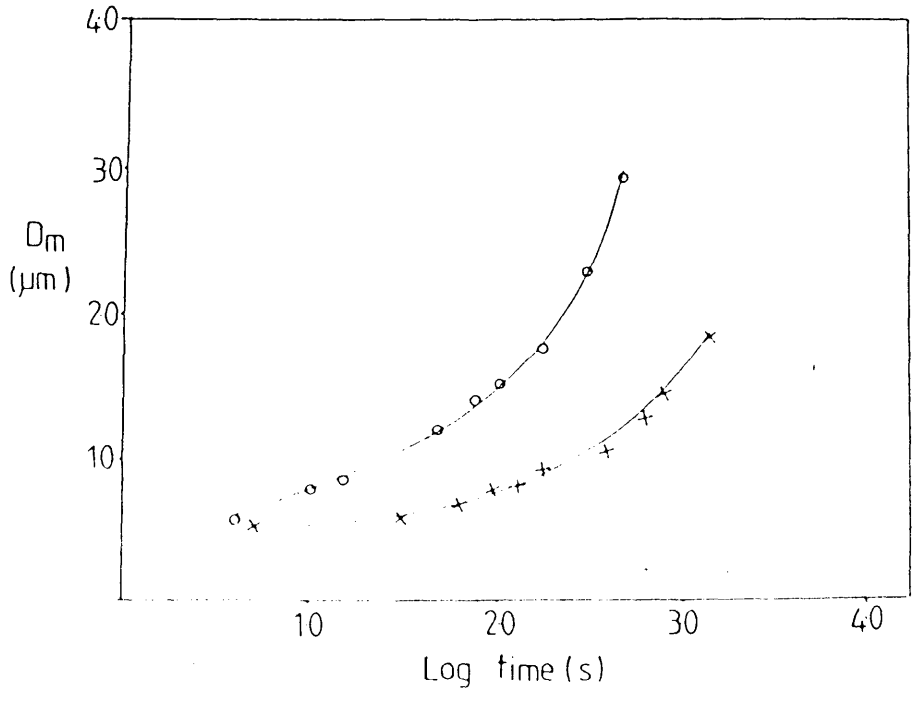


Fig.46 Plot of the correlation length (Dm) against log time for an EVA$^{45/3}$/SCPE$^{50/5}$ blend containing 46% EVA at two temperatures X = 96.3°C ◦ = 137·4°C.

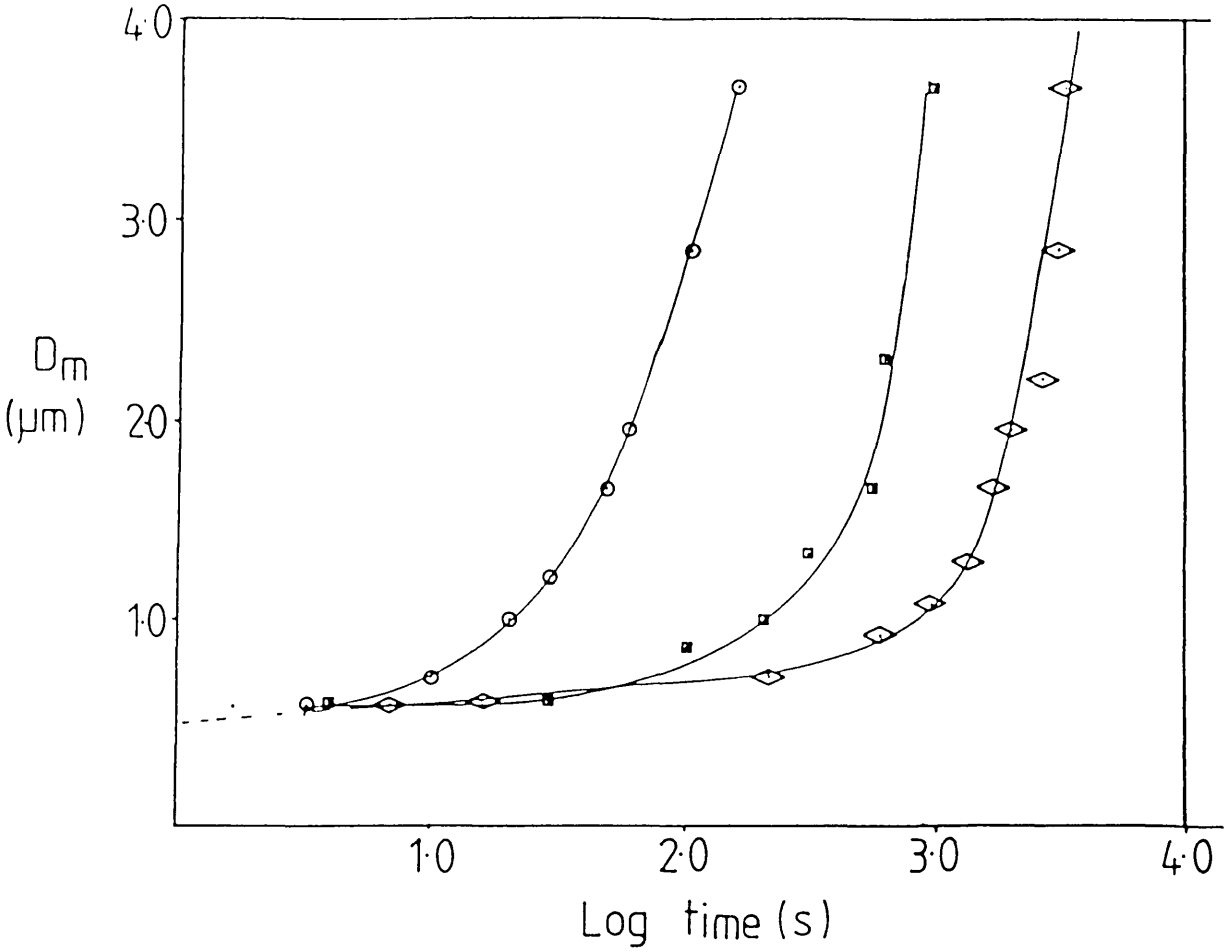


Fig.47 Plot of the correlation length (Dm) against log time for an EVA$^{45/3}$/SCPE$^{50/5}$ blend containing 13% EVA at three temperatures 53.3^{0}C, ▫ = 64.9^{0}C and ◇ = 83.3^{0}C.

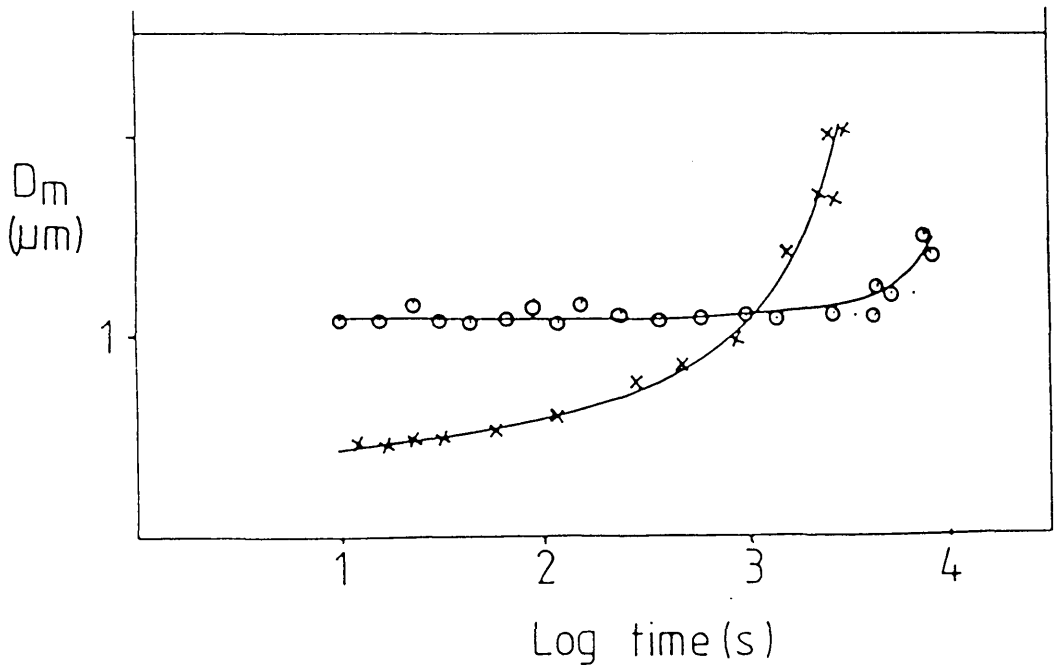


Fig.48 Plot of the correlation length (m) against log time for an EVA$^{45/3}$/SCPER$^{50/5}$ blend containiong 55% EVA at two temperatures. Note the quench depth dependence x = 139.9^{0}C. o = 115.9°C

FIGURE CAPTIONS FOR PHOTOMICROGRAPHS

Fig. 49 Optical micrograph of an EVA/SCPE blend containing 24% EVA heated for 300s at 90°C. Note the interconnected morphology.

Fig. 50 Optical micrograph of an EVA/SCPE blend containing 55% EVA heated for 300s at 100°C. Note the interconnected structure intermingled with a dispersed phase denoted by arrows.

Fig. 51 Optical micrograph of an EVA/SCPE blend containing 55% EVA heated for 900s at 100°C. Note the interconnected structure now has a larger wavelength.

Fig. 52 Optical micrograph of an EVA/SCPE blend containing 62% EVA heated for 300s at 137°C. Note the interconnected structure in contrast to Fig. 53 which was taken from the same sample but close to a heterogeneous particle.

Fig. 53 Optical micrograph of an EVA/SCPE blend containing 62% EVA heated for 300s at 137°C. Note the distinct particles surrounding the dust particles. (arrow).

Fig. 56 Electron micrograph of a thin section of a PMMA/SCPE[67] blend containing 55% SCPE heat treated for 8s at 175°C.

Fig. 57 Electron micrograph of a thin section made by copreciptation of a PMMA/SCPE[67] blend containing 55% SCPE then heat treated at 110°C for two hours.

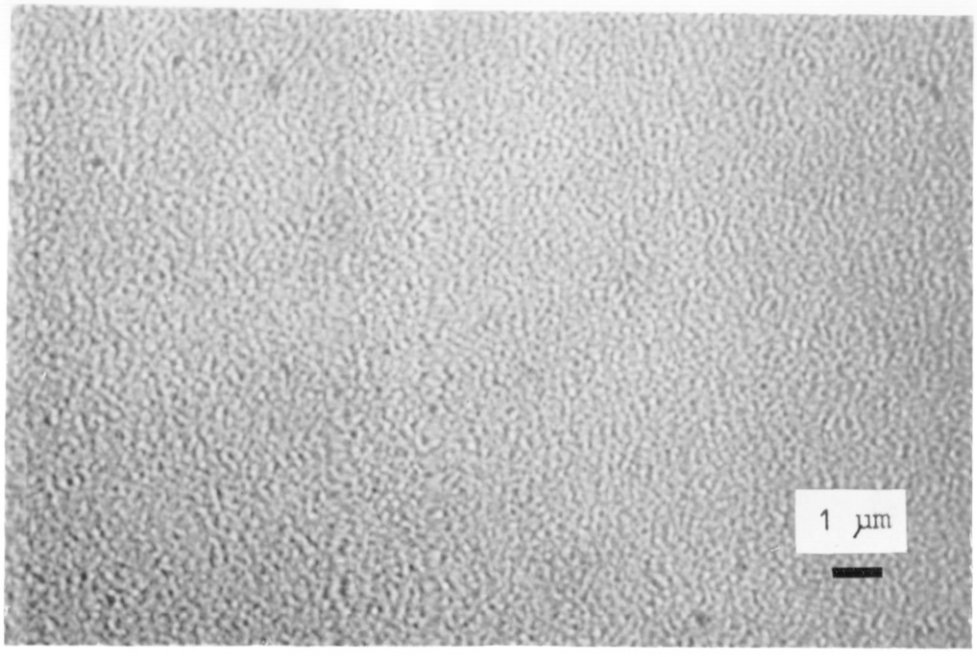


Fig. 49

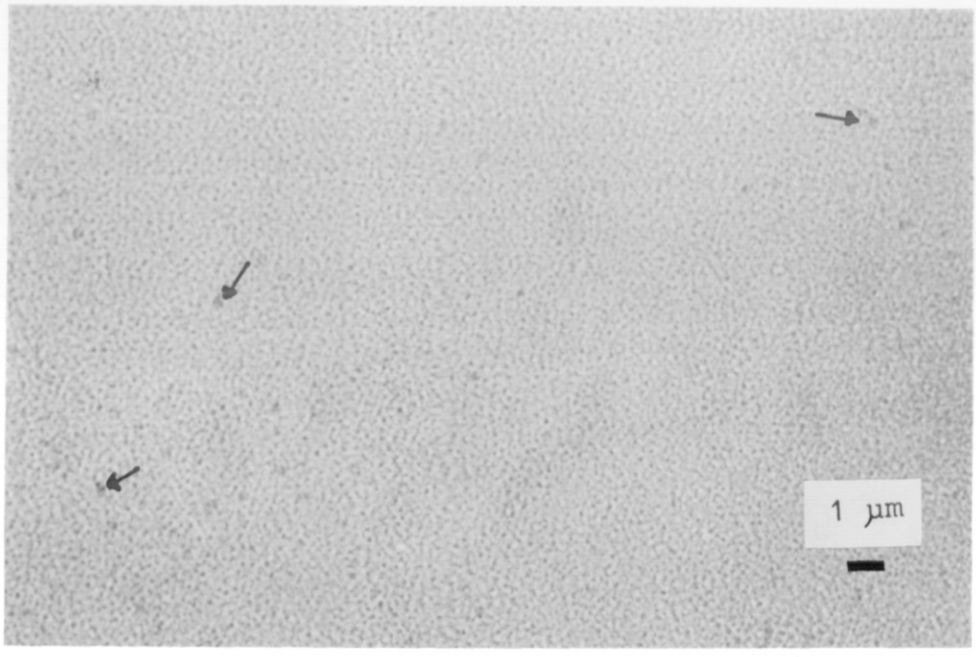


Fig. 50

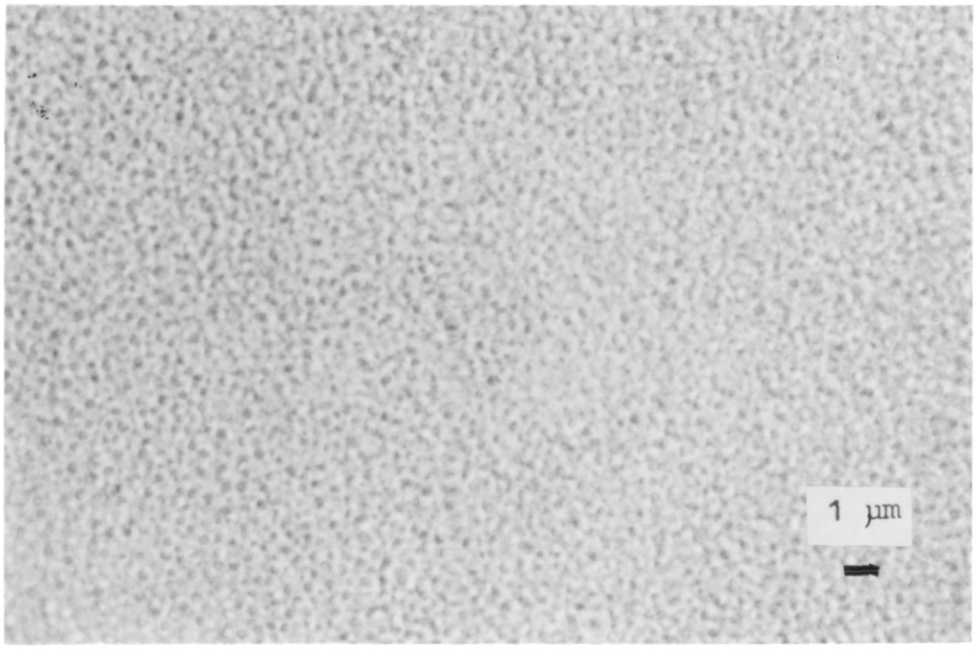


Fig. 51

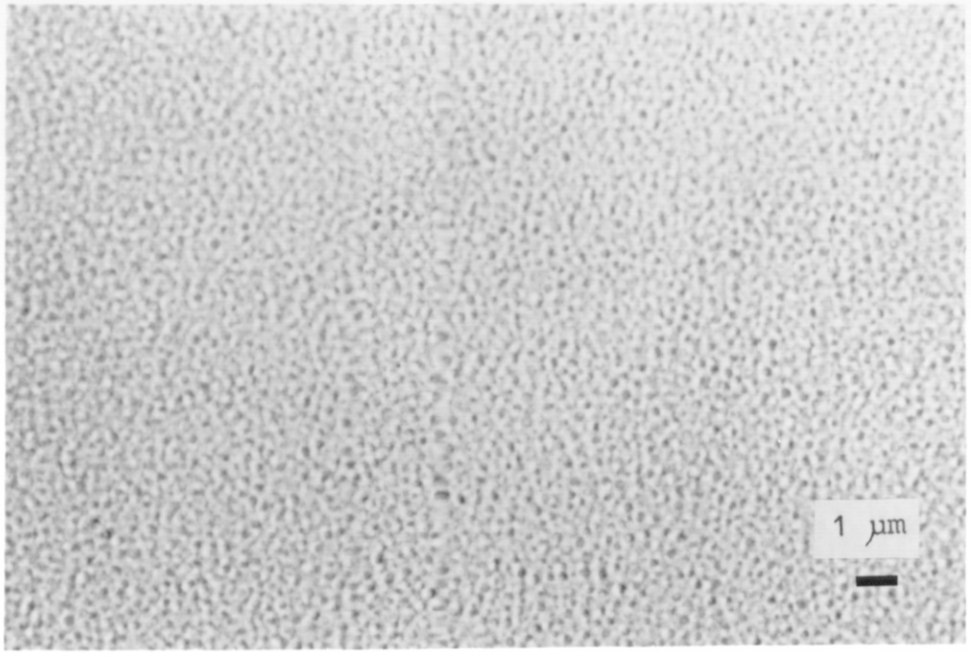


Fig. 52

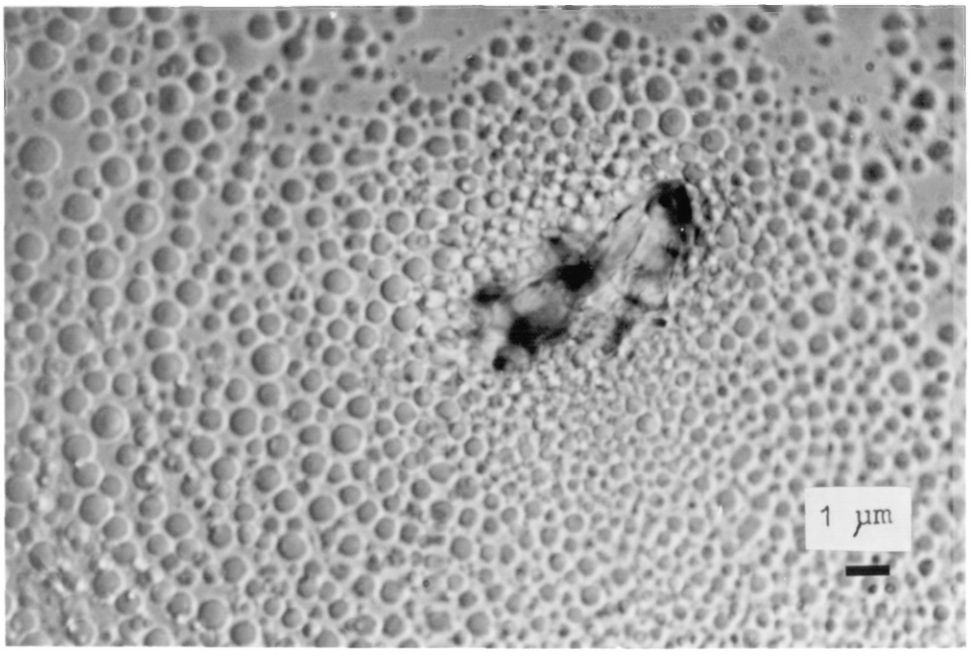


Fig. 53

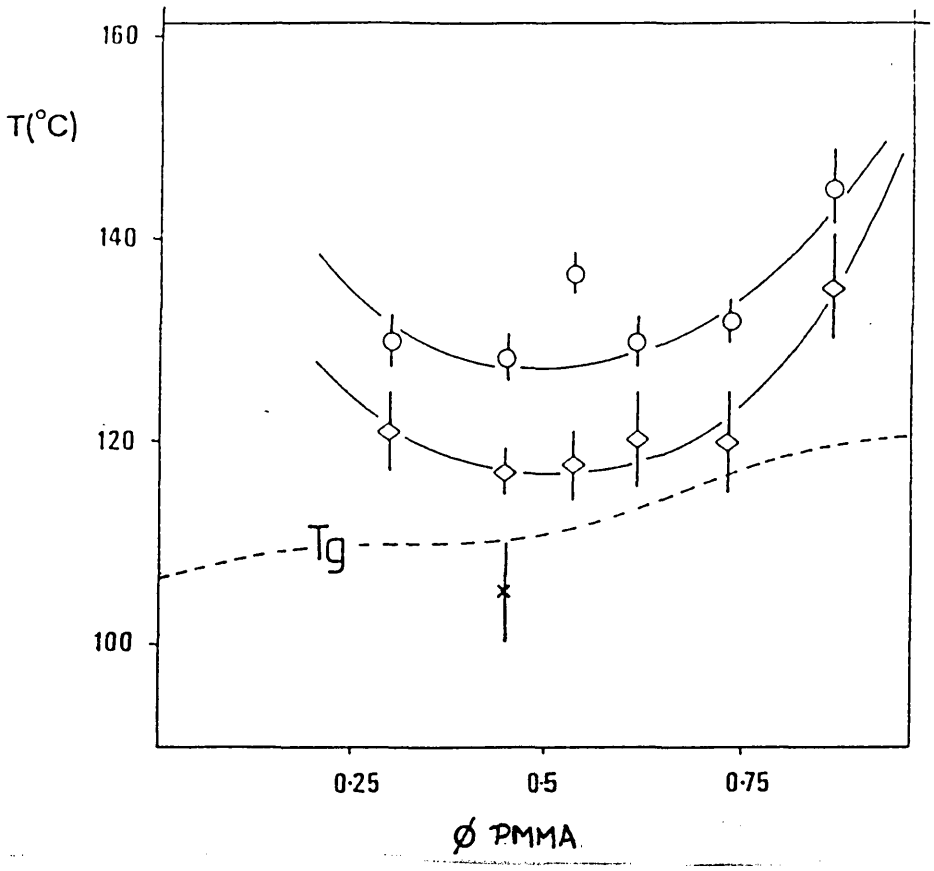


Fig.54 Phase boundaries determined using light scattering o and small angle Xray scattering◇(for the PMMA/SCPE[67]). The dashed line represents the glass transition temperatures of the blend calculated using the Flory-Fox equation.

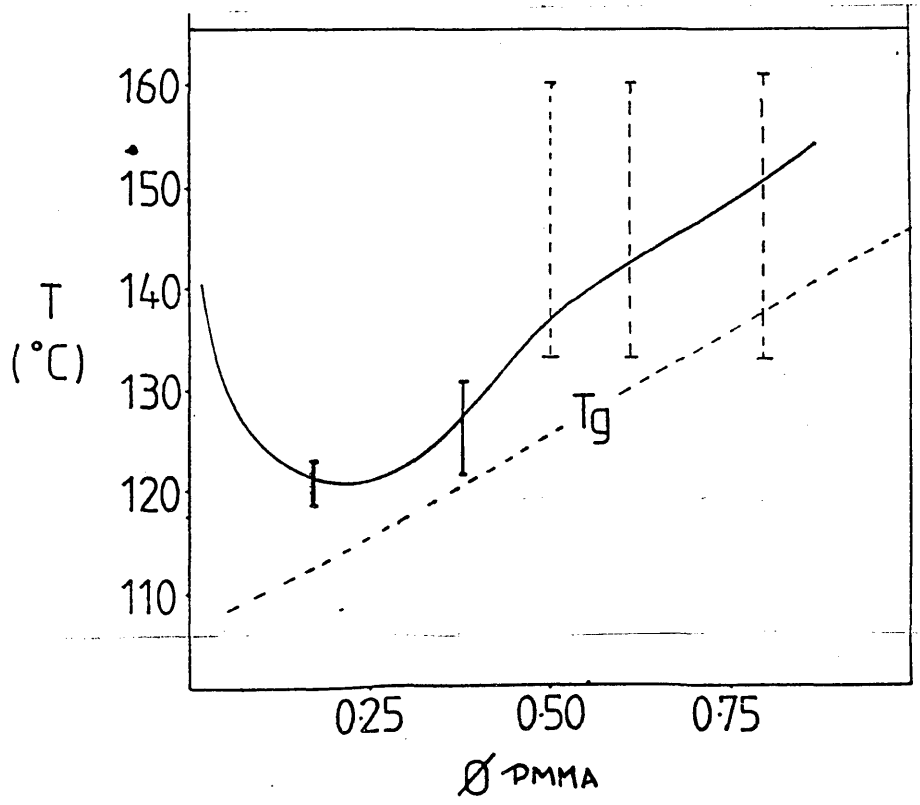


Fig.55 Phase boundary determined using small angle Xray scattering for the PMMA/SCPE[72] system. The dashed line represents the glass transition of the blend calculated using the Flory-Fox equation.

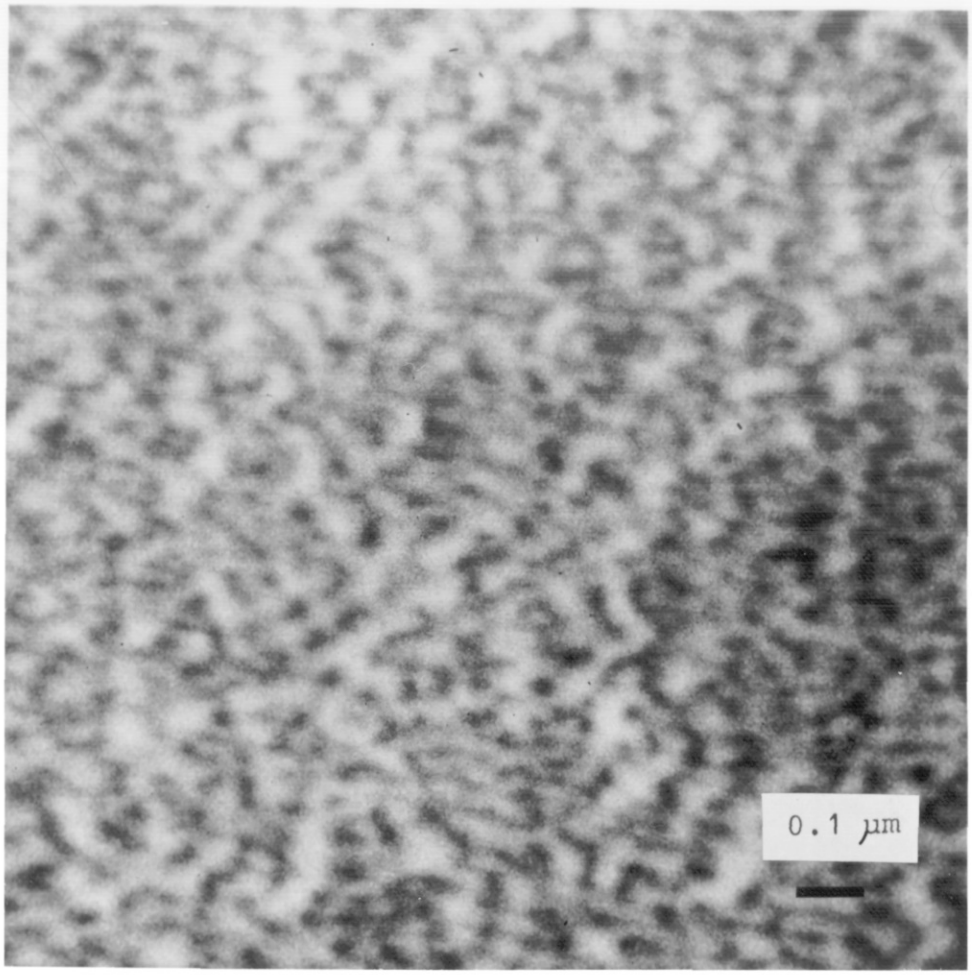


Fig. 56

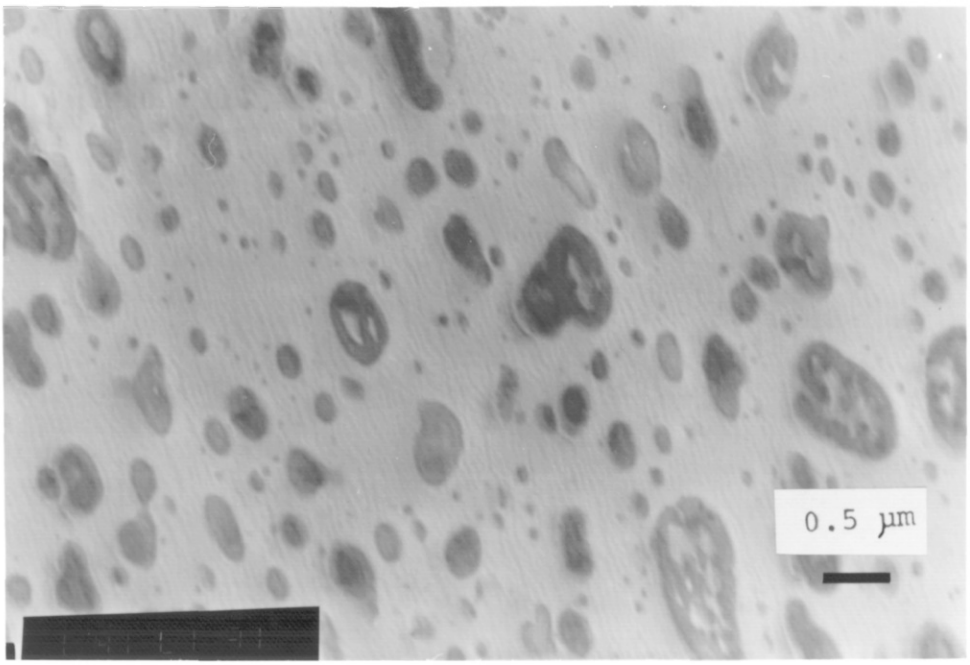


Fig. 57

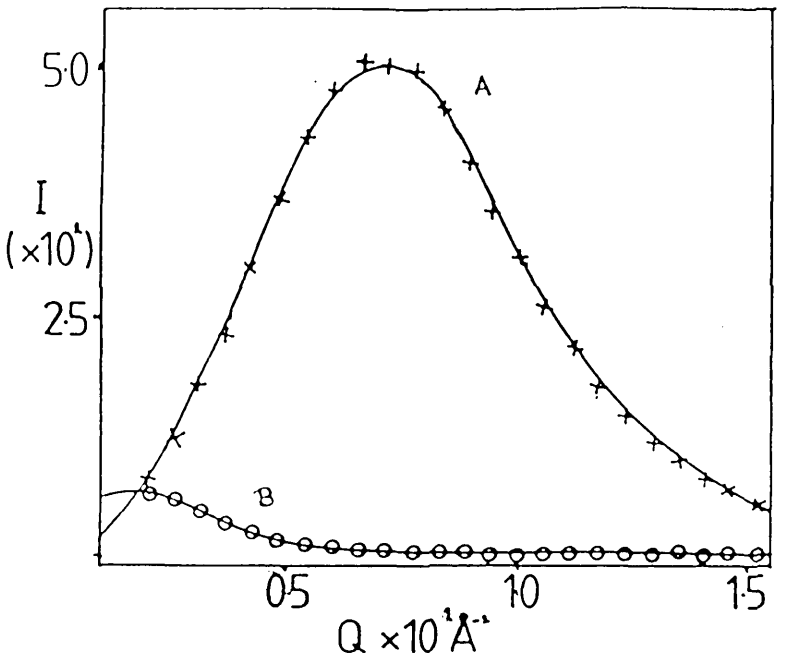


Fig.58 I(Q) plot obtained by SANS of (A) the sample shown in Fig.56 prior to sectioning and (B) a sample prior to any heat treatment.

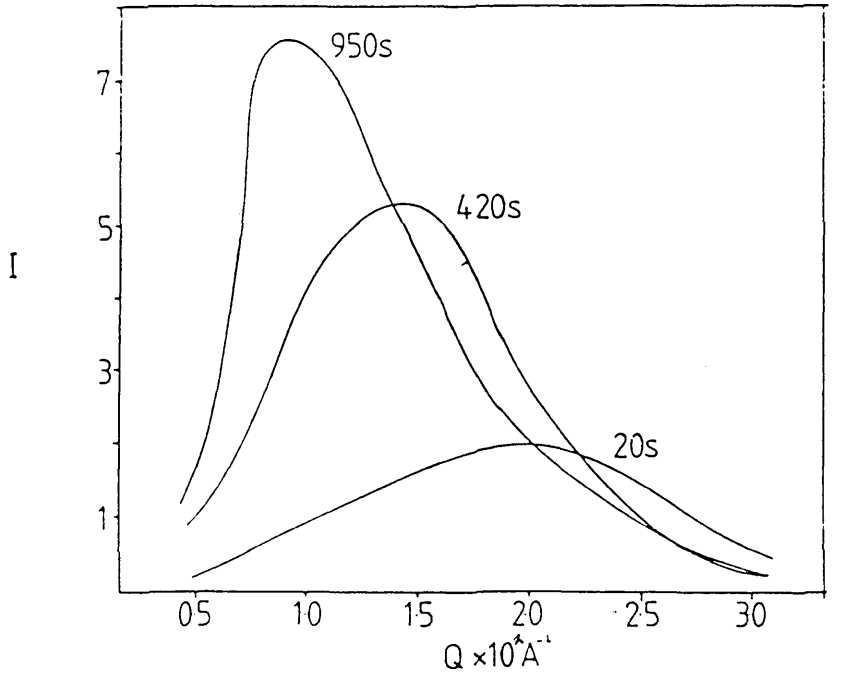


Fig.59 I(Q) plots determined by SAXS for a PMMA/SCPE[67] mixture containing 55% SCPE at 140°C.

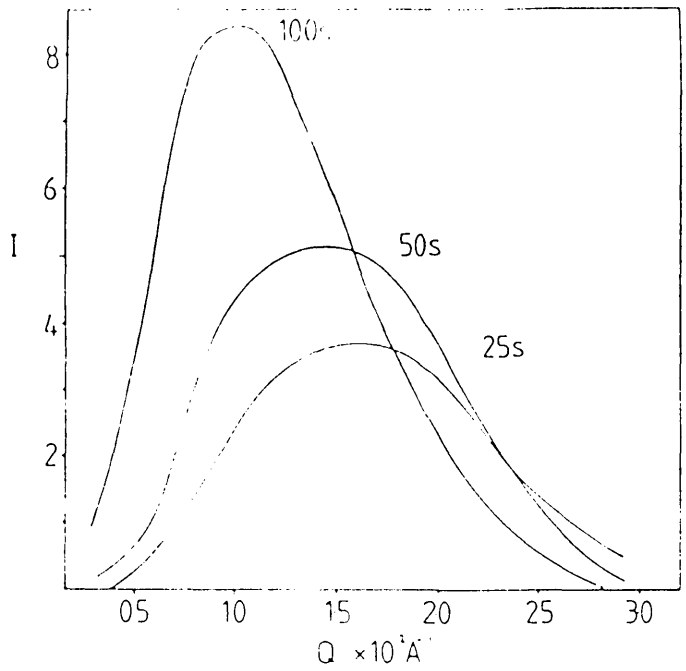


Fig.60 I(Q) plots determined by SAXS for a PMMA/SCPE[67] mixture containing 55% SCPE at 147°C.

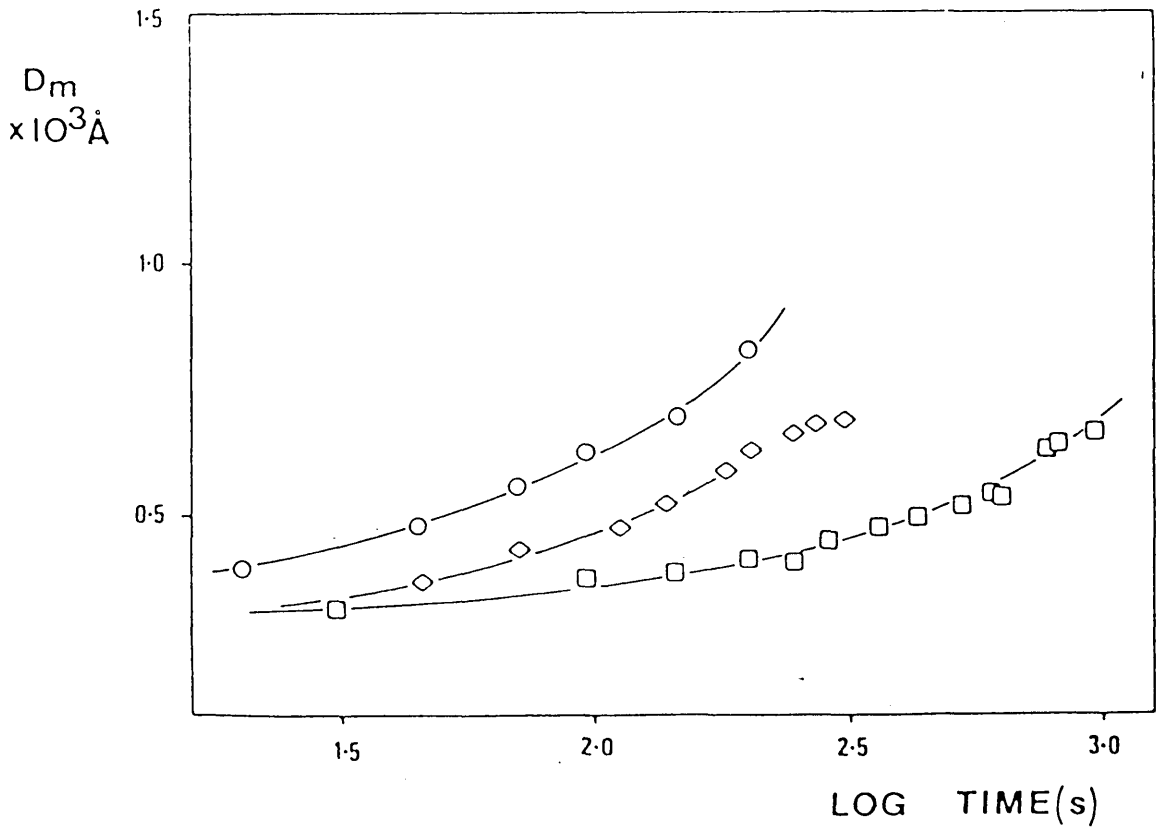


Fig.61 The development of the correlation lengt, Dm as a function of time for a hydrogenous sample containing 55% SCPE[67]. 147°C (○), 140°C (◇), and 130°C (□).

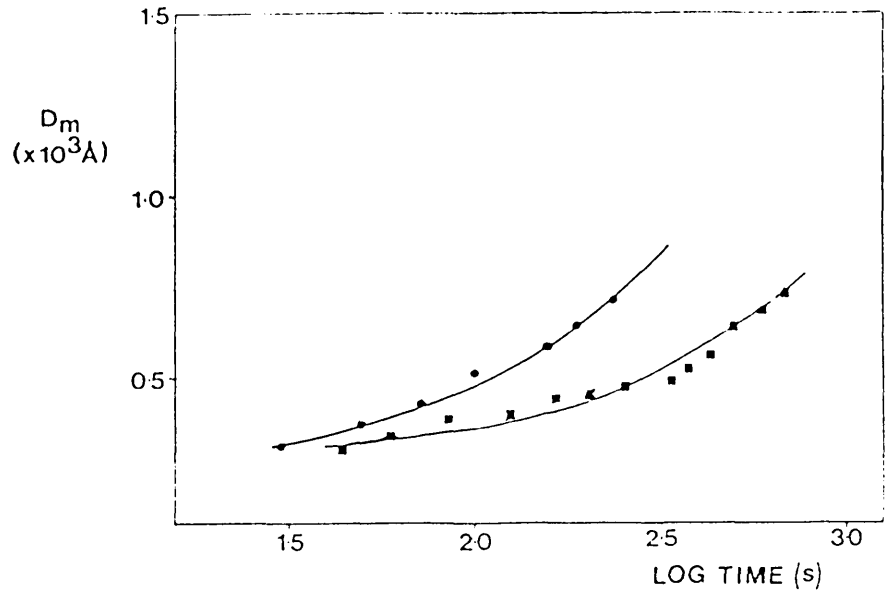


Fig.62 The development of the correlation length, Dm as a function of time for a hydrogenous sample containing 10% SCPE[67] at two temperatures ■ = 130 °C and ● 140 °C.

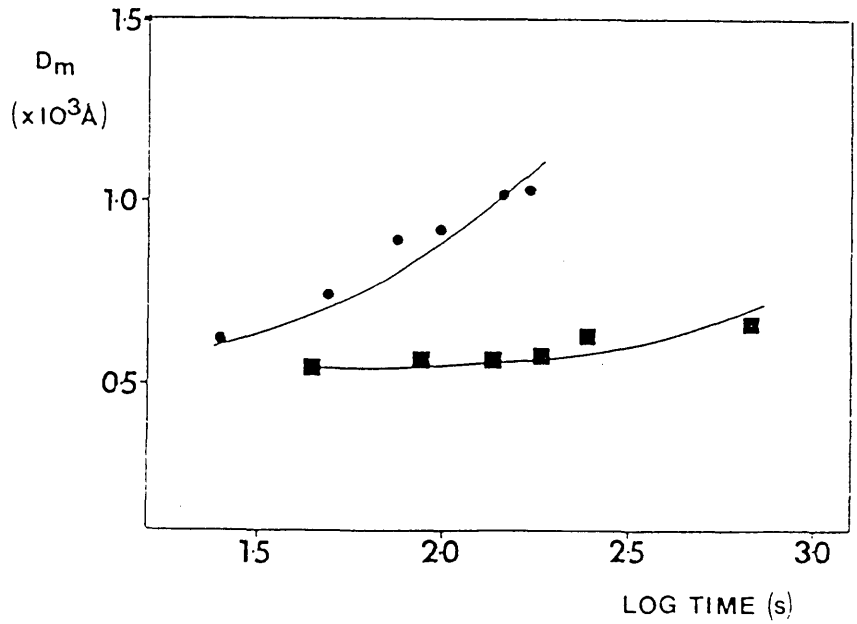


Fig.63 The development of the correlation length, Dm as a function of time for a hydrogenous sample containing 27% SCPE[67] at two temperatures ■ = 130 °C • = 48 °C.

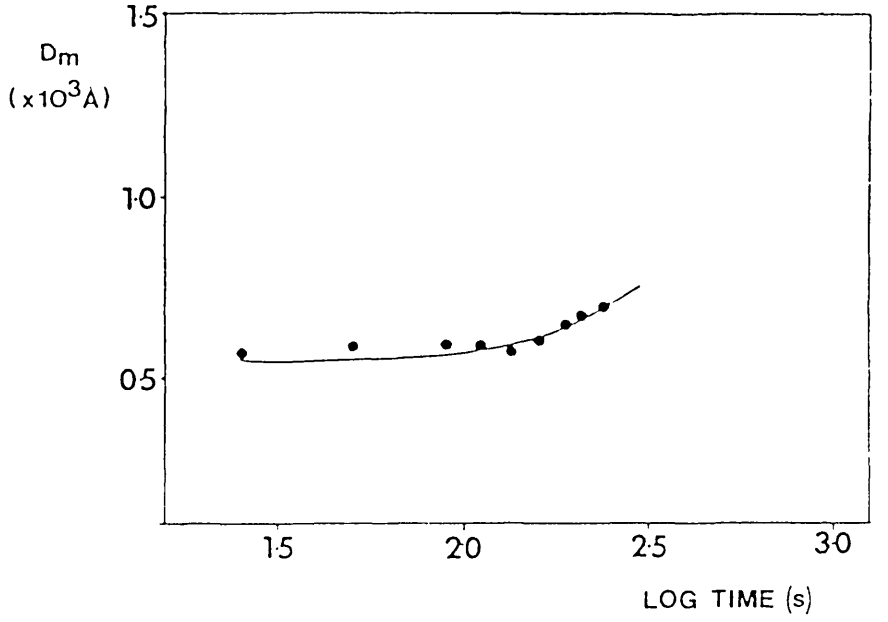


Fig.64 The development of the correlation length, Dm as a function of time for a hydrogenous sample containing 13% SCPE[67] at 140°C.

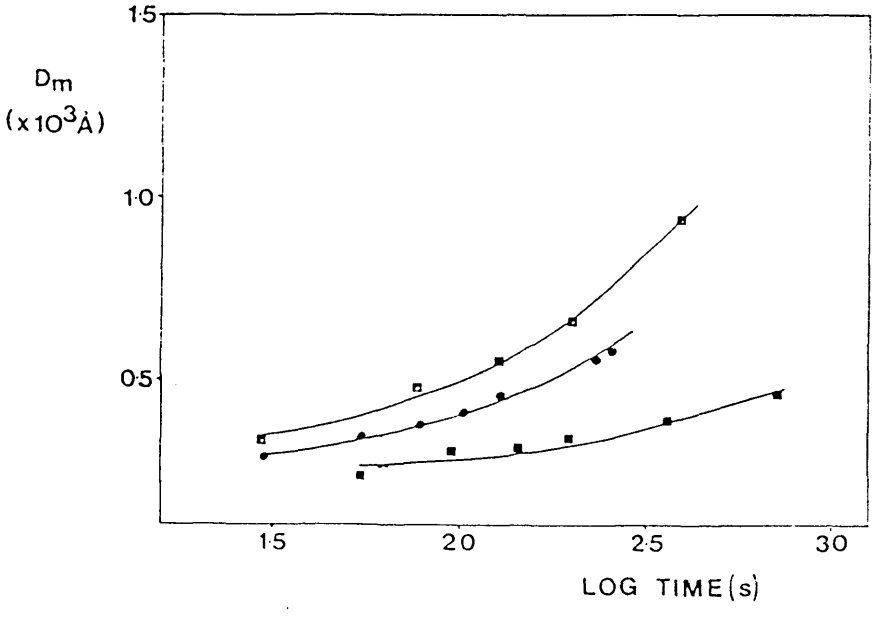


Fig.65 The development of the correlation length Dm as a function of time for a hydrogenous sample containing 80% SCPE[72] at three temperatures. ■ = 130°C, • = 140°C, ▼ = 148°C

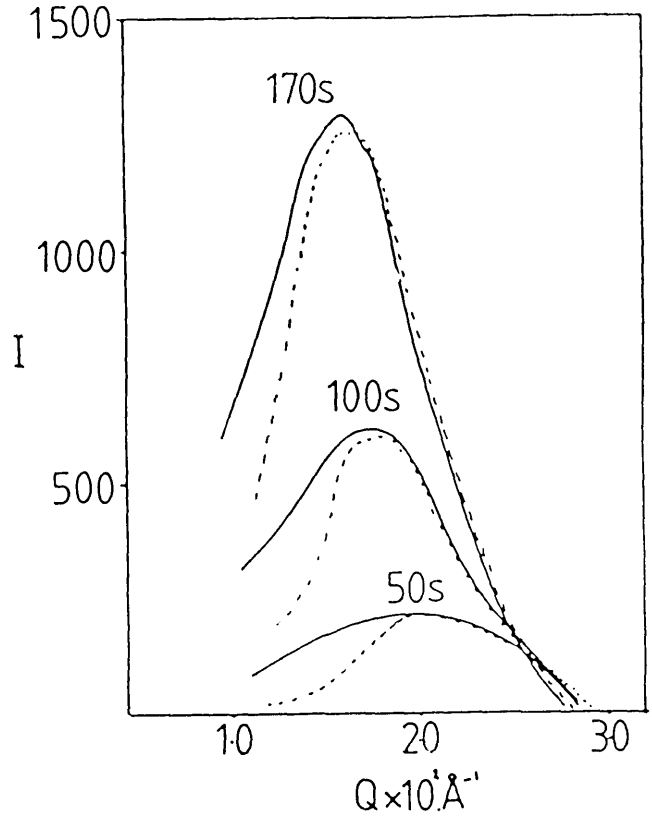


Fig.66 SAXS I(Q) plots for the two samples of PMMA/SCPE^{72} containing 80% SCPE^{72} at 126^{0}C.

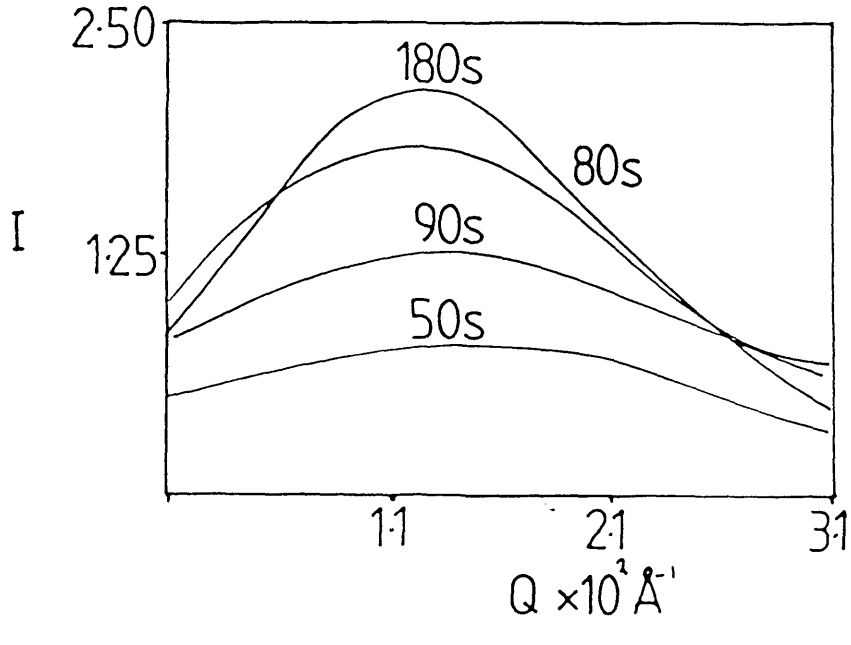


Fig.67 I(Q) plots determined by SANS from PMMA/SCPE^{72} blends containing 80% SCPE^{72} quenched after different times at 127^{0}C.

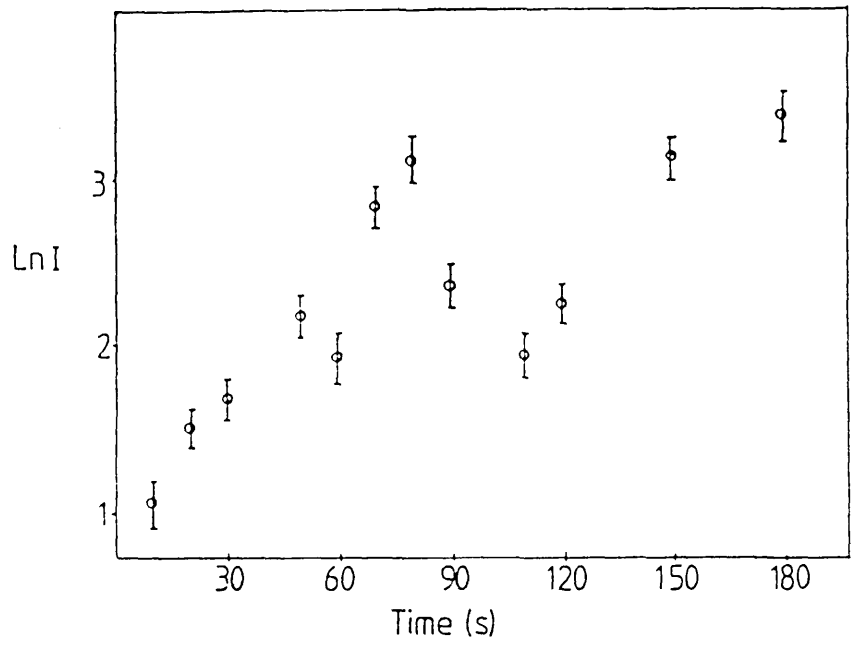


Fig.68 Plot of Ln(Intensity) against time for quenched samples of PMMA/SCPE[72] containing 20% SCPE at 127 ^{0}C.

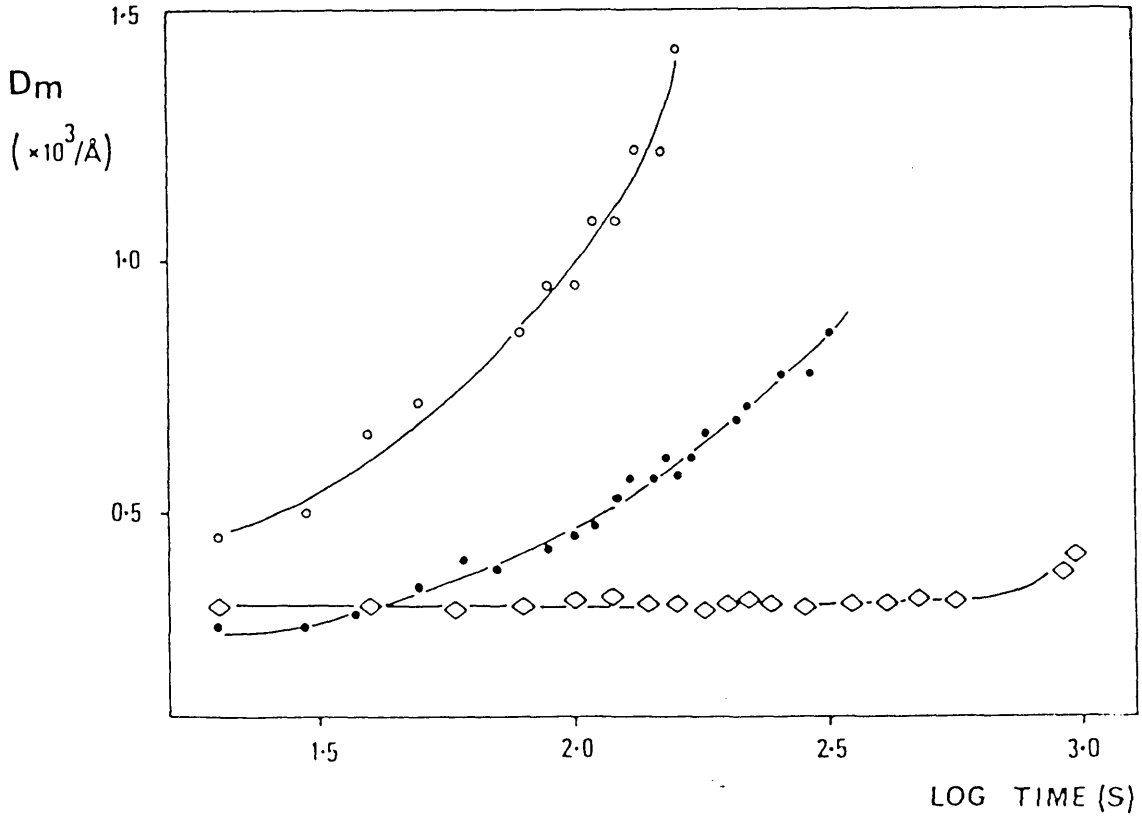


Fig.69 The development of the correlation length Dm as a function of time for samples containing deuterated PMMA and 55% SCPE (SANS data) o = 150^{0}c, • = 131^{0}c and ◇ = 113^{0}c.

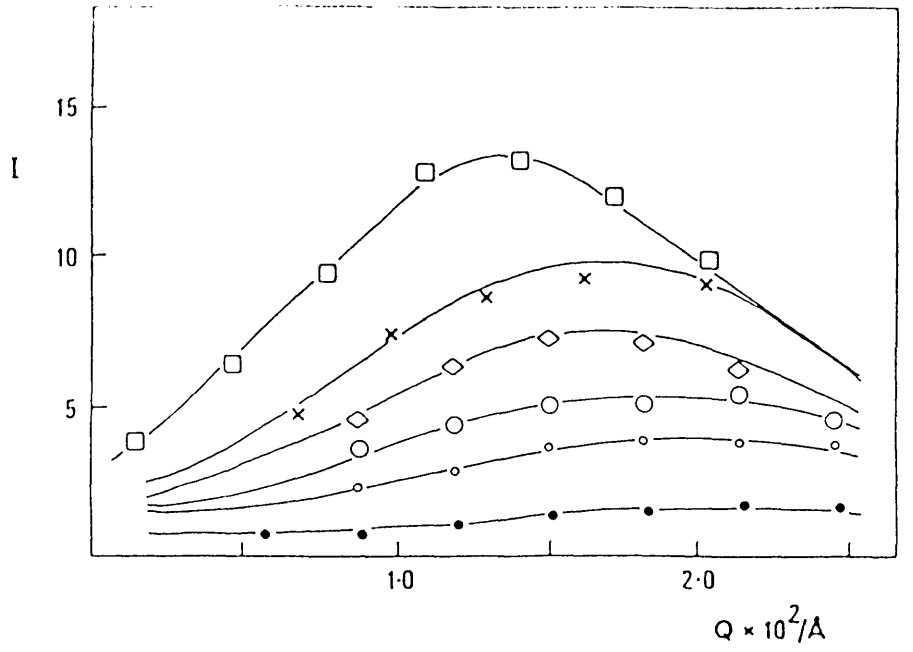


Fig.70 SANS data showing I(Q) as a function of time for a sample containing deuterated PMMA and 55% SCPE at 117°C • = 30s, o = 80s, 0 = 110s, ◇ = 150s x= 200s and □= 290s Most of the data points have been ommitted for clarity.

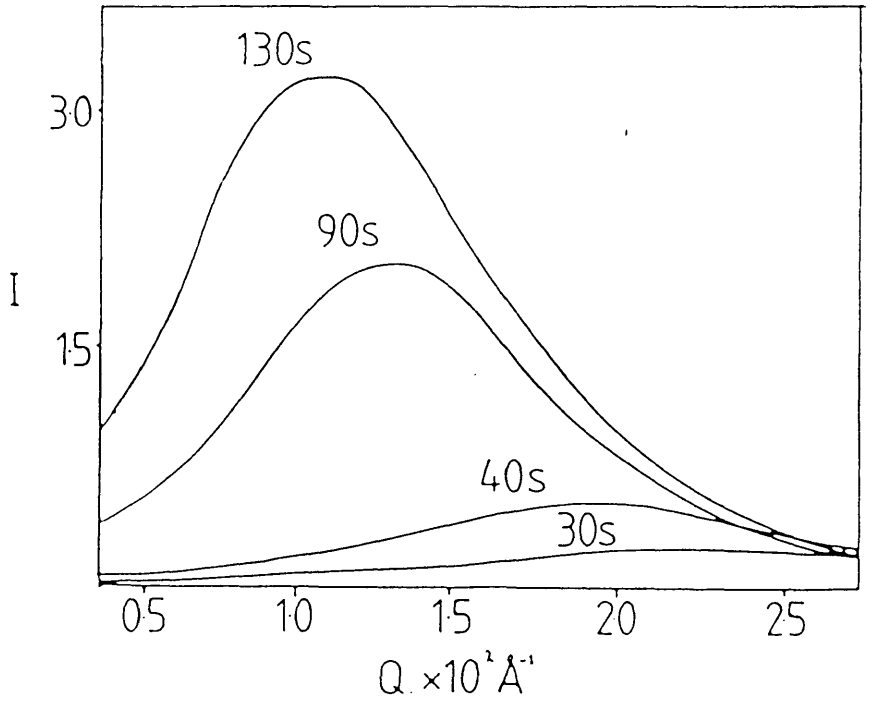


Fig.71 SANS data showing I(Q) as a function of time for a sample containing deuterated PMMA and 55% SCPE at 131°C.

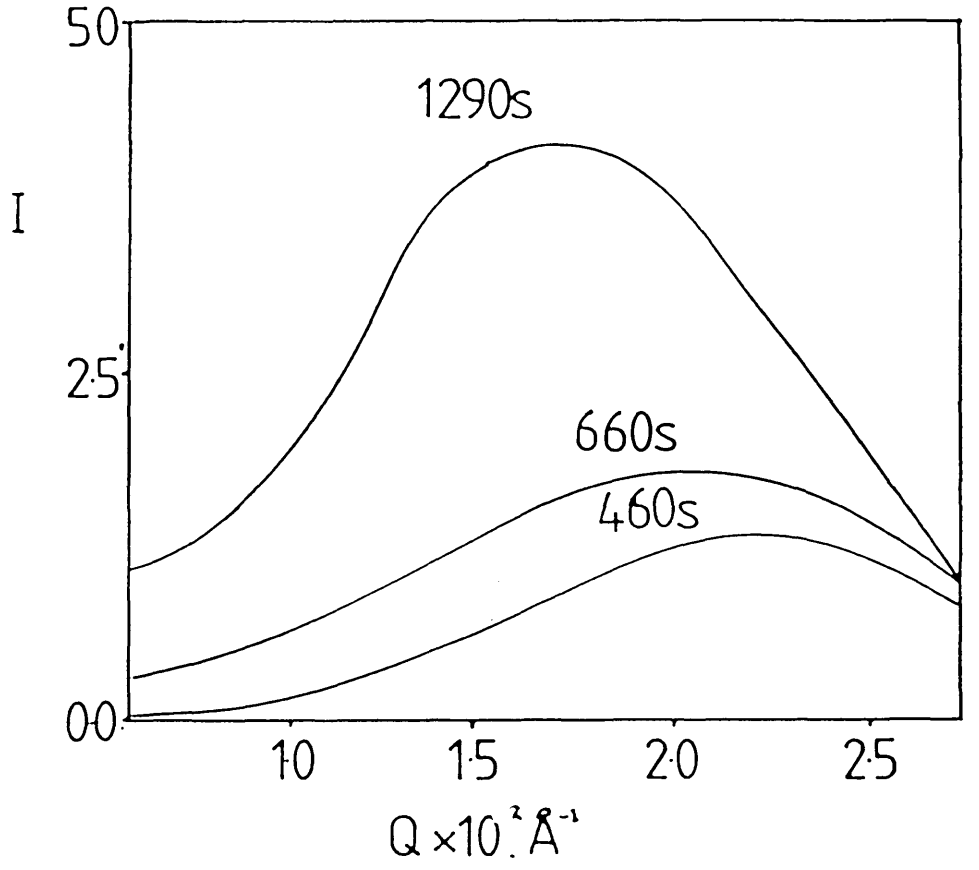


Fig.72 SANS data showing I(Q) as a function of time for a sample containing deuterated PMMA and 55% SCPE at 113°C.

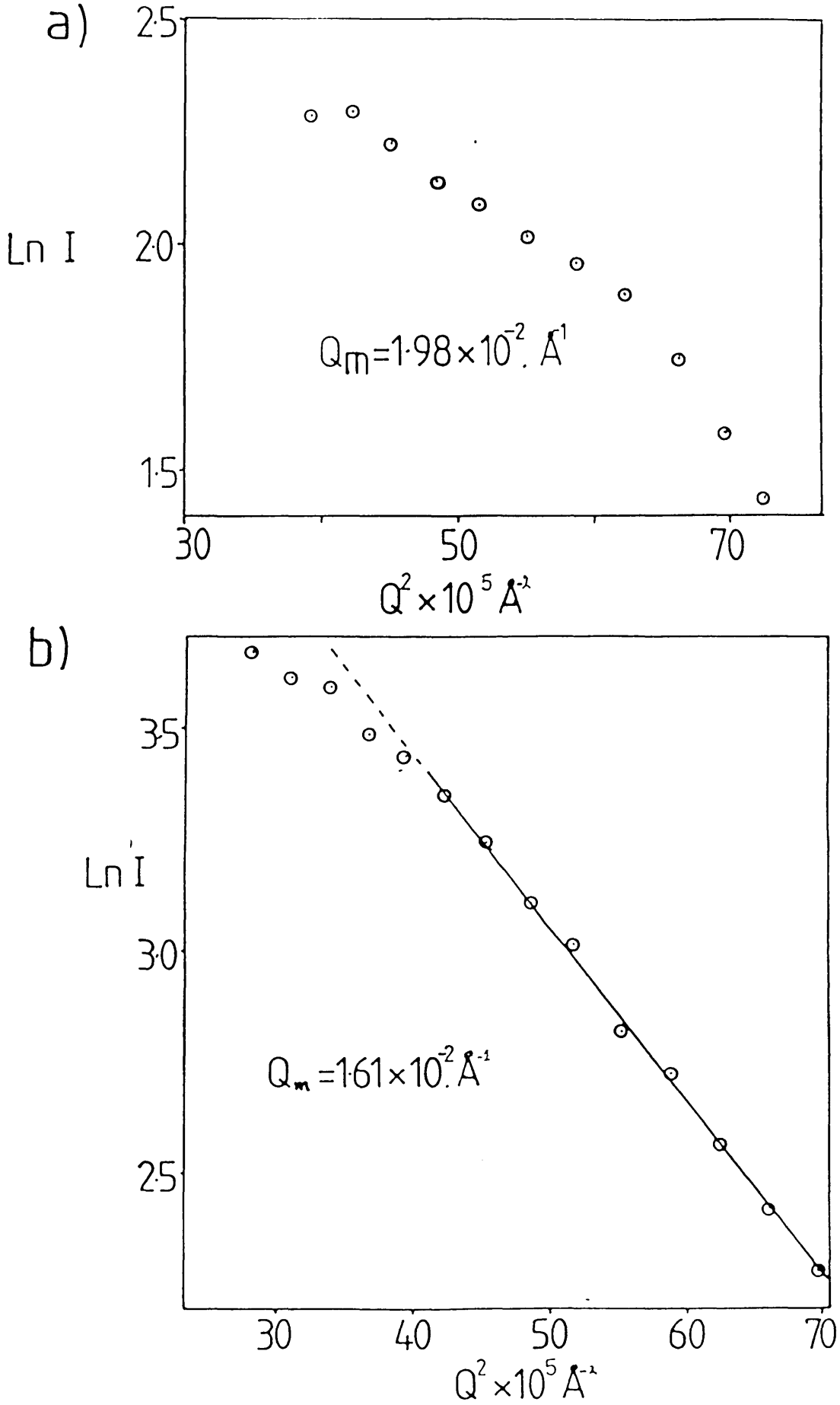


Fig.73 Plot of Ln(Intensity) against Q^2 (Guinier Plot) for a deuterated PMMA SCPE^{67} blend containing 55% SCPE^{67} a after 710 s at 113^{0}C b after 1580 s at 113^{0}C

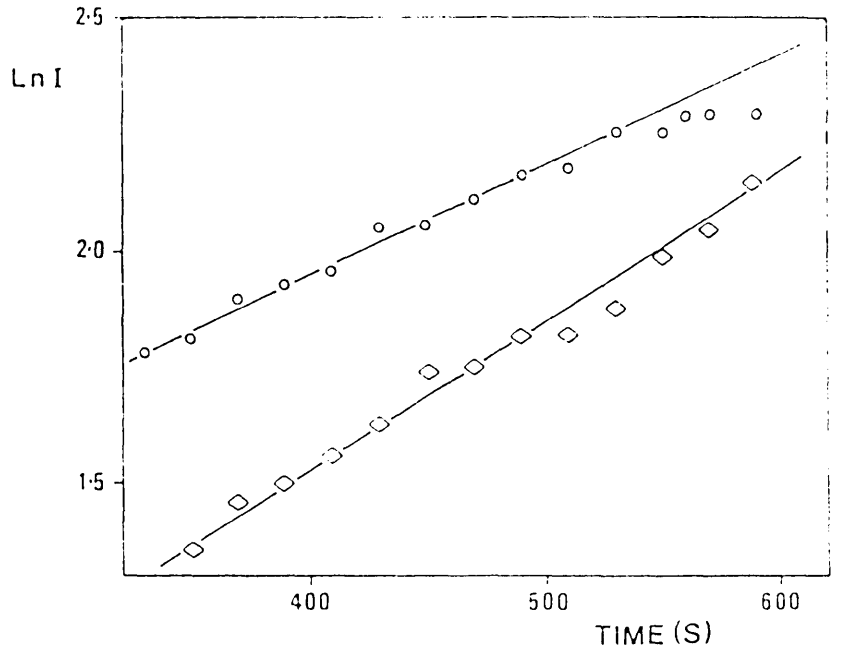


Fig.74 SANS data showing Ln(Intensity) as a function of time for a sample containing deuterated PMMA and 55% SCPE^{67} at 113^{0}. Q = 1.98 x 10^{-2} Å^{-1}(o) and Q = 2.70 X 10^{-2} A^{-1}(◇)

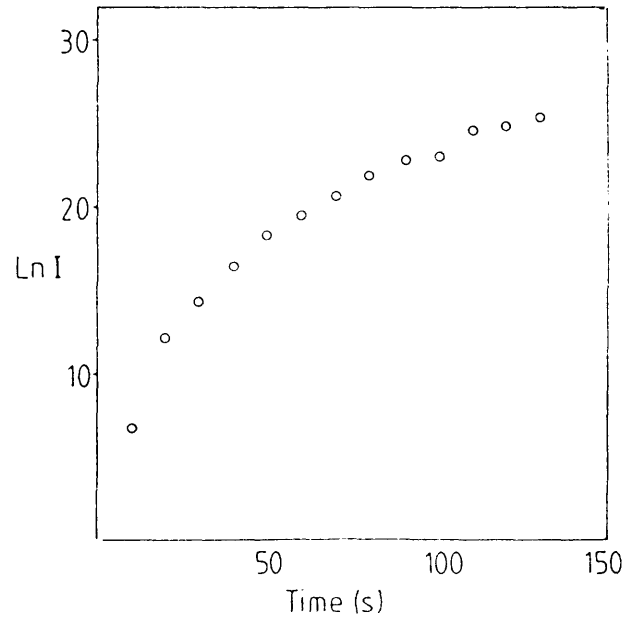


Fig.75 SANS data showing Ln (Intensity) as a function of time for a sample containing deuterated PMMA and 55% SCPE^{67} at 117^{0}C Q = 2.20 X 10^{-2} A^{-1}

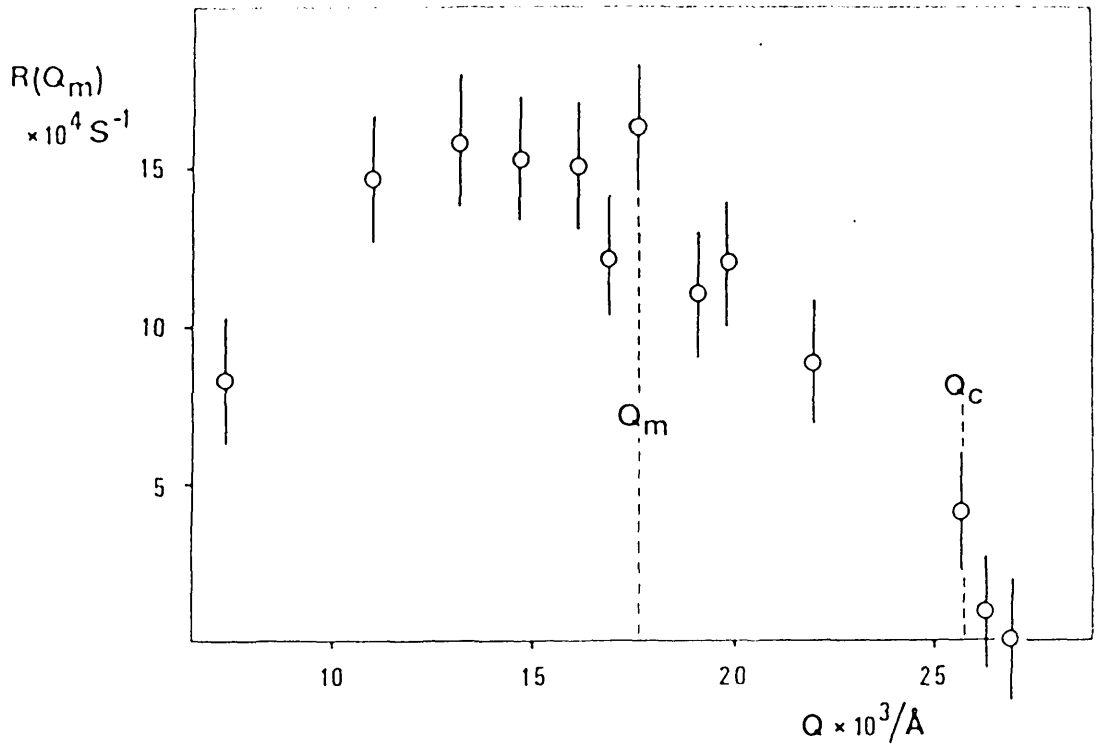


Fig.76 The Cahn-Hilluard growth rate R(Q) as a function of wavevector for a sample containing 55% SCPE and deuterated PMMA at 113°C.

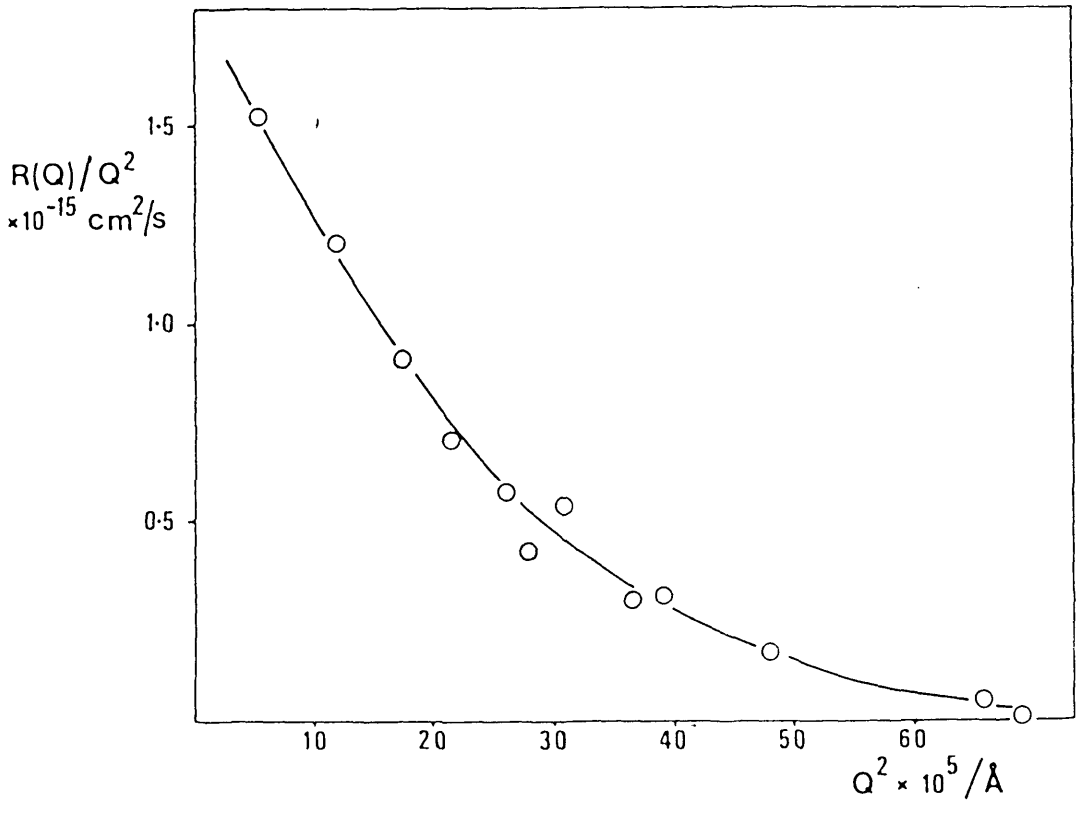


Fig.77 Plot of R(Q) against Q^2 for a PMMA (D)/SCPE^{67} blend containing 55% SCPE^{67}. The Cahn-Hilliard theory predicts this plot to be linear.

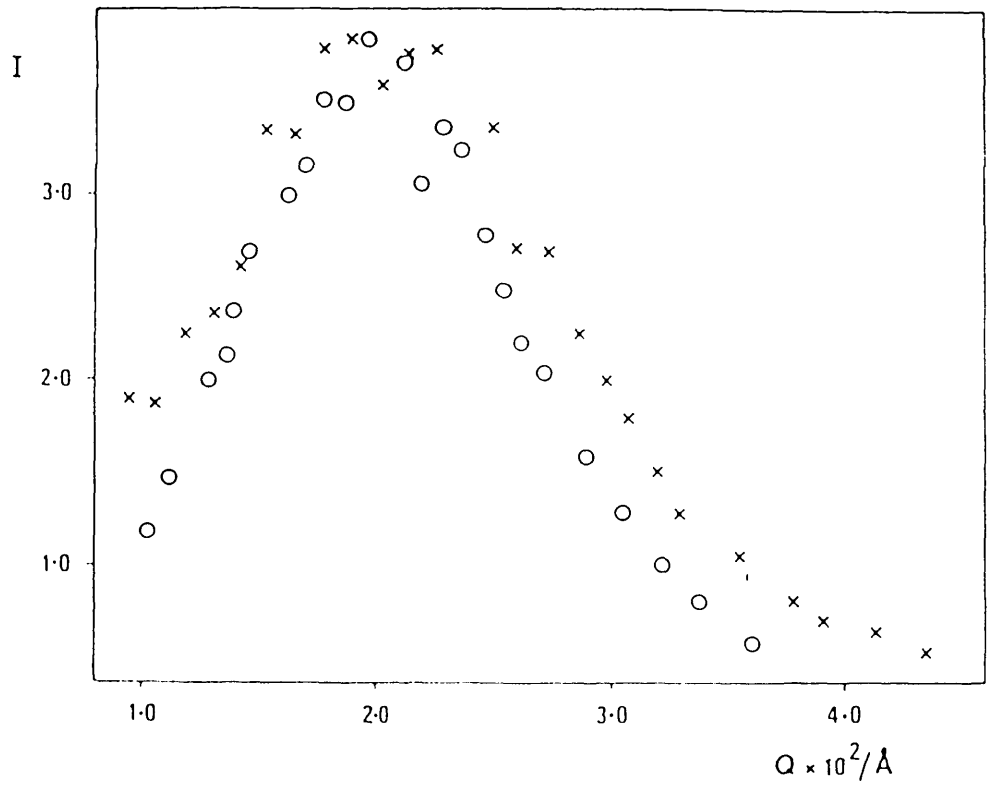


Fig. 78 Plots of intensity against Q for a hydrogenous sample which was quenched after being at 150°C for 30 seconds as observed by SAXS (O) and SANS (X).